Universidade de Aveiro Departamento de Engenharia Mecânica
2008

César Miguel Ramos Maranhão

FEM Analysis in Machining and Experimental Validation

Análise FEM na Maquinagem e Validação Experimental

Universidade de Aveiro Departamento de Engenharia Mecânica
2008

César Miguel Ramos Maranhão

FEM Analysis in Machining and Experimental Validation

Análise FEM na Maquinagem e Validação Experimental

dissertação apresentada à Universidade de Aveiro para cumprimento dos requisitos necessários à obtenção do grau de Mestre em Engenharia Mecânica, realizada sob a orientação científica do Doutor João Paulo Davim Tavares da Silva, Professor Auxiliar com Agregação do Departamento de Engenharia Mecânica da Universidade de Aveiro

Dedico este trabalho aos meus pais, Maria Clara e José Fernando, pelo incansável apoio que sempre me deram em toda a minha vida

o júri

presidente

Prof. Doutor Francisco José Queirós de Melo
prof. Associado da Universidade de Aveiro

Prof. Doutor Carlos Alberto da Conceição António
prof. Associado com Agregação da Faculdade de Engenharia da Universidade do Porto

Prof. Doutor João Paulo Davim Tavares da Silva
prof. Auxiliar com Agregação da Universidade de Aveiro

agradecimentos

Ao Prof. Doutor Paulo Davim, orientador, pela sua ajuda e orientação deste trabalho de investigação.

Ao MSc. Eng. António Festas e Doutor Paulo Faria, pela colaboração no desenrolar do trabalho prático.

Aos meus pais, Maria Clara e José Fernando, pela oportunidade que me deram de desenvolver este trabalho.

À minha namorada, Cíntia Sofia, e ao meu irmão, Nuno Filipe, por todo o apoio demonstrado.

palavras-chave

MEF, simulação numérica, validação experimental, forças de corte e de avanço, potência de corte, temperatura de corte máxima, deformação plástica, Al 7075, AISI 316

resumo

A presente investigação contempla a simulação numérica e validação experimental de processos de maquinagem. O estudo consiste na simulação numérica da maquinagem de materiais de alto desempenho como a liga de alumínio 7075 e o aço inox AISI 316 com validação experimental. Diversas simulações e validações foram conduzidas de modo a cobrir uma gama de parâmetros de maquinagem. Forças de corte e de avanço, potência de maquinagem, máxima temperatura de corte e deformação plástica foram validadas com sucesso. Finalmente, foram modeladas outras grandezas nomeadamente tensões residuais no aço inoxidável.

keywords

FEM, numerical simulation, experimental validation, cutting and feed forces, cutting power, maximum cutting temperature, plastic strain, Al 7075, AISI 316

abstract

The present investigation contemplates numerical simulation and experimental validation of machining processes. The study consists in simulating the machining of high performance materials like aluminium alloy 7075 and stainless steel AISI 316 with experimental validation. Several simulations and validations were conducted in order to cover a wide range of machining parameters. Cutting and feed forces, cutting power, maximum cutting temperature and plastic strain were validated with success. Finally, residual stresses in stainless steel were also modelled.

Contents

Nomenclature

This document employs specific symbols and abbreviations as possible. To accommodate for an easier reading, symbols and abbreviations will be listed.

Symbols

A	Yield strength (MPa)
a_p	Depth of cut (mm)
b	Chip width (mm)
B	Hardening modulus (MPa)
c	Workpiece specific heat (J/(Kg.K))
C	Strain rate sensitivity coefficient
D	Diameter of the workpiece (mm)
f	feed rate (mm/rev)
Fc	Cutting force (N)
Ff	Feed force (N)
Fτ	Cutting force in the shear plane (N)
HB	Hardness Brinell (HB)
k	Thermal conductivity coefficient (W/(m.K))
L	Length of the workpiece (mm)
lf	Contact length between chip and tool (mm)
Pc	Cutting power (W)
R	Thermal number
Ra	Arithmetic mean roughness (μm)
Rc	Cutting ratio
rpm	revolutions per minute
Rt	Maximum peak to valley height (μm)
RzD	Mean peak to valley height (μm)
t	Undeformed chip thickness (mm)
t’	Deformed chip thickness (mm)
T	Temperature (ºC)
Tm	Workpiece melting temperature (ºC)
Troom	Room temperature (ºC)
Vc	Cutting speed (m/min)
Vτ	Cutting speed in the shear plane (m/s)

Greek Symbols

α	Clearance angle (º)
γ	Rake angle (º)
Γ	Absorbed heat proportion
ε	Plastic strain
$\dot{\varepsilon}$	Plastic strain rate (s^{-1})
$\dot{\varepsilon}_0$	Reference plastic strain rate (s^{-1})
ρ	Workpiece specific weight (Kg/m^3)
θ	Maximum cutting temperature (ºC)
θf	Mean temperature in the tool-chip interface (ºC)
θm	Secondary shear zone temperature (ºC)
θs	Primary shear zone temperature (ºC)
μ	Friction coefficient
Φ	Shear plane angle (º)
χ	Position angle (º)

Abbreviations

AISI 316	Stainless steel 316
Al 7075	Aluminium alloy 7075
CNC	Computerized numerical command
FEM	Finite element method
ISO	International Standard Organization
PCD	Polycrystalline diamond tool
RTS	Relative tool sharpness

Chapter 1)

Introduction

Nowadays, FEM (finite element method) analysis machining is increasing in popularity among researchers when metal cutting operations are concerned. However, without experimental validation, FEM analysis in machining is nothing but a skeptical approach to the machining process. FEM analysis in machining is still in its early stages of life and because of this fact, a careless FEM development can lead to uncertain results. Experimental validations are detrimental to understand the validity of such FEM analysis.

In the present thesis, a prediction of the thermo mechanical behavior when machining an aluminium alloy is made, using a polycrystalline diamond cutting tool with variable feed rate. A similar study was also made but in stainless steel with a coated cemented carbide cutting tool, also with a variable feed rate. To aid the study, a commercial machining finite element software was used and several parameters could be studied like cutting and feed forces,

cutting power, maximum cutting temperature, plastic strain and plastic strain rate, maximum shear stress and residual stresses (the latter only for stainless steel). In figure 1.1, an example of a mesh used by the FEM software can be seen in the tool, workpiece, chip and burr.

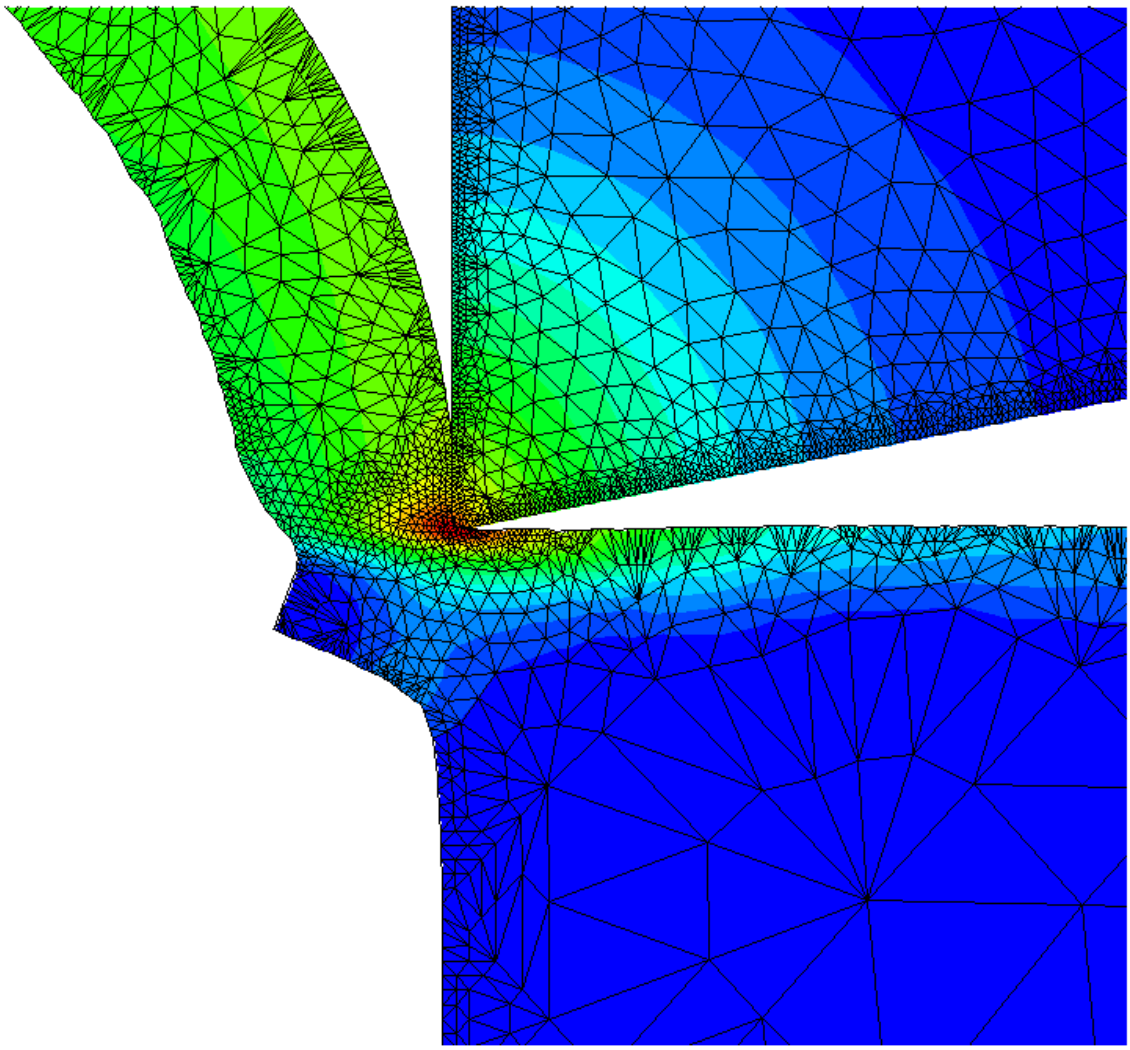

Figure 1.1: Example of a mesh in the tool, workpiece, chip and burr employed by the FEM software

Therefore, the main objective of the thesis is to make an experimental validation of the orthogonal cut applied to both materials using the FEM approach.

Input parameters were established and the experimental work took place. Afterwards, the experimentation was replicated with the aid of the FEM machining software in order to verify if the experimental results met what was made through simulation. Several cases of study were conducted for each workpiece material, being the feed rate and cutting tool the only difference between them. Several experimental validations were obtained for each material

for all cases of study. Experimental validations consisted in comparing experimental cutting and feed forces, cutting power, maximum cutting temperature and plastic strain to the respective simulated counterparts.

From the simulations and experimental work that has been conducted for the past several months, it can be concluded that FEM is a valid approach to predict the thermo mechanical behaviour of both materials used in this study. Parameters like cutting and feed forces, cutting power, maximum cutting temperature, plastic strain, plastic strain rate, maximum shear stress and residual stresses were studied for both materials (the latter being a stainless steel exclusive).

In the following paragraph, a brief note will be given to provide a better understanding on how this document is organized.

This investigation will be presented through several chapters. ***Chapter 2*** will be focused in the state of the art and will debate results from other researchers, some theories related with the current project and possible difficulties to be encountered through the investigation. ***Chapter 3*** will give an overview on FEM machining software by providing a brief description on how the software works and some notes from the user point of view. The mechanical characteristics of the workpiece materials in study will also be presented. It will also give an in depth analysis on how the experimental work was conducted in the workshop and all the hardware that was used. Input parameters of the simulations are also detailed. Finally, the employed analytic models will be explained. ***Chapter 4*** will be focussed upon the results and their discussion. It will start with a description on the studied workpiece materials and the motive of their choosing and their respective cutting tools. The measured experimental data and the obtained results when the mathematical models are applied will also be presented. In the following subsection, a FEM analysis validation with the Coulomb friction coefficient will be addressed followed by a FEM analysis validation with an adjustment to the Coulomb friction coefficient. Last but not least, a modelling and prediction section will give a more detailed analysis of the studied parameters for all cases of study (cutting and feed forces, cutting power, maximum cutting temperature, plastic strain and plastic strain rate, maximum shear stresses and residual stresses). Finally, ***Chapter 5*** will address the conclusions that are important to withdraw from all the work. The references of the bibliographic revision are also indicated.

Chapter 2)

FEM analysis in machining - a state of the art

2.1 FEM overview

Metal cutting is one of the most common manufacturing processes and the finite element method (FEM) has become the main instrument to simulate machining operations *(Bil et al, 2004).* It constitutes a complex process involving a variety of physical phenomena, such as plastic deformation, frictional contact, thermo-mechanical coupling and chip and burr formation mechanisms *(Trent and Wright, 2000).* Experimental approaches to study the machining processes are important but they can be replaced by FEM analysis, especially when a wide range of parameters is involved such as machining conditions, material of the workpiece, and tool types are involved. Process features such as tool geometry and cutting parameters directly influence cutting forces, chip morphology, tool life, and final product quality *(Marusich and Ortiz, 1995).* In figure 2.1, an example taken from Advantedge^{TM} of

plastic strain distribution in the chip and workpiece is shown. Also of relevance are the cutting and feed forces and maximum cutting temperature evolution along the time.

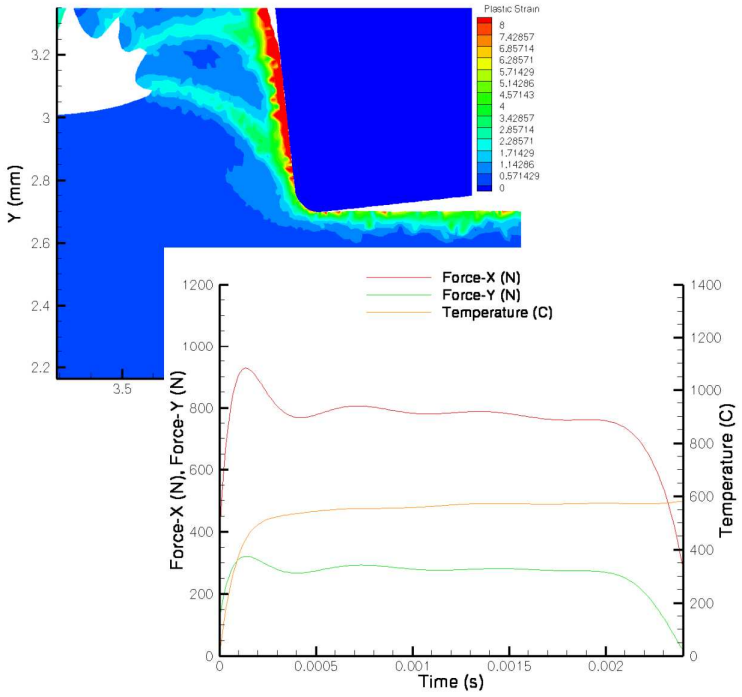

Figure 2.1: FEM software with a prediction of cutting and feed forces and cutting temperature along the time and plastic strain distribution in the workpiece and chip (Advantedge^{TM})

Experimental procedures are directly related with spending time and money in the workshop and there resides one of the advantages of using numerical simulation (it is possible to determine the thermo mechanical behaviour of both the tool and the workpiece). However, the accuracy of the obtained results with numerical simulation depends largely upon the accuracy of the input data. *Sartkulvanich et al (2005)* stated that the most important parameters that will influence the accuracy of the numerical simulations are the flow stress curve of the workpiece material and the friction coefficient along the tool-chip interface.

Computer simulation of the cutting process can potentially reduce the number of design iterations and that results in substantial cost savings. Therefore, considerable effort has been devoted to the development of computational models. In order to reduce costs and increase efficiency in mechanical cutting operations, understanding of the metal cutting process must be improved and an effective way is to model and simulate the process. Predictive models of cutting processes are used to forecast and evaluate cutting performance indicators such as chip formation, cutting force, cutting temperature, tool wear and surface finish *(Sartkulvanich et al, 2005; Barge et al, 2005; Bil et al, 2004; Yen et al, 2004).* Currently, numerical cutting

simulations (in two and three-dimensions) are commonly used and represent a very useful and powerful tool for understanding chip flow in machining and to obtain information that is difficult to acquire experimentally. In figure 2.2, an example of the applied mesh in 2D in the cutting tool, workpiece and chip is shown. Both cutting forces are displayed along the time.

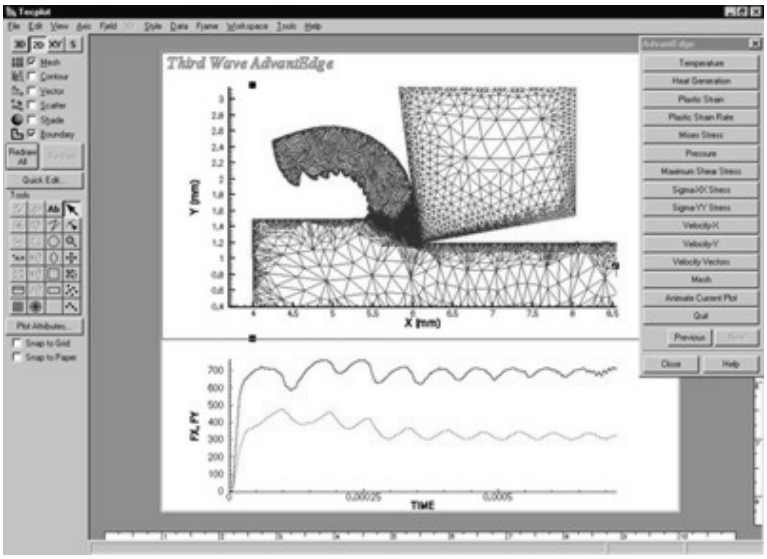

Figure 2.2: Mesh in the tool, workpiece, and chip with the respective prediction of cutting and feed forces along the time (Advantedge^{TM})

Changing a cutting input parameter and examining its effects on the final solution allows researchers to isolate regions and physical quantities most affected by the change. This provides for a previous reasoning in the specific matter which can result in multiple solution data sets for comparison. Like already stated, the reliability of the results obtained with FEM simulation depend upon the accuracy of the input values. Among these inputs, flow stress data of the workpiece and the friction along tool–chip interface are of extreme importance for the prediction of cutting variables such as cutting forces, chip formation and temperature distributions *(Fang, 2005; Grzesik et al, 2005; MacGinley and Monaghan, 2001; Ozel, 2006).*

2.2 Commercial Software's

The choice of finite element software for machining analysis is an important factor in determining the quality and scope of analysis that can be performed. Three of the most common software for FEM analysis machining are presented*: Deform^{TM}, Abaqus^{TM} and AdvantEdge^{TM}. Given the complexity of the finite element method, the choice of package is very important for the type of analysis that can be performed the quality of the results as well.

* Well described by Gardner et al, Comparative Study of Finite Element Software, 2005

This is because the type of analysis that can be performed as well as the quality of the results. This is because different packages have different capabilities and it is critical to select the package with the appropriate feature set. Furthermore, the assumptions and solver techniques used in the package have far reaching consequences in the results obtained from the simulations.

Deform™ (Design Environment for Forming), is a commercially available FEM solver that can be applied to several manufacturing processes. Deform™ original area of specialty was in metal forming operations like forging. It has since expanded to include modules that support machining operations. As an advantage, Deform™ machining modules can be used to quickly set up standard machining processes like turning, milling and drilling. The user has to supply the workpiece and tool geometry as well as the process parameters. The solver then uses a standard solver configuration and finds the solution. Alternatively, the user has the ability to adjust solver parameters like mesh-size, nodal boundary conditions, and tool-workpiece interaction properties, for example. Given that many of these parameters remain constant from one simulation to the next, the pre-programmed modules can work very effectively. Deform also has an extensive material library containing models of several common materials and alloys. The program also has the capability of defining new materials based on stress/strain data and other key material properties. This contributes to the usability of the program to simulate actual process conditions and increases its applicability. Adaptive meshing controls accommodate high workpiece deformations that are very common in machining.

As for Deform™ disadvantages, workpiece tends to demand more and more elements as the simulation progresses, which causes the simulation to run slower with time. In addition, the simulation will stop periodically and the mesh size needs to be adjusted by the user. There are several fine points which accompany the learning curve for Deform™.

Abaqus™ is a general purpose FEM program that can solve a variety of problems. Abaqus™ does not have any modules/packages for machining simulations, and hence the user has to explicitly define the tool and the workpiece, the process parameters and the simulation controls (including boundary conditions and mesh geometry.) As for advantages, Abaqus™ comes with two solvers (Standard and Explicit) which can be used to run a variety of simulations. Simulations are setup in Abaqus™ by using keywords that define the functioning of the simulation. The user is free to model the machining operation using specific axioms,

thus providing a good deal of control over the simulation. Though Abaqus™ has no support for any materials, it allows users to configure the materials using a variety of models. The user also has very fine control over the meshing and the element types used in the model. Perhaps the biggest advantage of Abaqus™ is that is allows modelling at a high level of detail. The user is able to setup a very detailed model describing various kinds of behaviour, as well as a "bare-bones" model that provides general information. Moreover, the software is command-line accessible and supports scripting functionality. As for disadvantages, the open-ended nature of the program presents a steep learning curve. Also, it takes a lot of time to "setup" simulations using the software as the user has to manually set many of the simulation parameters. This is especially true in the case of mesh optimization.

AdvantEdge™ is a machining specific FEM package. It has pre-programmed modules for both 2D and 3D machining operations including turning and milling and is very intuitive. A more detailed analysis of this software will be addressed under FEM analysis section. In figure 2.3, a scheme on how FEM packages work is presented. As shown, in order to obtain results, several software inputs are required. In other words, a pre-programmed module has several fields that need to be specified before the simulation takes place. In this case, where machining operations are the objective, the inputs are based in machining parameters. Among these inputs, the friction coefficient and the material flow stress need special attention like already mentioned.

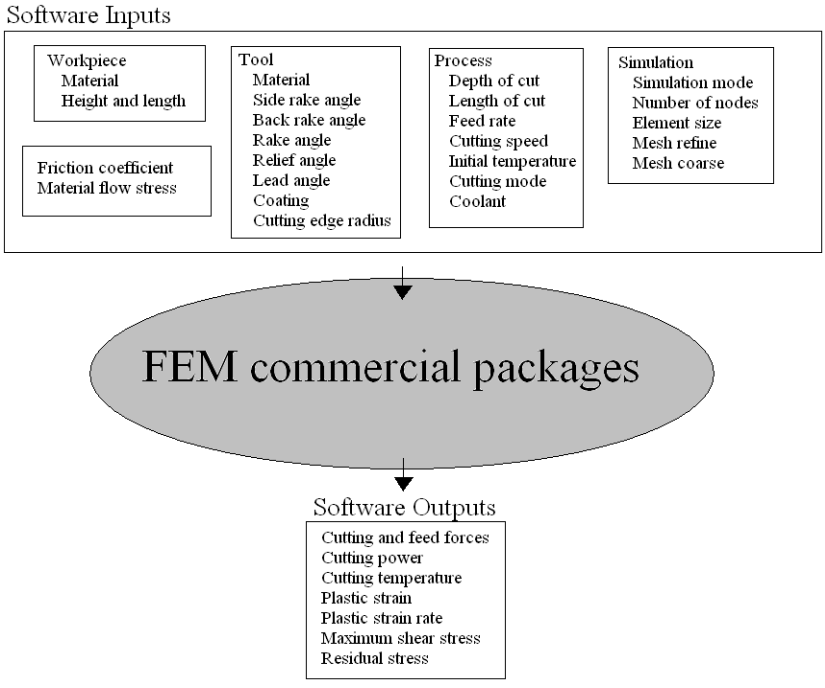

Figure 2.3: Typical FEM machining software inputs and outputs

2.3 FEM machining software inputs

FEM software demands several input values to predict the thermo mechanical behaviour of the machining operation. The inputs can be geometric like tool rake angle, cutting edge radius, etc. Cutting parameters like cutting speed, feed rate or depth of cut are also crucial as an input in the software. The number of nodes and the mesh also have weight in the FEM results. It is worth noting that although every input is important and if the cutting conditions are kept the same, the material flow stress and the friction coefficient, among all inputs, are the most representative in the simulations reliability.

2.4 Flow stress and friction coefficient

Finite element method for machining processes is constantly attracting researchers and scientists to continuously understand the chip formation mechanisms, heat generation, tool-chip friction and quality of the machined surfaces. When cutting metal, the cutting force is felt in a small area of the tool rake face which is in contact with the chip (this is known as the tool-chip interface) *(Astakhov and Outeiro, 2005)*. Of note is that the tool-chip interface is the zone immediately ahead of the cutting tool that is in contact with the chip. To understand better where the tool-chip interface is located, figure 2.4 shows a scheme of the orthogonal cut with the respective location and some geometric aspects of the cut are also detailed.

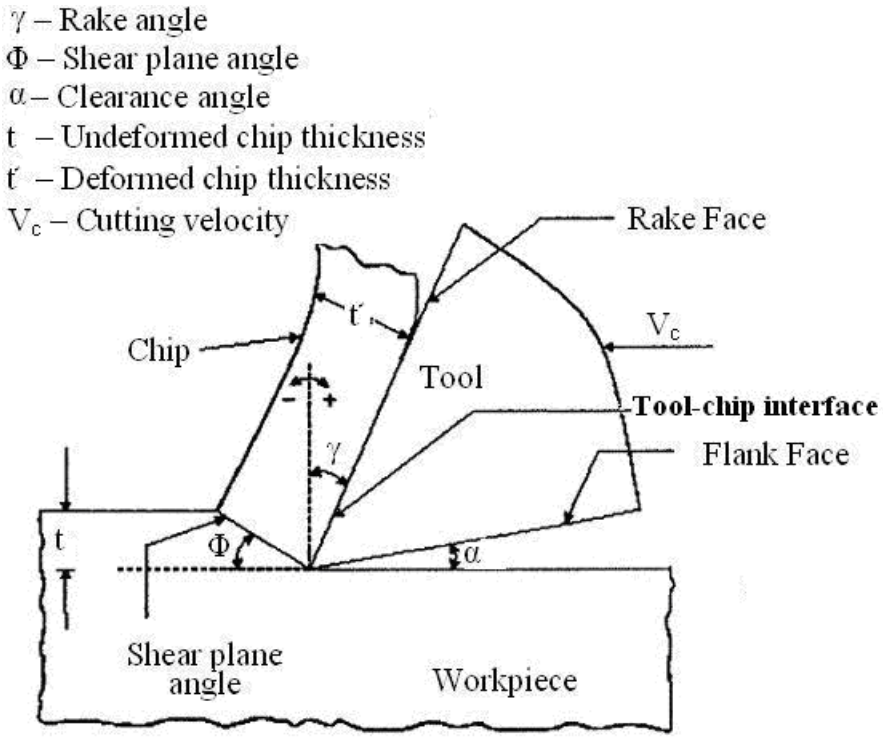

Figure 2.4: General view of the cutting process

When simulating machining processes, friction conditions at the tool-chip interface are one of the most important inputs to obtain reliable results. Despite of the development of high performance FEM software, simulating machining processes is a very hard task mainly due to the geometric complexity of the real tool-chip systems and the high cutting speed (requiring long simulation times). Because of these reasons, machining operations are not easy to simulate *(Filice et al, 2007).* FEM predictions are greatly influenced by the friction coefficient and by the material flow stress, however, the friction coefficient is the most important aspect when modelling machining operations. FEM machining simulation is essential to make reliable predictions in cutting forces, temperatures, stresses and strains in the chip, tool and machined surface. However, the reliability of the simulations is seriously compromised when the friction value is assumed. Friction is important in all engineering applications, wherever solid surfaces are sliding against each other. This relates directly with metal cutting processes, where a sliding pair of different surfaces are in contact and where plastic deformation of the softer material appear under high pressure. In orthogonal cutting, the frictional drag is encountered in the tool rake face (between the tool and the workpiece). The friction coefficient in these contact zones play a decisive role in chip formation, cutting forces, stresses, strains and work material flow in both the primary and secondary shear zones *(Das and Dundur, 2006; Filice et al, 2007).* Asperities of different kind and different distributions are present in metal surfaces, the surface roughness. This has an influence in the friction properties because each tool and each workpiece material have a specific and characteristic roughness, especially at the beginning of the cut, until the asperities are flattened (at the beginning of the cut, the tool is only in contact with the asperities of the workpiece material).

With the flattening of the asperities, the workpiece contact with the cutting tool gets larger leading to a varying friction coefficient *(Mahrenholtz et al, 2005).* The amount of crystalline precipitates on the outer surface of the workpiece can define the surface roughness. It can then be said that the interfacial friction force should be considered the force that resists the motion of the layers between the tool and the workpiece *(Li and Lovell, 2005).* Friction modelling is a challenging task that researchers have faced when metal cutting operations are involved. Friction modelling play a decisive role in residual stress prediction and residual stress is detrimental to determine fatigue life of a critical product *(Liu and Guo, 2005; Yang and Liu, 2002).* Friction occur mainly in two zones, the primary shear zone (where the major

shearing work takes place) and the secondary shear zone (adjacent to the tool-chip interface due to high stress contact conditions). Accurate predictions for variables such as forces, temperatures or stresses are of extreme importance to identify optimum cutting parameters, tool material and tool geometry in order to improve the quality of the final product. Therefore, a precise friction coefficient is crucial *(Filice et al, 2007; Ozel, 2006; Fang, 2005; Sartkulvanich et al, 2005; Raman et al, 2002, Marusich and Ortiz, 1995). Geiger et al (2001)* proved that the use of traditional friction coefficients can lead to erroneous results. A disagreement between the experimental and simulated results is usually present so it is very important to understand the influence of the input parameters upon the obtained results when dealing with FEM analysis (hence the sensitivity analysis of the friction coefficient in the FEM cutting simulations presented in this study). FEM simulation results show that the friction coefficient has a strong effect in cutting and feed forces, cutting temperature, stresses, strain, chip formations and tool wear predictions. An increase in the friction coefficient causes a larger tool-chip contact area and more work is required to form a chip (higher cutting forces are obtained). The cutting temperature also increases because more heat is generated *(Sartkulvanich et al, 2005).* Coulomb friction model is commonly used in most finite element analysis. This model contemplates a constant and average friction coefficient along the time and consists of the sticking region where the friction is constant and the sliding region where the friction varies linearly *(Fratini at al, 2006).* The amount of power consumed is a reflection of the friction and this have an impact in the tool wear. Therefore, an accurate predictive model of the friction boundary is critical for tool design and tool coatings. As the friction coefficient increases, sticking begins to occur at the tool tip and the slipline fields are modified to take care of the sticking and slipping friction in the interface *(Maity and Das, 2001).*

Zorev et al (1964) proposed that shear and normal stresses can be assumed in the tool rake face. According to *Zorev et al (1964),* a sticking region appears in the tool-chip contact area (near the cutting edge) and the frictional shearing at the sticking region can be assumed equal to an average shear flow stress at the tool-chip interface. A sliding region forms over the remainder of the tool-chip contact area and the frictional shearing stress can be determined by using a friction coefficient μ. When the normal stress distribution over the rake face is fully defined and μ is known, the frictional stress can be determined. Accordingly, the shear

stress distribution of the tool rake face can be represented in two distinct regions: the sticking and the sliding regions *(Ozel and Zeren, 2007).*

In machining processes, values of the mean friction coefficient can reach a level of 2, such as in aluminium machining with HSS tools having large positive rake angles. However, PCD drastically reduce the friction coefficient and nowadays 0.1 to 0.5 are typical values. When machining steels, the friction coefficient can vary from 0.6 to 1, depending on the machining conditions and cutting tools. The influence of the cutting speed and feed rate is felt in the friction coefficient. One can observe a substantial decrease in the friction coefficient with the increase of both the cutting speed and the feed rate. This fact can be explained by the thermal softening phenomenon with the increase in cutting speed and the rise of the normal load when varying the feed rate. Materials with low thermal conductivity generate higher contact temperatures and tend to produce higher friction coefficients *(Grzesik, 2008).*

The microscopic and macroscopic response of the material under high strain rate loadings is seriously affected by the plastic strain, plastic strain rate, temperature and microstructure of the workpiece material. Therefore, the knowledge of material constitutive behavior (material flow stress) under severe loading conditions is a requisite. The correct selection of the appropriate constitutive equation is often regarded as a critical step to predict variable with FEM software. In figure 2.5, Johnson-Cook constitutive law is presented for a fixed temperature but different constants. Therefore, for the same material, different constants can be found *(Umbrello et al, 2007).*

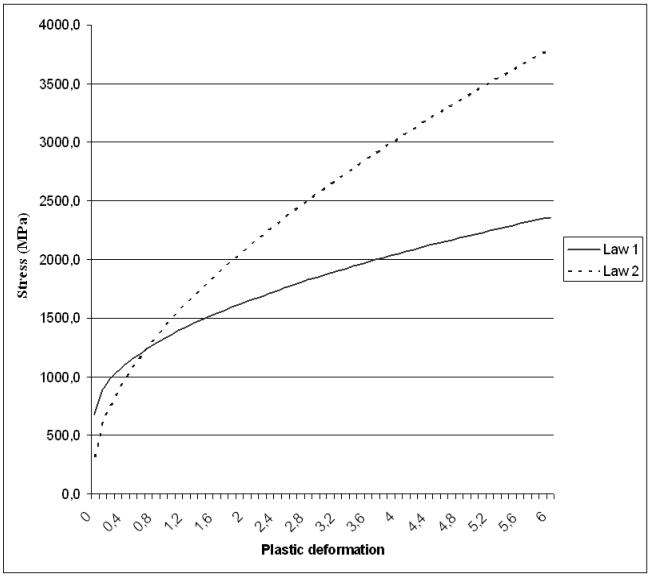

Figure 2.5: Example of AISI 316 flow stress (Johnson-Cook Law) curves for a fixed temperature

Like *Ozel (2006)* stated, the uncertainty of the flow stress can be avoided by using Lagrangian numerical models. In the present research, an updated formulation is used to simulate a continuous chip formation process in the orthogonal cut of both the aluminium alloy and the stainless steel. In figure 2.6, an example of a continuous chip formation can be seen in a 3D numerical simulation.

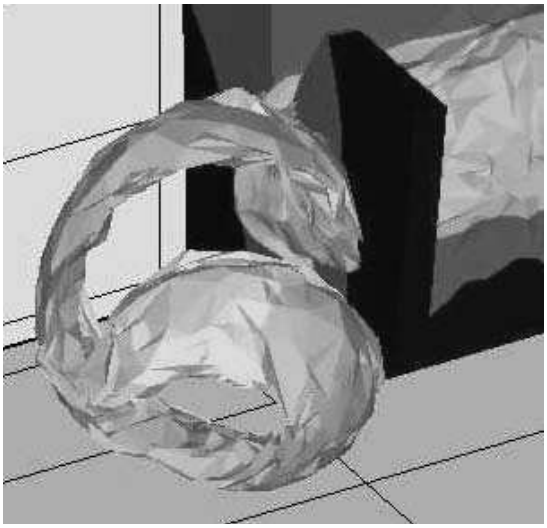

Figure 2.6: Continuous chip formation in 3D, typical of Lagrangian models (Advantedge^{TM})

In simulations, a rigid tool is advancing incrementally into the deformable workpiece which is remeshed whenever needed. There is no separation criterion defined since chip formation is assumed to be due to plastic flow, therefore, the chip is formed by continuously remeshing the workpiece. It remeshes the workpiece periodically to refine large elements, remesh distorted elements, and coarsen small elements. There is no user control for the remeshing process *(Bil et al, 2004).*

2.5 FEM machining software outputs

2.5.1 Cutting forces

Force modelling in metal cutting is important for a multitude of purposes, including thermal analysis, tool life estimation, chatter prediction, and tool condition monitoring. In addition to the effect of workpiece materials, cutting parameters, and process configurations, cutting tool thermal properties can also contribute to the level of cutting forces.

List et al (2005) showed the effect of the friction coefficient in the cutting and feed forces like can be seen in figure 2.7a. As the friction keeps increasing, also the forces show an

increase. In figure 2.7b, the experimental forces are shown along the cutting time. The aluminium alloy in study is Al 2024 with an uncoated cemented carbide cutting tool.

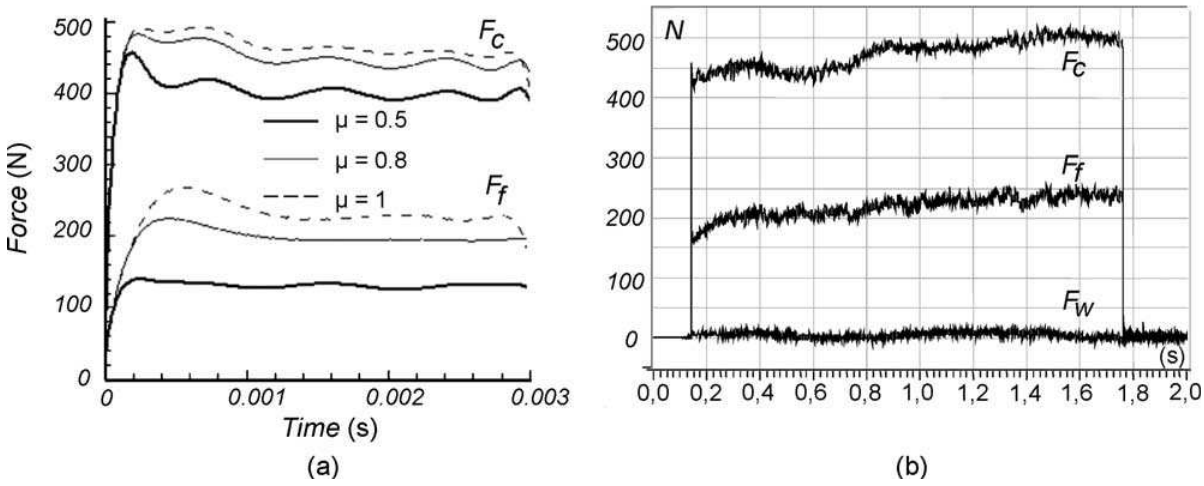

Figure 2.7: Influence of friction coefficient on the force components in the machining (dry) of Al 2024 with an uncoated cemented carbide cutting tool with *V*c = 60 m/min, *f* = 0.1 mm/rev and a_p = 4 mm a) simulated results b) experimental results *(List et al, 2005)*

2.5.2 Cutting temperature

Cutting temperature exercises extreme influence in tool wear. Tool wear is an important aspect when metal cutting processes are involved because process conditions are chosen with the maximization of tool life in mind. High contact temperatures at the tool-chip and tool-workpiece interfaces lead to softening of the tool material, which promotes tool wear.

These interfaces are subject of high pressure and sliding of work material layers, which promotes abrasive and adhesion wear. Finally, cyclic chip formation process can cause cracking due to thermal fatigue. Cutting tool wear occurs due to the independent wear mechanisms like adhesion, abrasion, diffusion, oxidation, etc., occurring simultaneously. Cutting speed, from all machining parameters, is regarded as having the strongest effect in tool wear because higher cutting speeds tend to generate more heat, resulting in more wear. In figure 2.8, a detailed distribution of the cutting temperature can be seen in the tool, chip and workpiece.

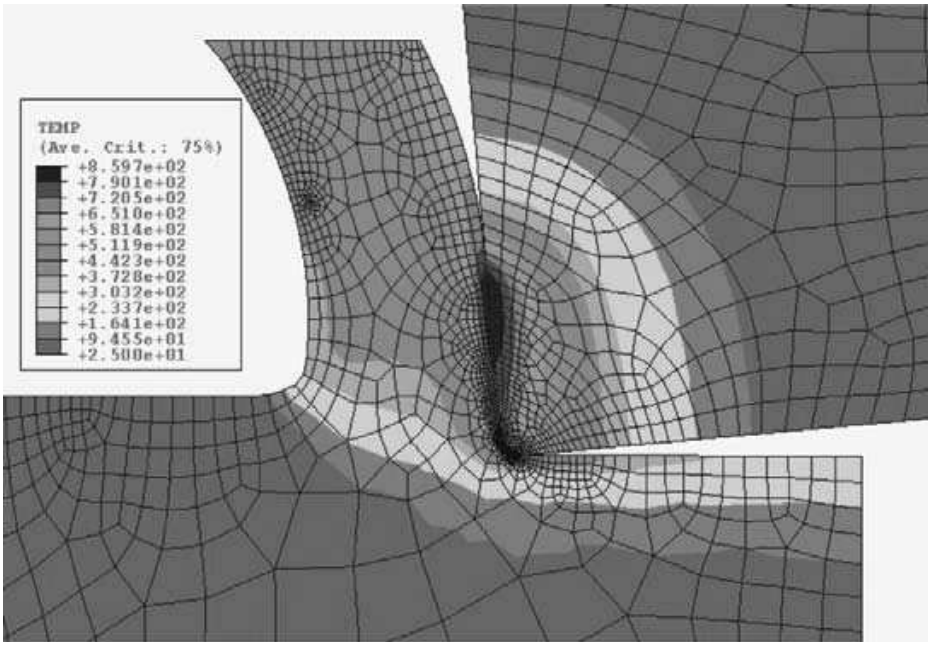

Figure 2.8: Chip formation and temperature distribution for machining of AISI 1045 steel *(Ozel et al, 2007)*

Also of note is that at the optimal cutting temperature, the increase of the cutting feed leads to increased dimensional tool life. The influence of the depth of cut on the tool wear rate is negligibly small if the machining is carried out at the optimum cutting regime. The diameter of the workpiece also has a strong influence on the cutting temperature and, consequently, on the tool wear rate and the roughness of the machined surface. This is because the diameter affects the static and dynamic rigidity of the machining system, curvature of the surface being cut, and interaction of the thermal and deformation waves in the layer being removed. In the range of optimum cutting speeds, the smaller the diameter of the hole being machined, the smaller the optimum cutting speed, the greater the chip compression ratio, and, thus, the work of plastic deformation, the greater the tool wear rate *(Astakhov, 2007).* Once again, *Aslan et al (2007)* concluded in their study (in different materials) that the cutting speed is the most significant factor influencing tool wear because it is responsible for 30% of the total variation. The friction coefficient besides having a strong effect in the cutting forces, is also felt in the cutting temperature like *List et al (2005)* have proven when machining Al 2024 with an uncoated cemented carbide cutting tool. In figure 2.9, it can be seen how the cutting temperature varies with the variation of the friction coefficient along the distance. As the friction keeps increasing, the temperature also keeps increasing.

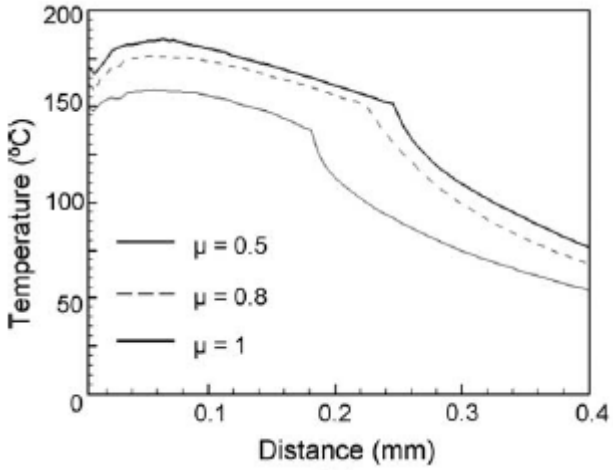

Figure 2.9: Effect of the friction coefficient on the cutting temperature in the tool-chip interface in the machining (dry) of Al 2024 with an uncoated cemented carbide cutting tool with *V*c = 60 m/min, *f* = 0.1 mm/rev and a_p = 4 mm *(List et al, 2005)*

2.5.3 Plastic strain and plastic strain rate

It is also worth noting the role of the plastic strain and plastic strain rate and how both relate with cutting temperature when dealing with metal cutting processes. The complex coupling between deformation and temperature isn't completely understood nowadays because the machining of metals is a non-linear process. The deformation process is concentrated in a small zone and the temperatures that are generated in this zone greatly affect the tool and the workpiece. High cutting temperatures strongly influence tool wear, tool life, workpiece surface integrity, chip formation mechanism and also contribute to thermal deformation of the cutting tool. An increase in temperature in the primary deformation zone softens the material, allowing for lower cutting forces and less energy in the shear process *(Abukhshim et al, 2006).* It is well known that during the cutting of a metal, a great amount of deformation energy is transformed into heat near the tool cutting edge. A small percentage of heat is transferred through conduction to the uncut material ahead of the cutting tool, having an effect in the integrity of the machined workpiece. However, the bigger percentage of heat remains in the removed chip and this produces a local increase of temperature in a narrow zone where high strain occurs and adiabatic shear bands are formed *(Velasquez et al, 2007).* The nature of plastic strain of materials and related phenomenon still remain considerably unclear nowadays. It has been realized that the strain rate and temperature affect material properties, although the strain rate have a greater effect on the flow stress in hot working range and a smaller effect in the cold working range, especially when large strains are present

(Lee and Yeh, 1997; Gnevko et al, 2002). In the figure 2.10, a detailed strain rate distribution is showed along the chip formation.

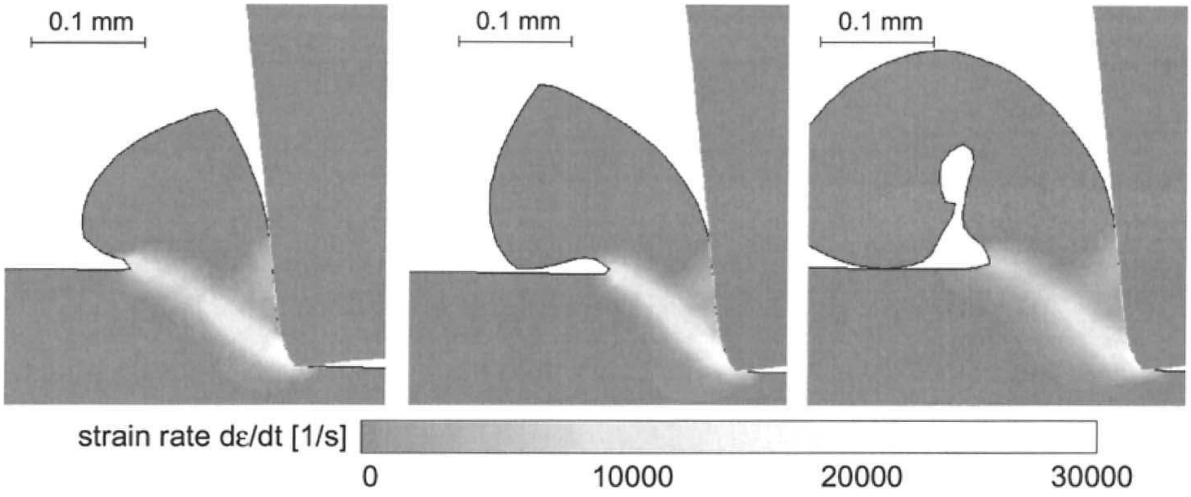

Figure 2.10: Strain rate distribution in discontinuous chip formation at 3000 m/min. ***(Ozel et al, 2000)***

Plastic deformation of steel is temperature sensitive and the rate at which the deformation takes place also have an effect in the plastic strain. This sensitivity is directly related with time and temperature dependency of the mechanisms that govern the deformation and the evolution of the deformation in the material. The main mechanism by which plastic strain takes place is thermally activated motion of dislocations past obstacles that exist within the lattice over a wide range of strain rates and cutting temperatures. The nature and density of the obstacles significantly affect the material response, which may change as the deformation takes place. When dealing with metals, experimental results show that the stress required for plastic strain often reduces with the increase of temperature and with the decrease of plastic strain rate. It can be concluded that cutting temperature and plastic strain rate strongly influence the material response. In general, the stress decreases with the increasing of temperature and decreasing of the plastic strain rate *(Gilat and Wu, 1997).* Actually, temperature and strain rate effects are coupled, since one influences the other. Temperature affects the rate of deformation, which is controlled mainly by a thermally activated mechanism. On the other hand, plastic strain at high rate generates significant heating and cause an increase in temperature which leads to mechanical instability and the localization of deformation into narrow sheets of material (called adiabatic shear bands), which act as a

precursor to eventual material failure *(Lee and Yeh, 1997).* An example of this phenomenon can be seen in figure 2.11.

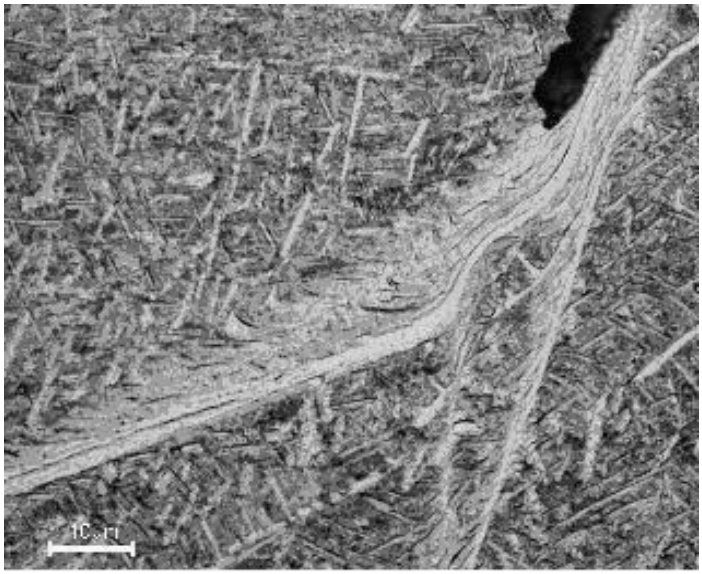

Figure 2.11: Example of adiabatic shear banding in Ti-6Al-4V alloy

Deformation at low strain rates or under quasi-static loading, is relatively homogeneous because is governed by slip and twinning mechanisms. On the contrary, deformation at high strain rates is a much complex phenomenon that is characterized by extreme strain localization along the adiabatic shear bands. Each material has a different susceptibility to adiabatic shear because it depends on properties like heat capacity, heat conductivity, strength level, microstructure, geometry, defects and strain rates. It is also known that adiabatic shear banding precedes material failures at high strain rates. Adiabatic shear banding is usually accompanied by a loss in stress capacity owing to intense thermal softening in the shear bands and, in many cases, shear bands serve as sites for crack initiation and growth during subsequent dynamic fracture *(Odeshi et al, 2005).* Localized adiabatic shearing can be considered a unique consequence of severe plastic deformation at high strain rates. As both thermal and strain softening lead to rapid deformation localization, a shear band forms via a nearly adiabatic process. Also of note is that grain refinement can occur within shear bands and severe plastic strain (which can reach 5 to 20) can also appear within these shear bands *(Xue et al, 2005).* In figure 2.12, it can be seen where the primary and secondary deformation zones are present when metal cutting.

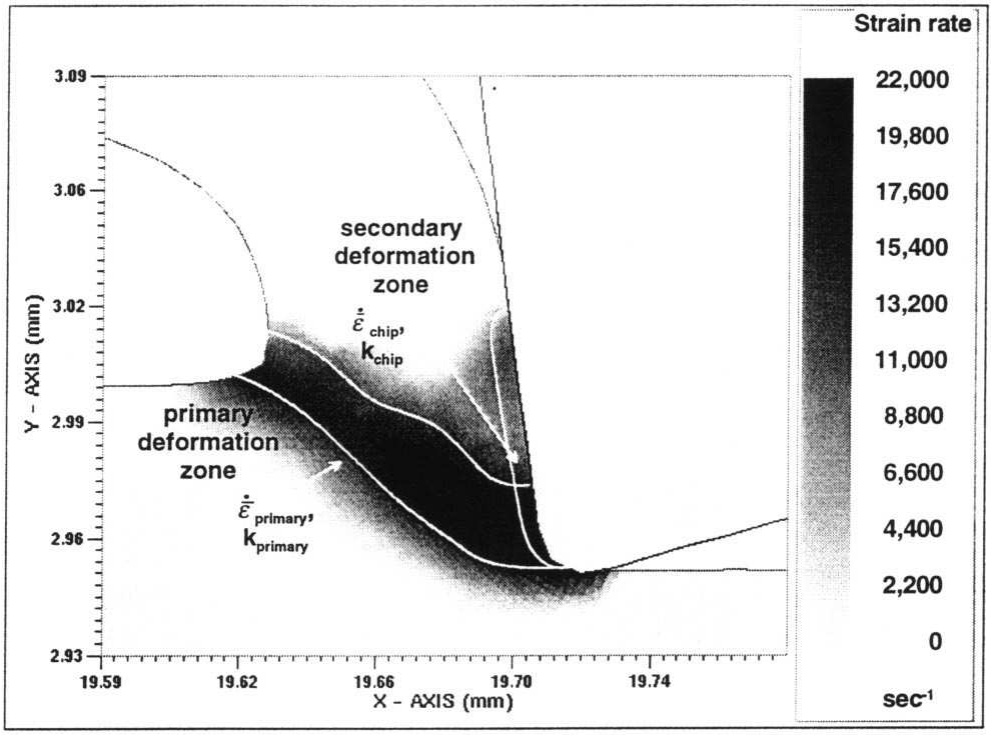

Figure 2.12: Predicted strain-rate distribution and identified primary and secondary regions in orthogonal cutting of P20 mold steel *(Ozel et al, 2000)*

Plastic strain rate can be divided in three zones: the low strain rate region (<1 s^{-1}), the medium rate region (comprehended between the low and high strain rate region values) and the high strain rate region (above 10^3 or 10^4 s^{-1}). The influence of these zones on the flow stress is, respectively, weak, sensitive and great *(Lee and Yeh, 1997).*

Duan et al (2006) showed that the plastic strain rate increases with the increase of the cutting speed. These authors also concluded that the hardness of the workpiece is able to influence the chip formation and the deformation mechanism.

2.5.4 Shear stress

Stress is a measure of the average amount of force exerted per unit area. It is a measure of the intensity of the total internal forces acting within a body across imaginary internal surfaces, as a reaction to external applied forces and body forces. Shear stress is a stress state where the stress is parallel or tangential to a face of the material, as opposed to normal stress when the stress is perpendicular to the face. The area is always the area resisting the shear, and not the area that the force is acting on. Structural members that are often considered to be in pure shear stress are riveted and bolted joints.

2.5.5 Residual stress

Surface quality and integrity can be divided in three main fields: surface roughness, microstructure transformations and residual stress. The occurrence of surface roughness is affected by cutting tool geometry, depth of cut, cutting speed, feed rate, workpiece microstructure and the rigidity of the lathe. When the working parameters are not selected properly, the cutting tool wears quickly or gets broken abruptly. The parameters affecting the surface roughness are, in order of importance: feed rate, insert radius and depth of cut. A good combination among these parameters should be addressed to provide better surface quality *(Gokkaya and Nalbant, 2007; Sahin and Motorcu, 2005).* An evident way to judge the surface quality is surface roughness. However, residual stress is not as evident as surface roughness but plays a decisive role in component performance. An investigation will be conducted to find out if the surface roughness has any relation with the residual stresses profile in the machining of AISI 316.

Fatigue life is an important dynamic property and it is strongly affected by the surface condition produced during machining. The fatigue crack, in general, nucleates at the surface of the part, and then propagates into the bulk. As the crack extends, the resistant section is reduced and when the residual section can no longer withstand the applied load, component fatigue occurs. Consequently, it is the state of stress at the surface, where the crack nucleates, that is of paramount importance. This state is the sum of the stress due to the applied load and of the residual stresses (or self stresses) generated during machining. Residual stress is the result of various mechanical and thermal events, which occur in the surface region during machining *(El-Axir, 2002).*

It is commonly found that the absolute value of the residual stress close to the surface of the workpiece is high and decreases as the depth increases. Residual stress can be tensile or compressive and the stressed layer can have multiple depths, depending upon the cutting conditions, working material, cutting tool geometry and contact conditions at the tool/chip and tool/workpiece interfaces. Compressive residual stresses generally improve component performance and life because they promote a service (working) tensile stresses and prevent crack nucleation. On the other hand, tensile residual stresses tend to increase service (working) stresses which lead to premature failure of components. These residual stresses may affect dramatically the performance of the machined part causing its premature failure, excessive wear, corrosion, part distortion (which leads to assembly problems), etc *(Outeiro et*

al, 2006a; El-Axir, 2002; Outeiro et al, 2006b). An example of a premature component failure is presented in figure 2.13.

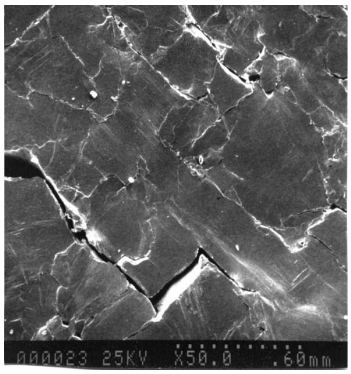

Figure 2.13: Fatigue cracks prefer to form along specific weak crystallographic planes or along the interfaces between crystals in the metal

To optimize processing factors and tool geometry and to predict the final surface residual stress, cutting temperature and thermal deformation all can improve the accuracy and integrity of the machined surface. With advancements and development of advanced science and technology and the increase in requirements regarding machining accuracy, the optimization for cutting parameters and prediction for machined surface quality are essential *(Ikawa et al, 1991; Mackerle, 2003).*

Residual stresses increase with most of the cutting parameters, including cutting speed, uncut chip thickness and tool cutting edge radius *(Outeiro et al, 2006b).* Compressive residual stresses are usually desirable on the machined surface and the subsurface, because these stresses generally increase the fatigue life *(Outeiro et al, 2006a).* An example of a desirable residual stress profile is given in figure 2.14.

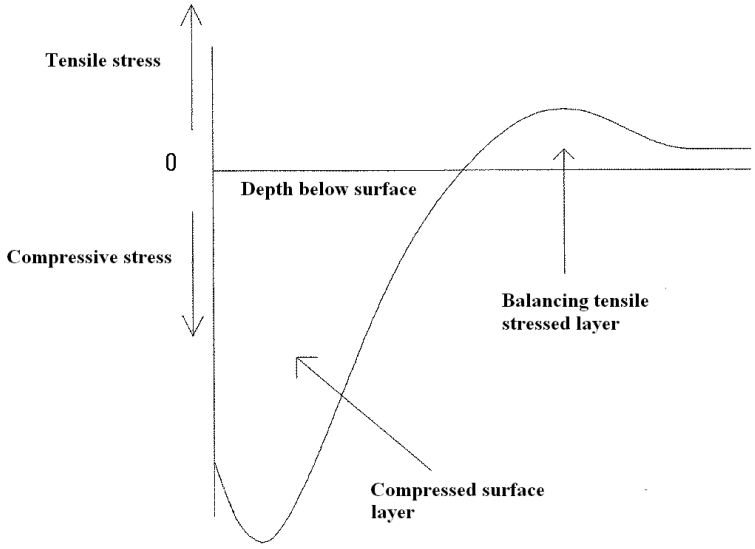

Figure 2.14: Example of a residual stress distribution along the depth below surface

The cutting edge geometry has a direct impact on the stress levels generated in finish hard turning because the increased edge hone radius on the insert generates higher cutting forces. A higher passive force tangential to the surface generates higher compressive residual stresses. When using a large hone radius together with low feeds and depths, solely the radius cuts the material. In tests performed by *Capello (2005)*, the influence of feed rate and nose radius was reported to have an impact on residual stresses at the surface. Increased feed generates significantly higher compressive stresses *(Dahlman et al, 2004).* Like can be seen in figure 2.15, the more the feed rate, the more residual stresses. However, the affected depth by the tensile stress remains practically the same among all feeds. The study was made in AISI 52100 using solid CBN inserts (CBN 100).

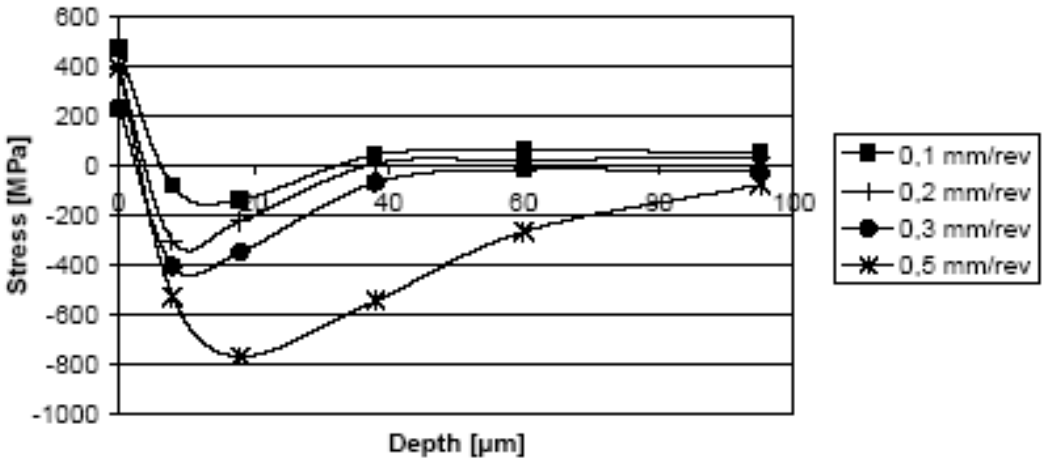

Figure 2.15: Residual stress profile in the machining of AISI 52100 with CBN 100 cutting tool with Vc= 110 m/min and with a_p= 0.1 mm in function of the feed rate *(Dahlman et al, 2004)*

Gunnberg et al (2006) also concluded that cutting speed increases the tensile residual stress on the surface and that the heat generated from higher cutting speeds does not penetrate more deeply into the workpiece. As *Dahlman et al (2004)* had already stated, *Gunnberg et al (2006)* also concluded that increased feed generates higher compressive stresses and a more negative rake angle produces more compressive stress. However, feed and nose radius have the greatest effect on the geometric surface values like already expected. In figure 2.16, an overview on how residual stresses evolve with cutting speed and geometric aspects is presented in the machining of AISI 316L with a coated cemented carbide cutting tool.

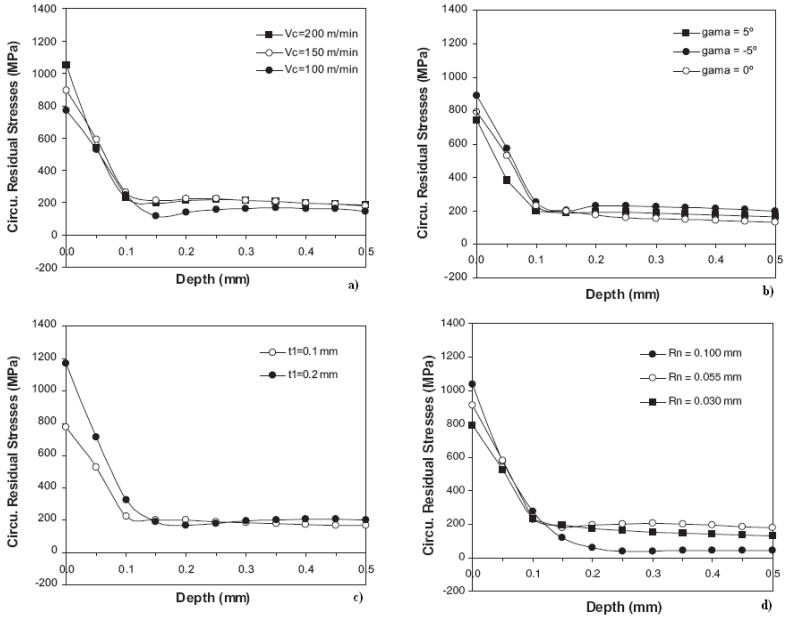

Figure 2.16: Circumferential residual stress for different cutting speeds b) circumferential residual stress for different rake angles c) circumferential residual stress for different uncut chip thickness d) circumferential residual stress for different cutting edge radii *(Outeiro et al, 2006b)*

Capello (2005) also performed an interesting analysis on how the residual stresses evolve. This researcher concluded that a material with higher mechanical properties will present larger (more tensile) residual stresses. This researcher verified once again that the influence of the process parameters on residual stresses is as follows; feed rate, tool nose radius and, to a minor extent, entrance angle influence residual stresses. The depth of cut, on the contrary, does not seem to influence residual stresses. *Dahlman et al (2004)* also showed that the depth of cut doesn't have a big impact in residual stress formation like can be seen in figure 2.17. In this investigation, the residual stress profiles are almost the same for the various depths of cut in the machining of AISI 52100 using solid CBN inserts (CBN 100).

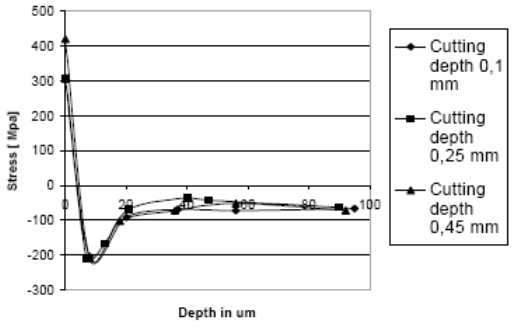

Figure 2.17: Residual stress profile in the machining of AISI 52100 with CBN 100 cutting tools with Vc= 110 m/min and f= 0.1 mm/rev in function of depth of cut *(Dahlman et al, 2004)*

Also the cutting velocity and the primary rake angle play a minor role. Consequently, it can be stated that the key parameters that control residual stresses in turning are the feed rate and the nose radius. Several researchers showed that these results are consistent with three investigated steels, suggesting that the residual stress mechanism is influenced by process parameters in a common way *(Dahlman et al, 2004; Capello, 2005).*

Besides several researchers stated that the rake angle has a minor influence in residual stress, it is acknowledged that a greater negative rake angle gives higher compressive stresses as well as a deeper affected zone below the surface. In case of an increase of rake angles, the maximum stress position is located into the material *(Capello, 2005; Dahlman et al, 2004).*

2.6 Synthesis

The aim of the thesis is to make an experimental validation of the cutting process. Despite numerical simulation being common among researchers to predict cutting forces, cutting power, cutting temperature, plastic strain, plastic strain rate, maximum shear stresses and residual stresses, there aren't publications that validate the experimental process in all these areas. Therefore, all the referred variables will be validated with the exception of the plastic strain rate, maximum shear stresses and residual stresses and here lies the originality of this work. Validating the experiment is an essential section that hopefully will show that numerical simulation can be used to predict several machining variables with precision.

Following the presented extensive state of the art revision, the most relevant ideas for this study will be stressed in the following section.

FEM accuracy and modelling

- The accuracy of the obtained results with numerical simulation depends largely upon the accuracy of the input data being the flow stress and friction coefficient the most important (although the friction coefficient is the most influential)
- FEM is widely applied to predict the thermo mechanical behaviour of machining processes

Mesh and remeshing

- Workpiece is remeshed periodically to refine large elements, remesh distorted elements, and coarsen small elements

- Chip formation is assumed to be due to plastic flow, therefore, the chip is formed by continuously remeshing the workpiece

Friction coefficient

- The use of traditional friction coefficients can lead to a disagreement between the experimental and simulated results
- Coulomb friction model is commonly used in most finite element analysis
- The rise of the normal load when varying the feed rate decreases the friction value

Flow stress

- The correct selection of the appropriate constitutive equation is often regarded as a critical step to predict variables with FEM software
- Material response under high strain rate loadings is seriously affected by the plastic strain, plastic strain rate, temperature and microstructure

Cutting temperature

- The cutting temperature and plastic strain rate strongly influence the material response
- High contact temperatures at the tool-chip and tool-workpiece interfaces lead to softening of the tool material, which promotes tool wear
- Cutting speed, from all machining parameters, is regarded as having the strongest effect in tool wear (higher cutting speeds tend to generate more heat, resulting in more wear)
- In general, the stress decreases with the increasing of temperature and decreasing of the plastic strain rate
- At the optimal cutting temperature, the increase of the cutting feed leads to increased dimensional tool life

Plastic strain and plastic strain rate

- The stress required for plastic strain often reduces with the increase of temperature and with the decrease of plastic strain rate

Surface quality and residual stress

- The parameters affecting the surface roughness are, in order of importance: feed rate,

insert radius and depth of cut

- Fatigue life is strongly affected by the surface quality produced during machining
- Compressive residual stresses generally improve component performance and life
- The influence of the process parameters on residual stresses is as follows; feed rate, tool nose radius and, to a minor extent, entrance angle
- Residual stresses are mostly influenced by feed rate and nose radius
- Increased feed generates significantly higher compressive stresses
- Residual stress mechanism is influenced by process parameters in a common way

Chapter 3)

FEM analysis, Experimental procedure and Analytic models

3.1 FEM analysis

The choice of finite element software for machining analysis is an important factor in determining the quality and scope of analysis that can be performed. When dealing with metal cutting, input parameters like friction coefficient and flow stress curves greatly influence the reliability and precision of the obtained results. Finite element software (specific for machining operations) was chosen to simulate the metal cutting process, therefore, Advantedge^{TM} 5.2 (provided by Third Wave Systems) was used to aid this study. In figure 3.1, an example of a mesh in 2D in the tool, chip and workpiece can be seen.

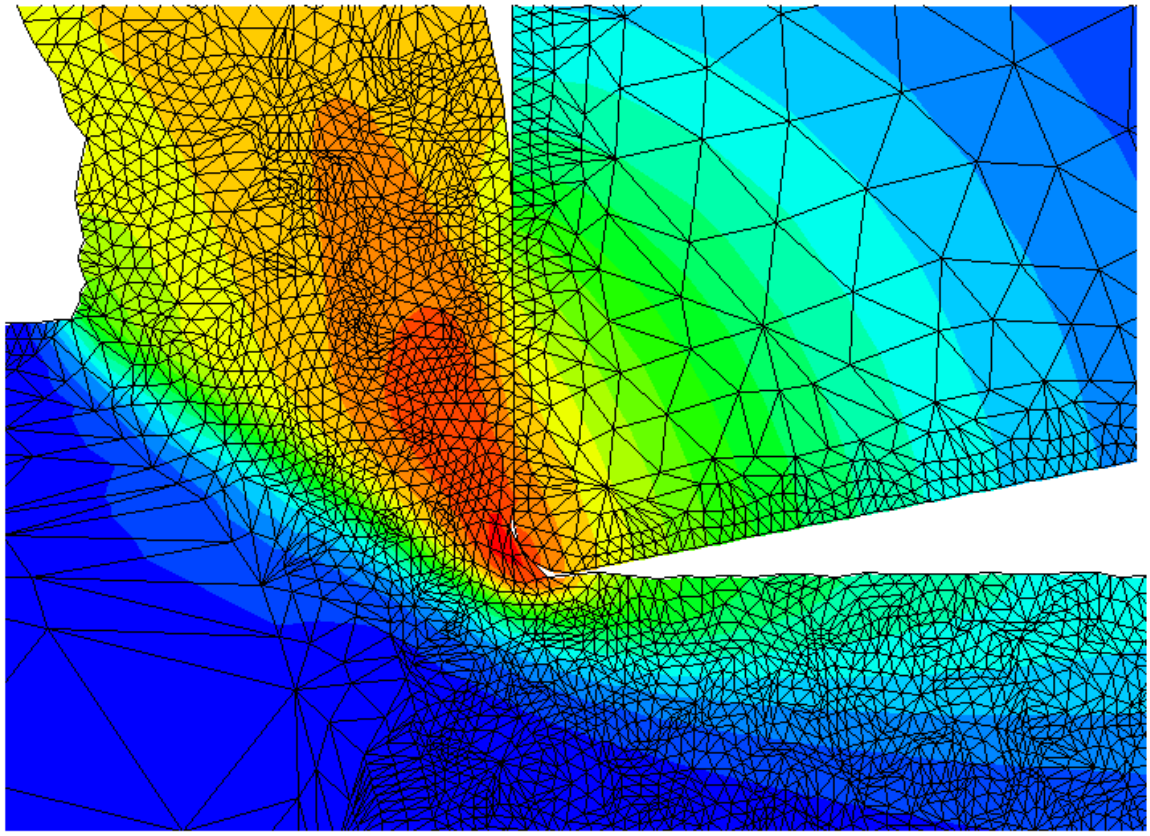

Figure 3.1: Example of a mesh using ThirdWave Advantedge™ commercial package

This commercial software was built with machining operations in mind, and this allows simulating turning, drilling, milling, micro machining, etc in two or three dimensions. It uses adaptive meshing to help to improve the quality and precision of the results and it also supports a wide variety of workpiece materials. The solver is controlled by the software itself and fast setups for several simulations can be done easily because of the clean software interface. AdvantEdge™ does not give the user much flexibility in configuring the controls of the solver. While this may be preferable in some cases, this means that the user is restricted to the preset controls of the software.

Third Wave Advantedge™ allows improvement and optimization of machining processes and with it, is possible to determine optimum machining parameters and tool configurations allowing lower cutting and feed forces and temperature, without spending time and money with experimental processes.

In the end, Advantedge™ allows for very fast setups with tool geometry libraries provided. It also has an extensive material model library with support for a wide range of materials, aerospace alloys included. It uses adaptive meshing but the controls cannot be

modified. In the overall control of the simulations, very minimal changes are allowed. In figure 3.2, some of the input parameters necessary for a two dimensional turning operation can be seen.

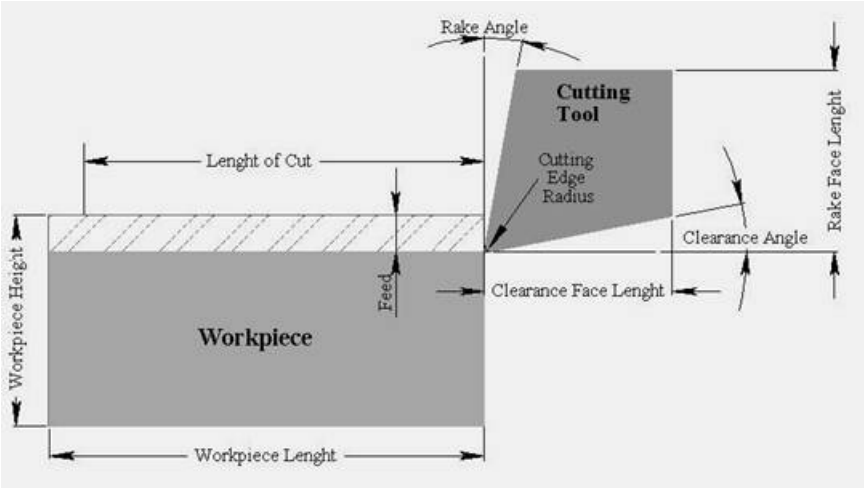

Figure 3.2: Software input parameters (Advantedge^{TM})

3.1.1 Rules to remember when simulating machining operations

Despite the software provide an easy to use interface, there are some rules to take into account in order to obtain reliable simulations. Some of these rules were found throughout the realization of the thesis, others were found in the literature. It is important to stress that the workpiece height should be more than 5 times bigger than the feed. This ratio is of extreme importance to obtain simulations with good precision. This way, the feed effect is negligible due to workpiece distortion being inexistent. Workpiece distortion can also be present if the workpiece height is bigger than the length so the length should be equal or bigger than the height. RTS (relative tool sharpness) is also an important aspect when machining with the FEM model. This relates the feed with the tool edge radius. If the relation is lower than the minimum value, the edge radius has an influence in the chip formation and the cut can't be considered orthogonal. RTS is defined by:

$$RTS = \frac{t_r}{r_n} \tag{3.1}$$

where t_r is the uncut chip thickness (mainly affected by the feed) and r_n is the tool edge radius *(Outeiro, 2007; Ozel et al, 2007).* 3 is considered to be the minimum RTS value to have an

orthogonal cut. The chip thickness should also have 3 layers of elements at least. The number of nodes is a subjective matter, although from a past study, it has been found that for 2D simulations within the elastic regime, 12000 nodes are sufficient. However, if 2D simulations are conducted within the elastic-plastic regime (necessary for residual stress predictions), 60000 nodes at least are required. In 3D, 100000 nodes are required in elastic regime and 180000 for elastic plastic regime.

To sum it up, it is important to take into account the following rules:

- Workpiece height more than 5 times bigger than the feed rate
- Workpiece length equal or bigger than the workpiece height
- RTS should be equal or bigger than 3 to have a consistent orthogonal cut
- Chip thickness with 3 or more layers of elements
- 12000 nodes for 2D elastic regime simulations
- 60000 nodes for 2D elastic plastic regime simulations
- 100000 nodes for 3D elastic regime simulations
- 180000 nodes for 3D elastic plastic regime simulations

With all these rules in mind, a careful analysis took place and it can be said that all simulations are reliable.

3.1.2 Material flow stress and Friction coefficient

To model the thermal-visco plastic behavior of the workpiece materials, the software uses a constitutive equation, the Johnson-Cook law, which can be represented by the following formula:

$$\sigma_{eq} = (A + B\varepsilon^{n})(1 + C\ln(\frac{\dot{\varepsilon}}{\dot{\varepsilon}_0}))(1 - (\frac{T - T_{room}}{T_m - T_{room}})^{m}) \quad (3.2)$$

where ε is the plastic strain, $\dot{\varepsilon}$ is the plastic strain rate (s^{-1}), $\dot{\varepsilon}_0$ is the reference plastic strain rate (s^{-1}), T is the temperature of the workpiece material (ºC), Tm is the melting temperature of the workpiece material (ºC), and Troom is the room temperature (ºC). Coefficient A is the

yield strength (MPa), B is the hardening modulus (MPa) and C is the strain rate sensitivity coefficient, n is the hardening coefficient and m the thermal softening coefficient.

The orthogonal model (Merchant, 1945) was followed in the machining of both the aluminium alloy and the stainless steel.

Experimental work was carried out in order to obtain the friction coefficient to use as an input in the FEM simulation and friction coefficient was calculated using the Coulomb model through the following formula:

$$u = \frac{Ff + Fc \times tan\gamma}{Fc - Ff \times tan\gamma} \tag{3.3}$$

where Ff represents the feed force, Fc the cutting force and γ is the tool rake angle. Both cutting forces were obtained experimentally for both materials.

3.2 Experimental procedure

In the following subsections, the experimental procedure will be detailed. It will start with a brief description of chemical and mechanical properties of the used workpiece materials followed by a step by step explanation on how the experimental work was conducted, which machine tools were used and which cutting tools were selected. Finally, an analysis of the analytic models will be given.

3.2.1 Materials

Both work bars (of aluminium and stainless steel) were tested in a Karl Frank GMBH Type 38180 durometer. Both hardness's were determined and they ranged from 161 to 207 HB for the aluminium alloy (being the harder zone found in the outside of the bar) and 180 to 187 HB for the stainless steel (being the harder zone found in the outside of the bar). When looking at the workpiece hardness's in the software, it is realized that the aluminium alloy has 150 HB and the stainless steel 250 HB.

The properties of the aluminium alloy in the study can be found in table 3.1.

Table 3.1: Chemical composition and mechanical properties of the aluminium alloy Al 7075

Chemical composition (%)	
Zn	5.6
Mg	2.5
Cu	1.6
Fe	0.5
Si	0.4
Mn	0.3
Cr	0.23
Ti	0.2
Mechanical properties	
Tensile Strength, Yield	260 MPa
Tensile Strength, Ultimate	360 MPa
Elongation at Break	Max 10 %
Modulus of Elasticity	70 GPa
Density	2.77 g/cm^3

Equally, the properties of the stainless steel can be found in table 3.2.

Table 3.2: Chemical composition and mechanical properties of AISI 316 stainless steel

Chemical composition (%)	
Cr	17.0
Ni	12.0
Mo	2.5
Mn	2.0
Si	1.0
C	0.08
S	0.03
P	0.0045
Mechanical properties	
Tensile Strenth, Yield	290 MPa
Tensile Strength, Ultimate	560 MPa
Elongation at Break	50%
Modulus of Elasticity	193 GPa
Density	8.0 g/cm^3

3.2.2 Machine tool and experimental setup

The turning tests were performed with a high rigidly lathe Kingsbury 50 CNC with 18kW spindle power and a maximum spindle speed of 4500 rpm like can be seen in figure 3.3.

Figure 3.3: CNC turning centre

The acquisition of the cutting, feed and depth forces (the latter being negligible due to the cut being orthogonal) was made with a piezoelectric Kistler® (model 9121) dynamometer like presented in figure 3.4.

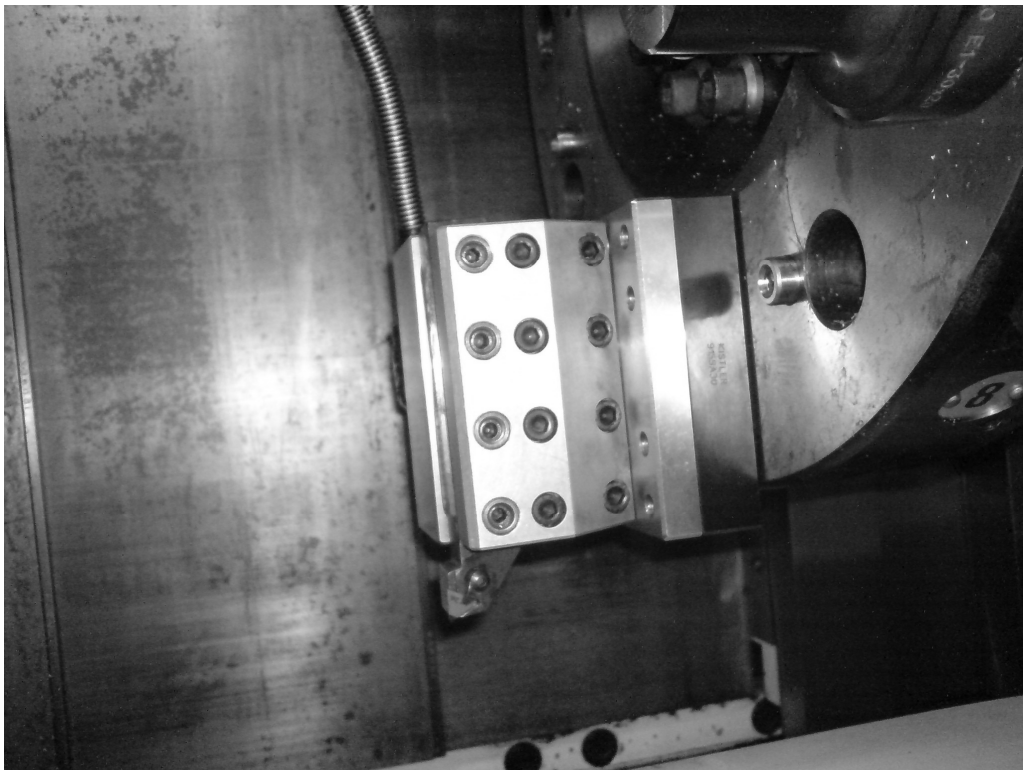

Figure 3.4: Assembly of the dynamometer in the turning turret

The cutting and feed forces were continuously monitored and acquired through out the test by using a charge amplifier (presented figure 3.5) with three independent channels (model 5019).

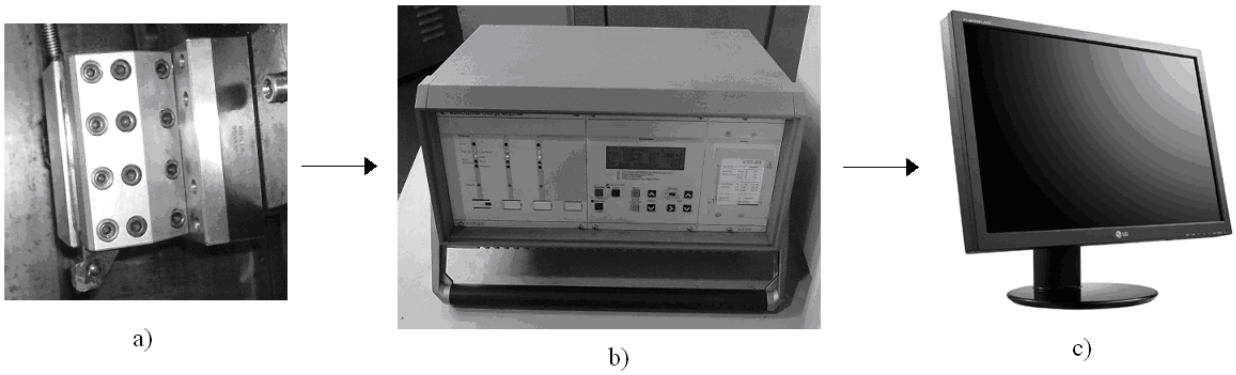

Figure 3.5: Cutting and feed forces data acquisition system a) piezoelectric dynamometer b) charge amplifier c) computer

The chip thickness and the contact between the tool and the chip were also measured. Figure 3.6 shows where the contact length between chip and tool should be measured.

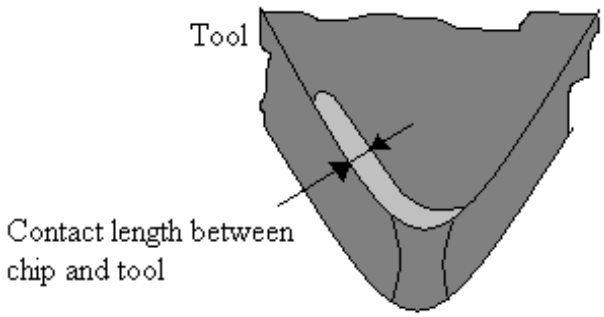

Figure 3.6: Contact length between chip and tool

The measurement of the surface roughness parameters Ra, RzD and Rt (only in AISI 316), were made with a Hommelwerke® T1000 profilometer (showed in figure 3.7), with a cut off (Lc) of 0.8 mm, according to ISO/DIS 4287/1E.

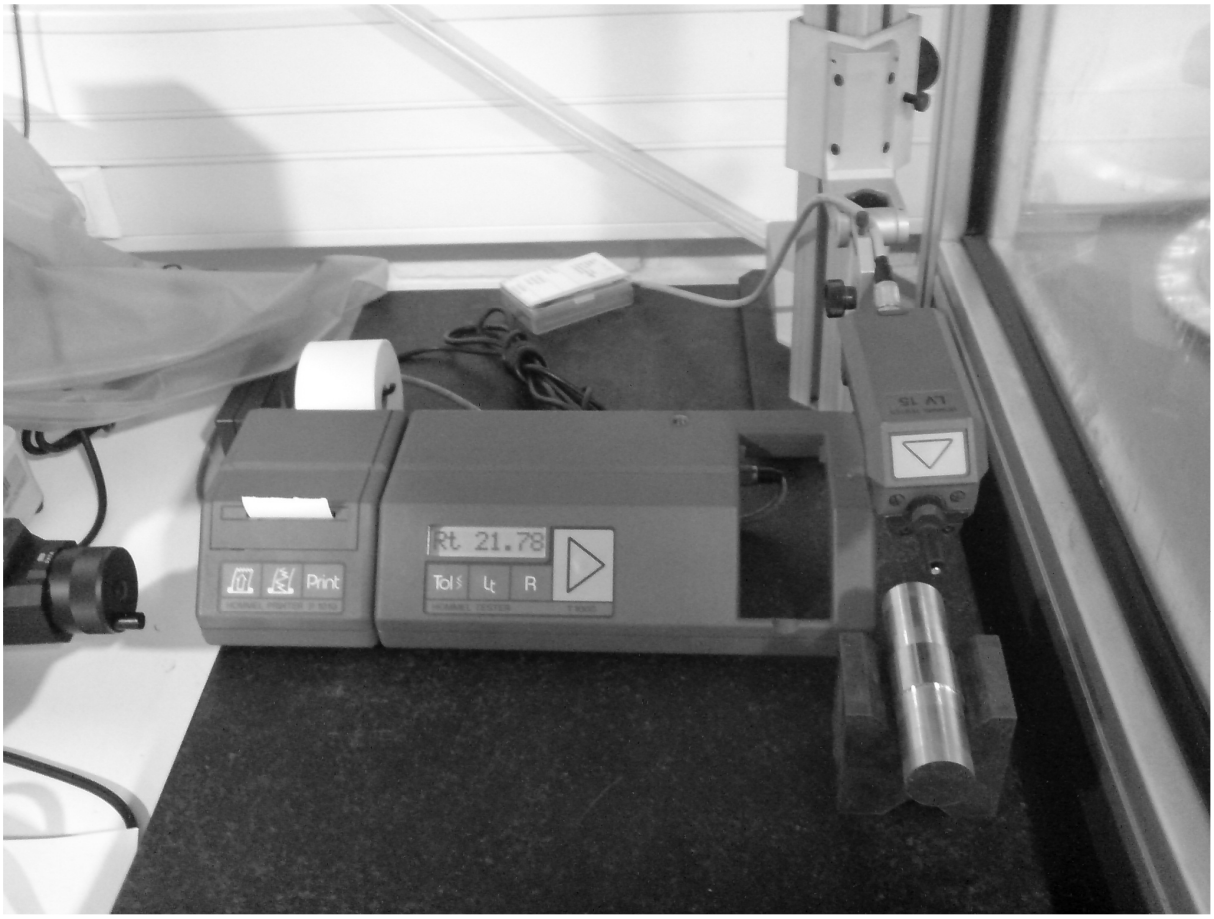

Figure 3.7: Profilometer acquiring the surface roughness in the AISI 316 stainless steel

3.2.3 Cutting tools

In the machining of the aluminium alloy, a PCD cutting tool (Sandvik TPUN 110304FP) was tested. It has 0º of rake angle and 7º of relief angle with 0.4 mm of nose radius. 91º edge major tool cutting angle and 0º cutting edge inclination angle were given by CTGPL 2020K11 (ISO) tool holder.

In the machining of the stainless steel, a triple layered custom cemented carbide (Sandvik DCMT 11T304-UM) cutting tool with a chip breaker was used. This tool has a 0.4 mm nose radius. The total thickness of the coating is 5.5 µm and consists of TiCN-Al_2O_3-TiN under a substrate with excellent resistance to thermal and mechanical shock. 90º edge major tool cutting angle with 0º cutting edge inclination angle given by SDJCL 2020K11 (ISO) tool holder were applied.

3.2.4 Cutting parameters and workpieces

The cutting parameters were the following in the machining of the aluminium alloy: cutting speed (V_c) of 500 m/min, feed rate (f) of 0.05 - 0.10 and 0.2 mm/rev and constant depth of cut (a_p) of 2 mm. Work bars of Al 7075 with 100 mm of diameter and 200 mm of length were tested. Because of avoiding vibrations, a tailstock was used when machining the aluminium. In figure 3.8, the aluminium workpiece is being held in place by the chuck and the tailstock.

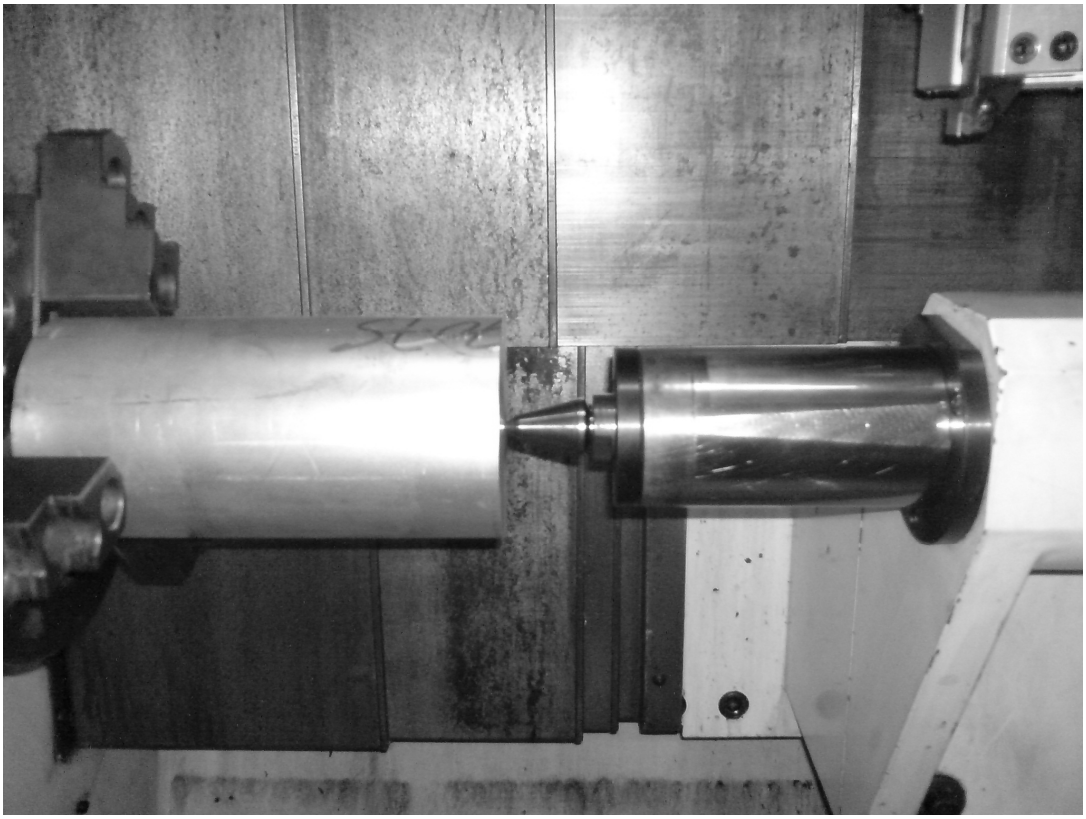

Figure 3.8: Aluminium bar being held in place by the chuck and the tailstock

A rule was followed to avoid vibrations. Because of using the tailstock when machining the aluminium alloy, it is as follows:

$$L \leq 15D \tag{3.4}$$

being L the length of the workpiece and D its diameter. An overall view of the experimental setup can be seen in figure 3.9, where the workpiece, chuck, tailstock and dynamometer are shown.

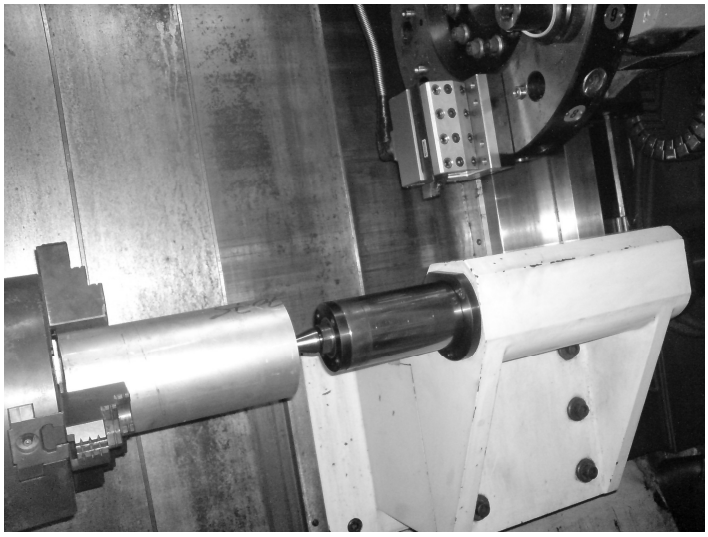

Figure 3.9: Overall view of the orthogonal cut applied in the aluminium alloy

The orthogonal cut was conducted under Merchant theory like in figure 3.10.

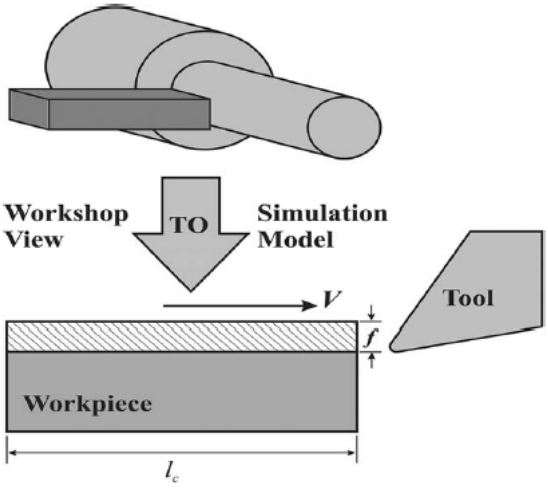

Figure 3.10: Schematic on how the experimental work was conducted and comparison with the finite element approach *(Bil et al, 2004)*

The same approach was considered for the machining of AISI 316 with the following cutting parameters: cutting speed (V_c) of 100 m/min, feed rate (f) of 0.05 - 0.10 and 0.2 mm/rev and constant depth of cut (a_p) of 1 mm. 20 mm diameter with 50 mm of length work bars were tested. Due to its reduced dimensions in comparison with the aluminium bars, the tailstock wasn't necessary.

The rule of avoiding vibration to apply in the machining of the stainless steel is slightly different because the tailstock wasn't necessary. Having that said, the following reasoning was applied:

$$L \leq 5D \tag{3.5}$$

being L the length of the workpiece and D its diameter.

3.3 FEM machining input parameters

The simulations were carried out in order to meet what was made experimentally, allowing for an experimental validation. The input parameters of the machining operation for the aluminium alloy are showed in table 3.3 and in table 3.4 for the stainless steel. The tool used to simulate the machining of the stainless steel is imported from the library and some information is not specified.

Table 3.3: Aluminium alloy input parameters

Workpiece	
Workpiece Length	6 mm
Workpiece Height	3 mm
Workpiece Material	Al 7075
Tool	
Rake Angle	0º
Rake Face Length	3 mm
Relief Angle	7 º
Relief Face Length	3 mm
Cutting Edge Radius	0.02 mm
Material	PCD
Process	
Depth of Cut	2 mm
Length of Cut	2 mm
Feed	0.05, 0.1, 0.2 mm/rev
Cutting Speed	500 m/min
Initial Temperature	20 ºC
Friction Coefficient	specific for each case
Coolant	not used
Simulation	
Maximum Number of Nodes	12000
Maximum Element Size	0.1 mm
Minimum Element Size	0.02 mm

Table 3.4: Stainless steel input parameters

Workpiece	
Workpiece Length	6 mm
Workpiece Height	3 mm
Workpiece Material	AISI 316
Tool	
Rake Angle	tool custom
Rake Face Length	tool custom
Relief Angle	tool custom
Relief Face Length	tool custom
Cutting Edge Radius	tool custom
Material	Triple layered cemented carbide
Process	
Depth of Cut	1 mm
Length of Cut	2 mm
Feed	0.05, 0.1, 0.2 mm/rev
Cutting Speed	100 m/min
Initial Temperature	20 ºC
Friction Coefficient	variable for each case
Coolant	not used
Simulation	
Maximum Number of Nodes	60000
Maximum Element Size	0.1 mm
Minimum Element Size	0.02 mm

3.4 Analytic models

This section is destined to explain the method of validating the experiments. The validation of the mean cutting and feed forces is direct. The forces are obtained using the dynamometer and directly compared to the mean forces obtained in the simulation and the same can be said for the cutting power. The cutting power is:

$$P_c = F_c^{med} \times V_c \tag{3.6}$$

where F_c^{med} is the average cutting force and V_c is the cutting speed in meters per second. This provides for a direct comparison with the average numerical cutting power.

A more elaborated method is necessary to find the maximum cutting temperature. During the cut of metal, high temperatures are generated in the shear zone. This fact increases tool wear so particular attention needs to be paid to determine the cutting temperature calculated using *Boothroyd (1989)* analytic model. That being said, the used expressions in this reasoning will be presented. The cutting angle was calculated by:

$$\phi = \arctan\left(\frac{\cos\gamma}{R_c - \sin\gamma}\right) \tag{3.7}$$

where γ is the rake angle and R_c is the cutting ratio. The cutting ratio can be obtained with the following formula:

$$R_c = \frac{t'}{t} \tag{3.8}$$

where t´ is the measured chip thickness within the experimental process and t is the theoretical chip thickness that can be obtained by:

$$t = f \times \sin\chi \tag{3.9}$$

where f is the feed rate and χ is the tool position angle. The chip width can be obtained by:

$$b = \frac{a_p}{\sin\chi} \tag{3.10}$$

where a_p is the depth of cut. The absorbed power P_τ by the chip in the rake face can be calculated by:

$$P_\tau = F_\tau \times V_\tau \tag{3.11}$$

where F_τ is the force and V_τ is the speed (both in the shear plane). The chip temperature in the primary shear zone θ_s can be obtained by:

$$\theta_s = \frac{(1-\Gamma)P\tau}{\rho \times c \times Vc \times t \times b} \tag{3.12}$$

where Γ is the absorbed heat proportion, ρ is the specific weight and c is the specific heat. The temperature in the secondary shear zone can be calculated by:

$$\theta_m = \theta_f \times \sqrt{\frac{R \times t}{l_f}} \tag{3.13}$$

where lf is the contact length between chip and tool and R is the thermal number and can be obtained by the following formula:

$$R = \frac{\rho \times c \times V_c \times t}{k} \tag{3.14}$$

where k is the thermal conductivity coefficient of the machined material. The average temperature that results from the friction between the chip and the rake face θ_f can be calculated through:

$$\theta_f = \frac{P\tau}{\rho \times c \times V_c \times t \times b} \tag{3.15}$$

The maximum cutting temperature θ can be obtained by:

$$\theta = \theta_s + \theta_m + \theta_0 \tag{3.16}$$

where θ_0 is the room temperature.

Regarding plastic strain, *Merchant, 1945* theory was followed. The plastic strain was calculated using the following equation:

$$\varepsilon = \frac{1 + R_c^{\,2} - 2R_c \times \sin\gamma}{R_c \times \cos\gamma} \tag{3.17}$$

Chapter 4)

Results and discussion

In this chapter, the core of the thesis will be presented. Therefore, a previous presentation on how this chapter is divided will be given. This chapter starts with a brief presentation of the studied materials and the main reason why these materials were chosen. A brief description on the cutting tools for both materials is also presented. The following subsection is destined to present the measured experimental values that will be used as an input in the analytical models. All tests are covered, including experimental results for all feeds for both aluminium alloy and stainless steel (cutting power, maximum cutting temperature and plastic strain).

The next section will consist of a single experimental validation (for each material with a fixed feed of 0.1 mm/rev) with the Coulomb friction coefficient to see what degree of

approximation this friction gives. In this section, experimental validation on cutting and feed forces, cutting power, maximum cutting temperature and plastic strain will be addressed for each material.

Finally, the same reasoning of the latter subsection will be taken, although this time for the iterated friction coefficients. All cases of study, on both the aluminium alloy and the stainless steel, will have the respective experimental validation.

Finally, a more detailed analysis will be conducted for each case of study with the presentation of distribution maps.

4.1 Workpiece materials and cutting tools

4.1.1 Al 7075 and PCD cutting tool

First of all, it is important to understand why PCD tools were chosen to machine the aluminium alloy. Machining aluminium with traditional cutting tools shortens the tool life and has an adverse effect on the surface and edge quality, because of the formation of built-up edges and burrs (aluminium parts require deburring and finishing processes after cutting, raising the cost of the workpiece on such processes). Burrs are damaging even during machining because they hit the cutting tool edge and cause groove wear (and groove wear, in turn, accelerates burr formation). Therefore, machining technology that does not form built up edges and produces very good surface is very much in demand, being PCD such material. If a degraded tool isn't identified early enough, a significant drop in the quality of the workpiece quality can occur (*Bouzid, 2005a; Li et al, 2002; Bouzid, 2005b; Kim and Kang, 1997).* The overall surface quality is influenced by tool geometry, chip flow, temperature generation, heat flow and tool wear *(Ceretti et al, 1996).*

PCD cutting tools are considered a noble material with substantial higher performance when compared to traditional cutting tool materials when machining aluminium alloys *(Davim et al, 2007).* Turning process with diamond tools is a technique of precision machining of automobile, aerospace, computer, optic components and moulding and die industry. With advancements and development of advanced science and technology and the increase in requirements regarding machining accuracy, the optimization for cutting parameters and prediction for machined surface quality are essential *(Ikawa et al, 1991).* To optimize processing factors and tool geometry and to predict the final surface residual stress,

cutting temperature and thermal deformation all can improve the accuracy and integrity of the machined surface *(Mackerle, 2003).*

Aluminium alloys have good machinability among metals due to outputting lower cutting forces, cutting temperatures, and tool wear rates. Machinability advantages concerned with aluminium alloys include tool life, chip characteristics, chip disposal, recycling potential and surface finish *(Kelly and Cottrell, 2002; Ezugwu el al, 2003).* Dry machining of aluminium alloys is especially difficult because aluminium exhibits high friction and therefore has a strong tendency of built-up edge (BUE) formation. Cutting tools used for machining aluminium should possess low affinity to aluminium, low friction coefficient, and high hardness which makes PCD tools the suitable choice due to ability to reduce significantly the built-up edge formation and hence improve cutting performance *(Fukui et al, 2004; Shen, 1996).*

For some alloys, the high tendency of aluminium to adhere during cutting presents a significant risk that can lead to tool breakage. Long, ductile chips, that complicate the machining process, are formed regardless of the cutting tool geometry chosen. From a thermal and a deformation point of view, aluminium alloys have many advantages like obtaining complex shapes with a lower demand in terms of power (due to a lower flow strengths), reducing this way the size of the necessary equipment *(Sartkulvanich et al, 2005).*

4.1.2 AISI 316 and coated cemented carbide cutting tool

On the other hand, AISI 316 is not easy to machine, even with specific coated tools. Stainless steels contain chromium with a content of 12-25% Cr which is responsible for corrosion resistance and about 25% Ni to produce an austenitic structure, which leads to extreme high work-hardening rates. Acid resistance can be obtained with the addition of molybdenum. AISI 316 is widely used to produce critical structural components in chemical industries and nuclear power stations because they provide a unique combination of high mechanical properties and corrosion resistance *(Outeiro et al, 2006b).*

Stainless steels are considered difficult to machine due to their high tensile strength, high ductility, high work hardening rate, low thermal conductivity and abrasive behaviour. These properties often lead to high cutting forces and high cutting temperature, fast tool wear rates, high susceptibility to notch wear, difficulties with chip breakability, BUE formation and poor surface finish. Because of these reasons, a coated tool with a chip breaker was used to

perform the cut. Work hardening can occur which leads to unstable chip formation and vibrations (which induces to mechanical modifications and behaviour heterogeneity on the machined surface). Due to their low thermal conductivity, heat conduction is difficult at the tool tip and heat concentrated areas may appear in the working material. These phenomenons affect the integrity of the piece and lead to residual stressed affected layers *(M'Saoubi et al, 1999).* Having that said, it is fundamental to study residual stresses when machining these types of materials.

The energy that is used to plastically deform the workpiece material during a turning operation is transformed into heat. The developed temperatures that appear during the machining operation are mainly related with the contact between the tool and chip, the level of cutting forces and the friction between tool and chip. Practically all the heat that occurs is transferred to the cutting tool and workpiece while a portion of it is dissipated through the chip. The shear zone is subject of the majority of heat therefore, the contact length between the chip and tool influences the cutting forces, cutting conditions of the tool, the tool performance and tool life *(Korkut et al, 2007).*

Therefore, to machine the aluminium alloy (Al 7075), a PCD cutting tool was chosen. Regarding the machining of the stainless steel (AISI 316), a triple coated cemented carbide cutting tool was used.

To sum it up, it is as follows:

- Aluminium alloys are widely used in automotive, mould and die and aeronautic industry
- PCD is perfectly suitable to machine aluminium alloys due to its properties
- Stainless steels are hard to machine because of its mechanical and chemical properties and are mainly used in chemical industries and nuclear power stations
- Coated cemented carbide tools are suitable to machine stainless steel

4.2 Experimental data

In table 4.1 and table 4.2, all experimental measured values will be detailed in function of the feed rate for both materials. For the machining of the aluminium alloy, the cutting speed was fixed at 500 m/min with a constant depth of cut of 2 mm. In the machining of the stainless steel, the cutting speed was fixed at 100 m/min while the depth of cut had a constant value of 1 mm.

4.2.1 Al 7075 with the PCD cutting tool

In table 4.1, experimental measured values are presented, in the machining of the aluminium alloy with the PCD cutting tool in function of the feed rate. Cutting and feed forces and contact length between the chip and tool are an average of two different experimental tests while the chip thickness is an average of six experimental measures.

Table 4.1: Experimental cutting and feed forces, chip thickness and contact length between chip and tool for the machining of the aluminium alloy with the PCD cutting tool with Vc= 500 m/min; f= 0.05 – 0.1 – 0.2 mm/rev; a_p= 2 mm

Feed rate [mm/rev]	Cutting force [N]	Feed force [N]	Chip thickness [mm]	Contact length between chip and tool [mm]
0.05	94.7	46.4	0.08	0.71
0.1	171.3	53.3	0.22	0.74
0.2	317.3	52.8	0.55	1.09

4.2.2 AISI 316 with the coated cemented carbide cutting tool

Experimental measured values are presented in table 4.2 for the machining of the stainless steel with the coated cemented carbide cutting tool in function of the feed rate. Cutting and feed forces and contact length between the chip and tool are an average of two different experimental tests while the chip thickness is an average of six experimental measures.

Table 4.2: Experimental cutting and feed forces, chip thickness and contact length between chip and tool for the machining of the stainless steel with the coated cemented carbide cutting tool with Vc= 100 m/min; f= 0.05 – 0.1 – 0.2 mm/rev; a_p= 1 mm

Feed [mm/rev]	Cutting force [N]	Feed force [N]	Chip thickness [mm]	Contact length between chip and tool [mm]
0.05	143.3	121.2	0.22	0.89
0.1	242.0	152.2	0.31	0.95
0.2	413.8	219.6	0.79	0.98

In table 4.3, the presented results are obtained through the application of the analytical models presented in chapter 3 and using the experimental values for both materials. Experimental (analytical) cutting power was based in equation (3.6), maximum cutting

temperature based in equation (3.16) and plastic strain based in equation (3.17) can be obtained in function of the variation of the feed rate.

Table 4.3: Experimental (analytical) cutting power, maximum cutting temperature and plastic strain for the machining of the aluminium alloy and stainless steel in function of the variation of the feed rate

	Al 7075			AISI 316		
Feed rate [mm/rev]	**Pc [W]**	**T [ºC]**	**ε**	**Pc [W]**	**T [ºC]**	**ε**
0.05	789.1	213.8	2.18	238.8	312.6	4.37
0.1	1427.2	268.1	2.65	403.3	542.5	3.18
0.2	2643.8	314.8	3.11	689.7	689.3	3.95

4.3 FEM analysis validation with Coulomb Friction coefficient

The Coulomb friction coefficients, obtained using equation (3.3) are presented in table 4.4, for aluminium alloy and stainless steel in function of the feed rate.

Table 4.4: Coulomb friction coefficients for both materials in function of the feed rate

Feed rate [mm/rev]	Al 7075	AISI 316
0.05	0.31	0.89
0.1	0.25	0.80
0.2	0.17	0.53

By comparing the obtained Coulomb friction coefficients with the friction coefficients found in the literature, it is possible to conclude that an agreement is established. Typically, aluminium alloys have friction coefficients lower than 0.5 and stainless steels above 0.5 and this fact is verified for all cases of study.

To provide an overview of the differences obtained between experimental work and simulation using the Coulomb friction coefficient, a single case of study will be presented for each workpiece material. An experimental validation on the cutting and feed forces, cutting power, maximum cutting temperature and plastic strain is addressed in order to verify if the simulations met what happened experimentally. The differences were calculated using the following formula:

$$difference = \frac{|\ Experimental \quad value - Simulated \quad value\ |}{Experimental \quad value} \times 100\% \tag{4.1}$$

4.3.1 Al 7075 with the PCD cutting tool

For a feed rate of 0.1 mm/rev and the respective Coulomb friction coefficient (0.25), the following results were obtained (cutting and feed forces, cutting power, maximum cutting temperature and plastic strain). Important to note is that all values are an average of two tests in the experimental work and an average of one simulation in the numerical simulation.

In figure 4.1, the experimental cutting force has a value of 171.3 N while the feed force has a value of 53.3 N. The numerical results are superior when compared to the simulated results. In the latter case, the cutting force presents a value of 197.9 N and the feed force 81.2 N.

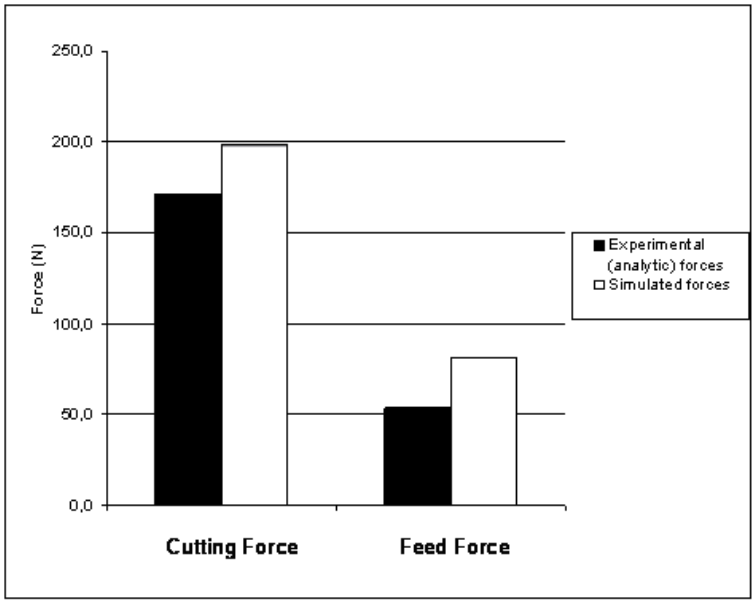

Figure 4.1: Comparison between experimental and simulated cutting and feed forces when machining the aluminium alloy with a feed rate of 0.1 mm/rev and the Coulomb friction coefficient (0.25)

The cutting power can also be compared between experimental and numerical approaches like showed in figure 4.2 a). While 1427.5 W were obtained experimentally, about 1641 W were obtained numerically.

The maximum cutting temperature has a minimum difference between experimentation and simulation when using the Coulomb friction coefficient like can be seen in figure 4.2 b). 268.2 ºC were obtained through the analytical models and 271.4 ºC in the numerical simulation.

The plastic strain presents 2.65 deformation in the experimental work and about 2.85 through numerical simulation like presented in figure 4.2 c).

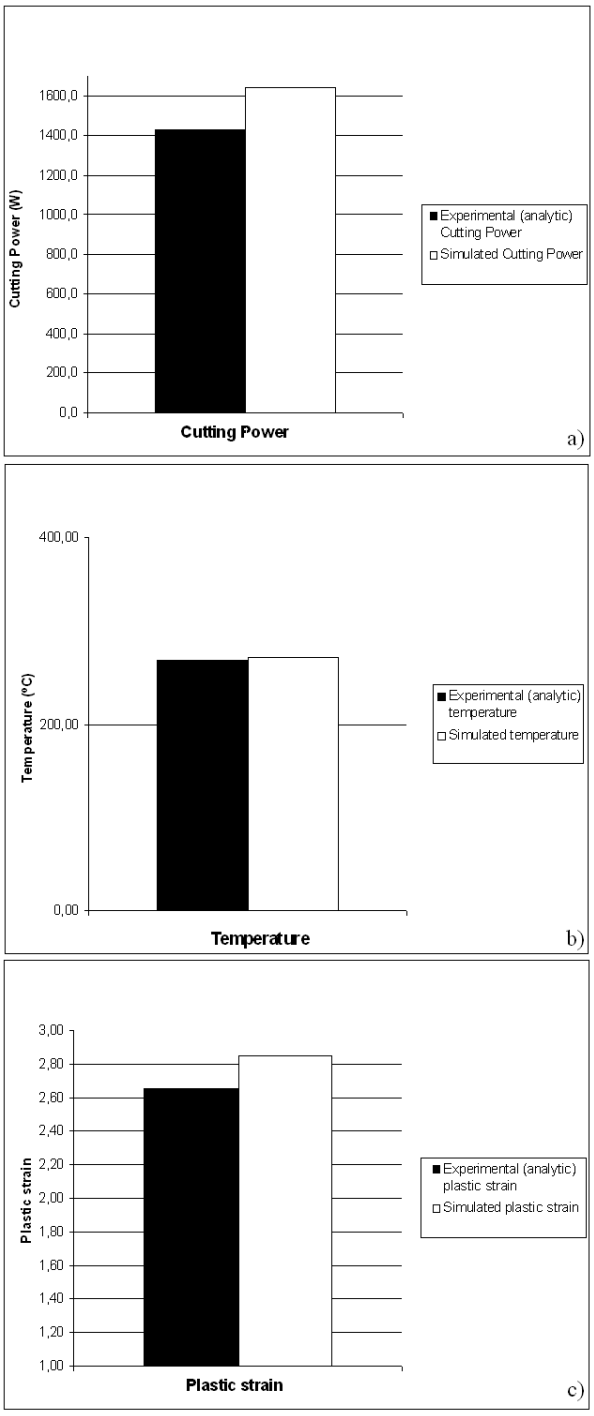

Figure 4.2: Comparison between experimental and simulated data when machining the aluminium alloy with a feed rate of 0.1 mm/rev and the Coulomb friction coefficient (0.25) a) cutting power b) maximum cutting temperature c) plastic strain

In table 4.5, the differences in percentage between the experimental results and simulated values are shown.

Table 4.5: Differences between experimental and simulated data for the machining of Al 7075 with the PCD cutting tool with a feed rate of 0.1 mm/rev

Differences [%]	
Cutting force (Fc)	15.5
Feed force (Fa)	52.3
Cutting power (Pc)	15
Maximum cutting temperature (T)	1.2
Plastic strain (ε)	7.4

The differences are reasonable for almost every case, only with the feed force presenting an unacceptable difference. This is due to the use of the Coulomb friction coefficient in the numerical simulation.

4.3.2 AISI 316 with the coated cemented carbide cutting tool

As for the stainless steel, the same reasoning will be presented. The results obtained experimentally through the analytical models will be compared with the results obtained by numerical simulation (cutting and feed forces, cutting power, maximum cutting temperature and plastic strain) using the Coulomb friction coefficient (0.80). Once again, experimental results are an average of two experiments while simulated results are an average of a single simulation.

In figure 4.3, the differences in the cutting and feed forces are evident. The experimental cutting force reached about 242 N and the feed force about 152.2 N. In the simulated results, the cutting force reached about 195.2 N and the feed force about 116.3 N.

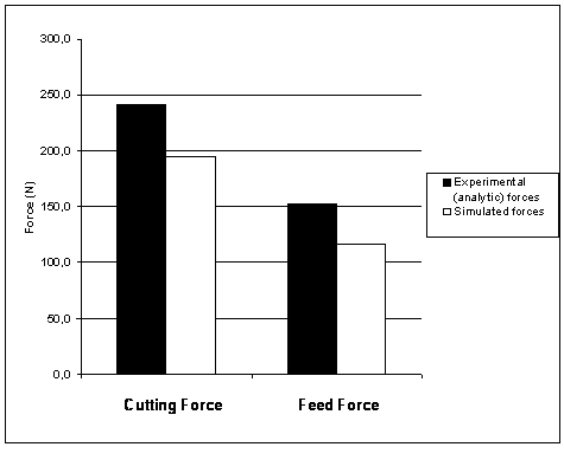

Figure 4.3: Comparison between experimental and simulated cutting and feed forces when machining the stainless steel with a feed rate of 0.1 mm/rev and the Coulomb friction coefficient (0.80)

Regarding cutting power, the experimental test reached 403.3 W and the simulated test about 366.4 W like showed in figure 4.4 a).

As for the maximum cutting temperature, the experimental approach resulted in 542.5 ºC and the simulated approach in 419.5 ºC like presented in figure 4.4 b).

In figure 4.4 c) it can be seen that the plastic strain reached about 3.18 with the analytical models and 3.88 in the simulated test.

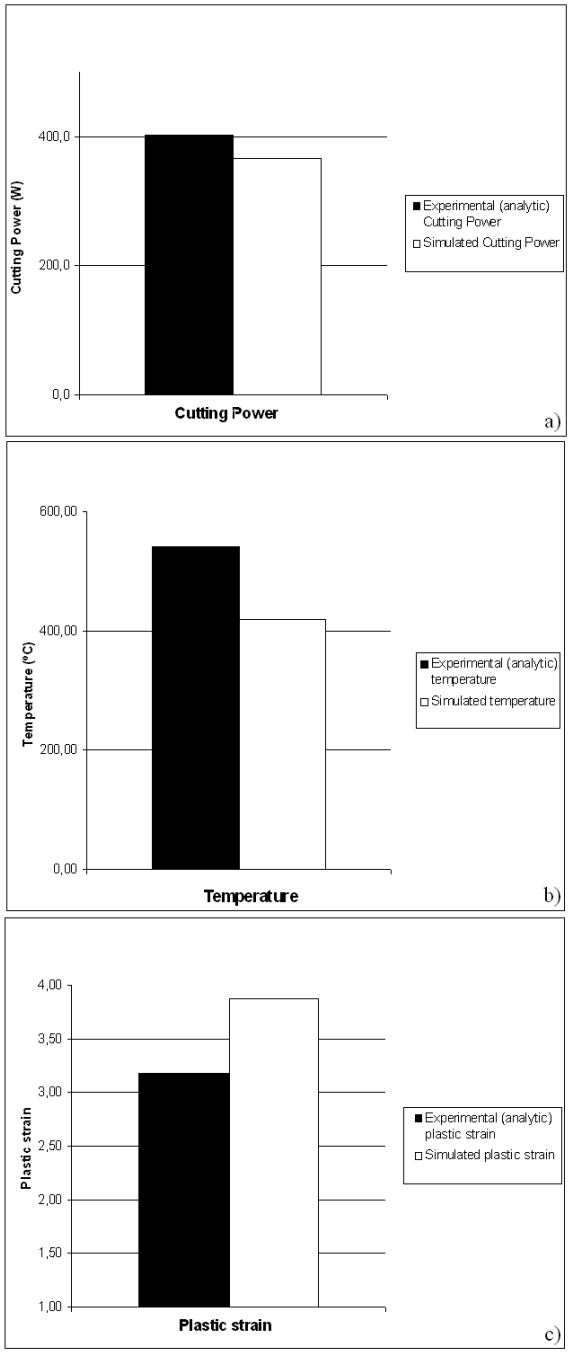

Figure 4.4: Comparison between experimental and simulated data when machining the stainless steel with a feed rate of 0.1 mm/rev and the Coulomb friction coefficient (0.80) a) cutting power b) maximum cutting temperature c) plastic strain

The differences between the experimental results and simulated values are shown in percentage for machining of the stainless steel in table 4.6.

Table 4.6: Differences between experimental and simulated data for the machining of AISI 316 with the coated cemented carbide cutting tool with a feed rate of 0.1 mm/rev

Differences [%]	
Cutting force (Fc)	19.3
Feed force (Fa)	23.6
Cutting power (Pc)	9.2
Maximum cutting temperature (T)	22.7
Plastic strain (ε)	22.1

The differences for the majority of cases are somewhat in the limit of being acceptable, being the cutting power the only case with a difference that is considered reasonable.

4.4 FEM analysis validation with Coulomb Friction adjustment

As showed in 4.3 subsection, the friction coefficient obtained through the Coulomb model doesn't provide a solution capable of outputting results close to the results obtained using the analytical models in any of the materials. Coulomb model is useful to provide a first approach to the friction value and, using that value as a starting point, several iterations must be carried until the results are satisfactory. Coulomb model is suitable as a starting point because it is able to define if the friction coefficient is bigger or smaller than the standard friction coefficient (0.5). The stopping criterion is found when the cutting and feed forces obtained through numerical simulation are comparable with the results found in the experimental work.

As already stated, the software is very closed in terms of changing Johnson-Cook coefficients so all the simulations were conducted using the software database flow stress. Even if the Johnson-Cook coefficients were improved to fit the experimental material used in the experiments, a disagreement between numerical and analytical results would have high chance of being present due to the critical friction coefficient. Besides, changing the friction coefficient is a fast and reliable way to improve differences between experimentation and simulation. Nowadays, industry is always pushing towards having results in less time and testing each material to find the appropriate parameters for the Johnson-Cook law is a very tedious task, not suitable for industry needs. Even more, with the change of material lot, new parameters have to be found and several tests need to be done on the material in order to find

the new constitutive law constants. This way, the software database flow stress was used and the friction coefficient iterated instead.

Therefore, the optimum friction coefficient for each material in function of the feed rate can be found in the table 4.7 (several simulations were made in order to adjust, for each case, the friction coefficient. A total number of 80 simulations were carried within this investigation along 9 months.

Table 4.7: Iterated friction coefficients for both materials in function of the feed rate

Feed rate [mm/rev]	Al 7075	AISI 316
0.05	0.1	1.1
0.1	0.1	1.0
0.2	0.06	0.95

4.4.1 Al 7075 with the PCD cutting tool

In this subsection, the experimental validations using equation 4.1 on cutting and feed forces, cutting power, maximum cutting temperature and plastic strain will be conducted. Figure 4.5 shows a comparison between the experimental and simulated cutting forces in function of the feed rate.

For a feed rate of 0.05 mm/rev, the iterated friction coefficient is 0.1 while the Coulomb friction coefficient is 0.31. In figure 4.5, it can be seen that the experimental cutting force has reached a value of 94.7 N while 97.8 N for the simulated result.

For a feed rate of 0.1 mm/rev, the iterated friction coefficient is 0.1 and Coulomb friction coefficient is 0.25. Once again, the experimental results are comparable to the numerical ones like presented in figure 4.5. The experimental cutting force reached a value of 171.3 N while the simulated results reached a value of 171.8 N.

For a feed rate of 0.2 mm/rev, the iterated friction coefficient is 0.06 and the Coulomb friction coefficient is 0.17. Differences between numerical and experimental values are minimal once again like figure 4.5 shows. The experimental cutting force reached a value of 317.3 N and the simulated results reached a value of 315.2 N.

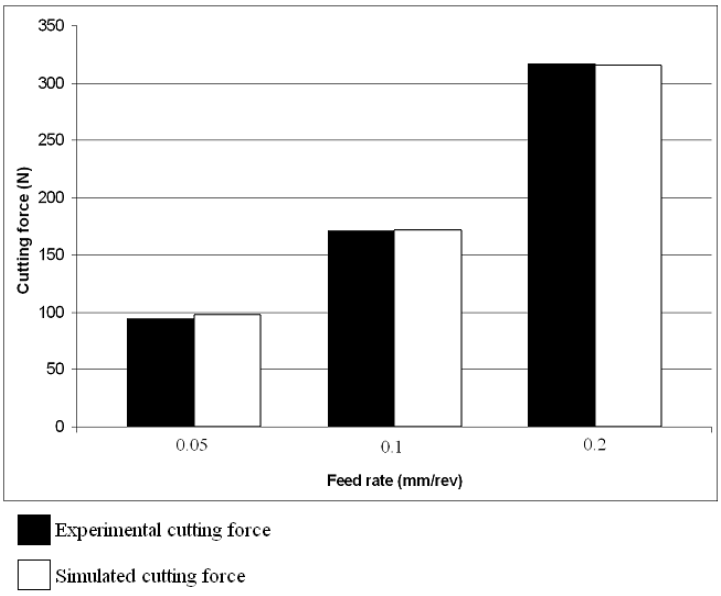

Figure 4.5: Comparison between experimental and simulated cutting forces when machining the aluminium alloy with the iterated friction coefficient in function of the feed rate and constant cutting speed of 500 m/min and fixed depth of cut of 2 mm

In figure 4.6, a comparison of feed force is shown between both methods in function of the feed rate. For a feed of 0.05 mm/rev, feed force has a value of 46.4 N for the experimental approach and 47.9 N for the simulated one. For 0.1 mm/rev, while the feed force reached a value of 53.3 N for experimentation, 57.8 N were reached in simulation. Last but not least, for a feed of 0.2 mm/rev, experimental feed force reached 52.8 N and 63.1 N in the simulation.

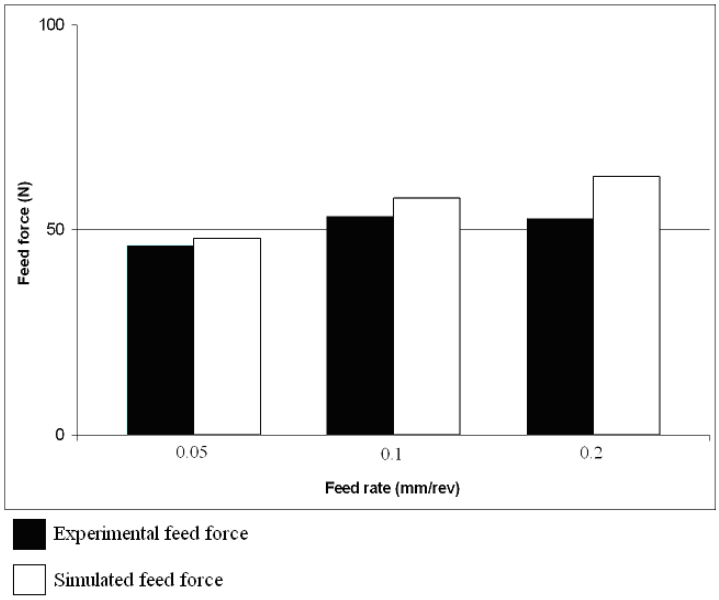

Figure 4.6: Comparison between experimental and simulated feed forces when machining the aluminium alloy with the iterated friction coefficient in function of the feed rate and constant cutting speed of 500 m/min and fixed depth of cut of 2 mm

Cutting power is also very close when experimental and numerical results are compared. Figure 4.7 shows the cutting power in function of the feed rate and for a feed of 0.05 mm/rev, 789.2 W were obtained with the analytical model and about 825.4 W through the simulation. For 0.01 mm/rev, experimental cutting power reached 1427.5 W while 1433.9 W were obtained through the simulation. For 0.2 mm/rev, the analytical model reached 2644.2 W while 2550.8 W were obtained through the simulation.

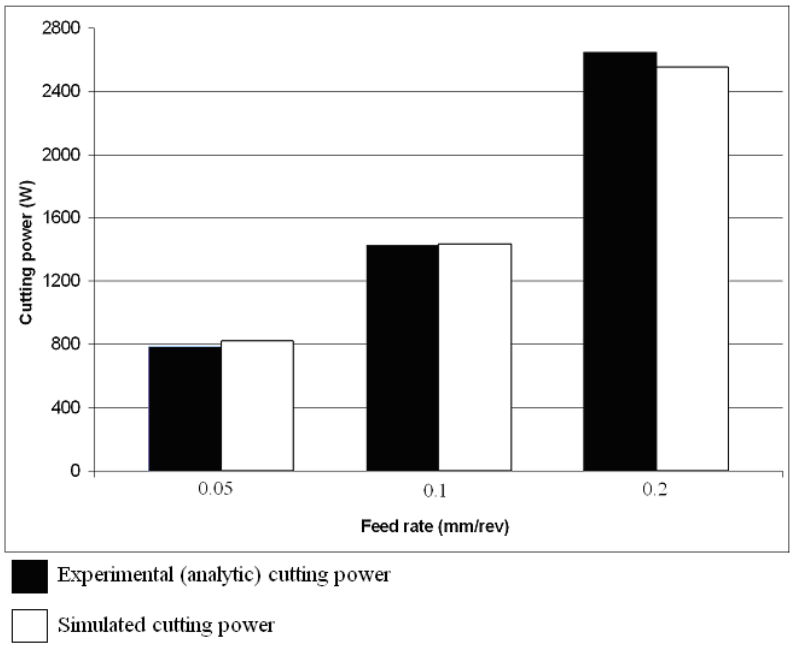

Figure 4.7: Comparison between experimental and simulated cutting power when machining the aluminium alloy with the iterated friction coefficient in function of the feed rate and constant cutting speed of 500 m/min and fixed depth of cut of 2 mm

Regarding maximum cutting temperature, once again the results are close between both methods like figure 4.8 suggests. Figure 4.8 compares the maximum cutting temperature obtained through the numerical models with the results found within the simulation in function of the feed rate. About 213.8 ºC were obtained through the analytical models and 224.2 ºC in the numerical simulation for a feed rate of 0.05 mm/rev. For 0.1 mm/rev, about 268.2 ºC were obtained through the analytical models and 252.5 ºC in the numerical simulation. For 0.2 mm/rev, about 314.8 ºC were obtained through the analytical models and 272.1 ºC in the numerical simulation.

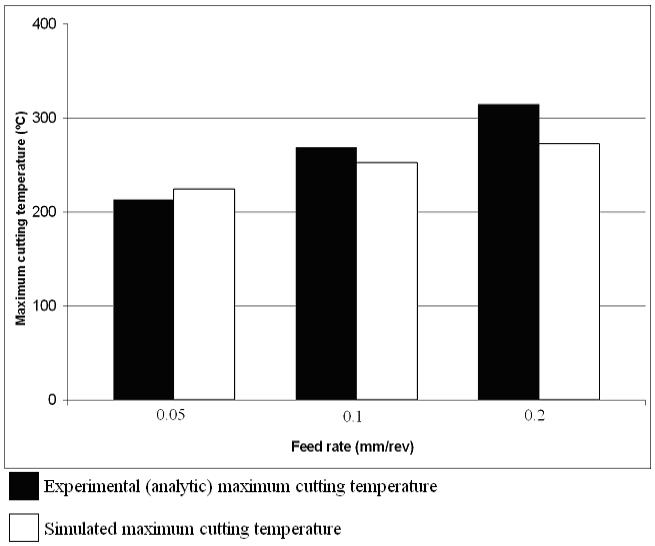

Figure 4.8: Comparison between experimental and simulated maximum cutting temperature when machining the aluminium alloy with the iterated friction coefficient in function of the feed rate and constant cutting speed of 500 m/min and fixed depth of cut of 2 mm

The plastic strain can be seen in figure 4.9 in function of the feed rate and presents 2.18 deformation in the experimental work and about 2.31 through numerical simulation for a feed rate of 0.05 mm/rev. For 0.1 mm/rev, the plastic strain reached 2.65 in the experimental work and about 2.84 through numerical simulation. Finally, for a feed rate of 0.2 mm/rev, the plastic strain reached 3.11 in the experimental work and about 2.85 through numerical simulation.

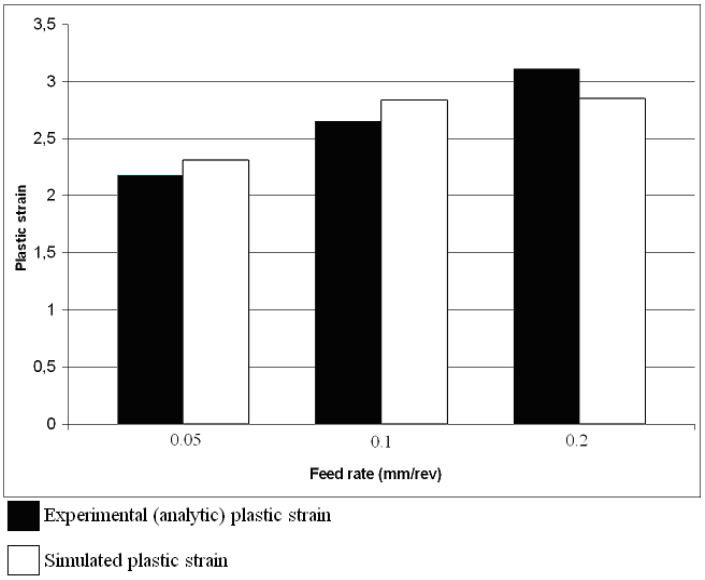

Figure 4.9: Comparison between experimental and simulated plastic strain when machining the aluminium alloy with the iterated friction coefficient in function of the feed rate and constant cutting speed of 500 m/min and fixed depth of cut of 2 mm

In table 4.8, the differences in percentage between the experimental results and simulated values are shown in function of the feed rate in the machining of the aluminium alloy.

Table 4.8: Differences between experimental and simulated data for the machining of Al 7075 with the PCD cutting tool with a variable feed rate

	Differences (%)				
Feed [mm/rev]	**Cutting force**	**Feed force**	**Cutting Power**	**Maximum Cutting Temperature**	**Plastic strain**
0.05	0.29	8.4	0.45	5.9	6.9
0.1	0.3	8.4	0.4	5.9	7.0
0.2	0.7	19.5	3.5	13.6	8.5

As can be seen, when Coulomb friction coefficient is iterated, very precise results are obtained for almost all cases of study. The most critical results were obtained with the simulation with 0.2 mm/rev. In this particular case, feed force has a difference of 19.5% but in general these results can be considered very satisfactory and much more precise when compared with the Coulomb friction results for all cases of study.

4.4.2 AISI 316 with the coated cemented carbide cutting tool

Experimental validations for cutting and feed forces, cutting power, maximum cutting temperature and plastic strain in the machining of the stainless steel will be addressed in the present subsection. Figure 4.10 shows a comparison between the experimental and simulated cutting forces in function of the feed rate.

For a feed rate of 0.05 mm/rev, the iterated friction coefficient is 1.1 and the Coulomb friction coefficient is 0.89. In figure 4.10, it can be seen that the experimental cutting force has a value of 143.3 N and the numerical cutting force about 133.2 N.

For a feed rate of 0.1 mm/rev, the iterated friction coefficient is 1.0 and the Coulomb friction coefficient is 0.80. Like figure 4.10 shows, the experimental cutting force reached a value of 242.0 N while the simulated result reached a value of 211.5 N.

For a feed rate of 0.2 mm/rev, the iterated friction coefficient is 0.95 and the Coulomb friction coefficient 0.95. The experimental cutting force reached a value of 413.8 N and 376.9 N for the simulation like presented in figure 4.10.

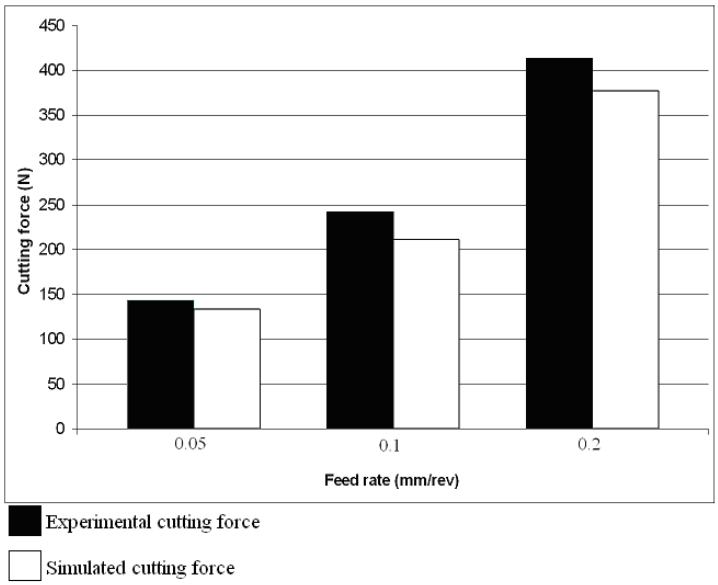

Figure 4.10: Comparison between experimental and simulated cutting forces when machining the stainless steel with the iterated friction coefficient in function of the feed rate and constant cutting speed of 100 m/min and fixed depth of cut of 1 mm

In figure 4.11, feed forces are compared between experimental and simulated work in function of the feed rate. For a feed of 0.05 mm/rev, feed force has a value of 102.5 N for the experimental approach and 121.2 N for the simulated one. For 0.1 mm/rev, while the feed force reached a value of 152.2 N for experimentation, 131.7 N were reached in simulation. Experimental feed force reached 219.6 N and 189.9 N in the simulation for a feed rate of 0.2 mm/rev.

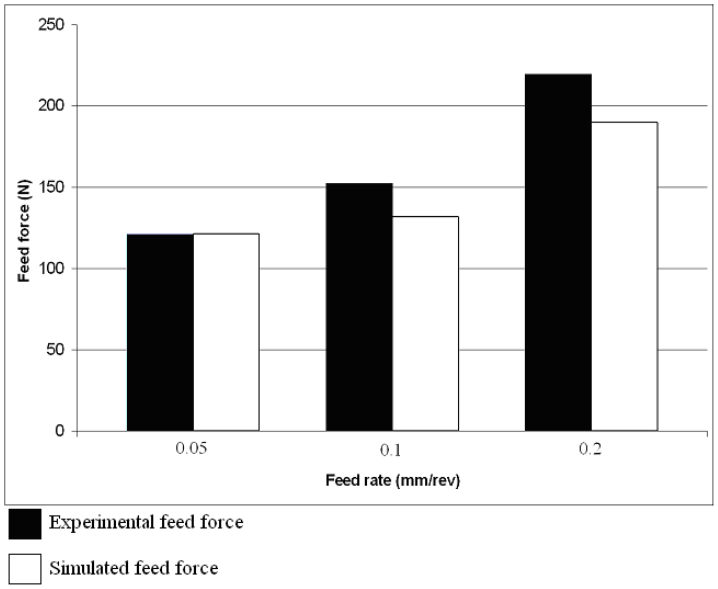

Figure 4.11: Comparison between experimental and simulated feed forces when machining the stainless steel with the iterated friction coefficient in function of the feed rate and constant cutting speed of 100 m/min and fixed depth of cut of 1 mm

Regarding cutting power, figure 4.12 shows its evolution in function of the feed rate. 238.8 W were obtained with the analytical model and about 232.8 W through the simulation for a feed rate of 0.05 mm/rev. For a feed rate of 0.1 mm/rev, experimental cutting power reached 403.3 W while 349.9 W were obtained through the simulation. Finally, for a feed rate of 0.2 mm/rev, using the analytical model reached 689.7 W while 620 W were obtained through the simulation.

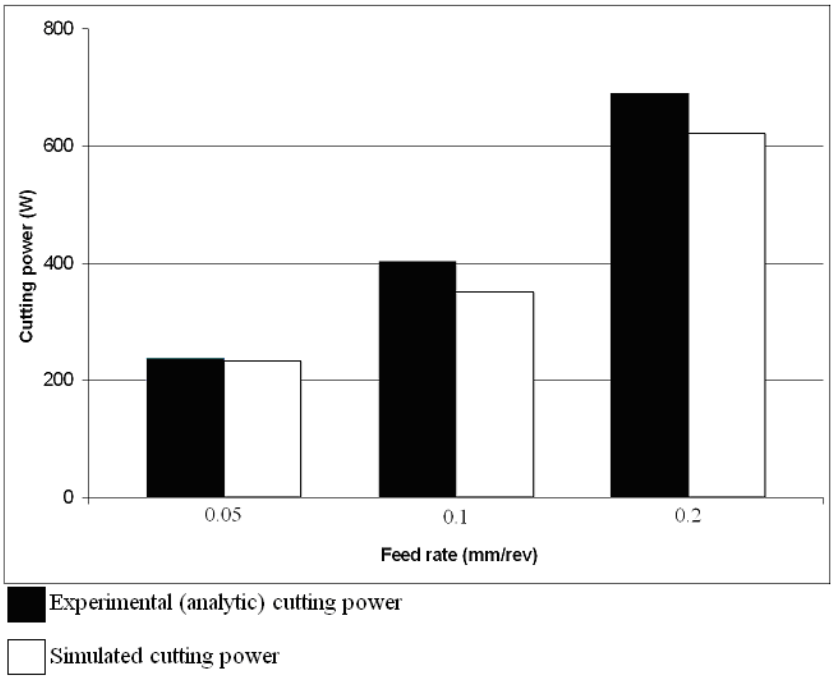

Figure 4.12: Comparison between experimental and simulated cutting power when machining the stainless steel with the iterated friction coefficient in function of the feed rate and constant cutting speed of 100 m/min and fixed depth of cut of 1 mm

As to what maximum cutting temperature is concerned, figure 4.13 shows its evolution in function of the feed rate. About 312.6 ºC were obtained through the analytical model and 251.2 ºC in the numerical simulation for the lower feed rate. About 542.5 ºC were obtained through the analytical model and 410 ºC in the numerical simulation for a feed rate of 0.1 mm/rev. For the higher feed rate, about 689.3 ºC were obtained through the analytical models and 519.8 ºC in the numerical simulation.

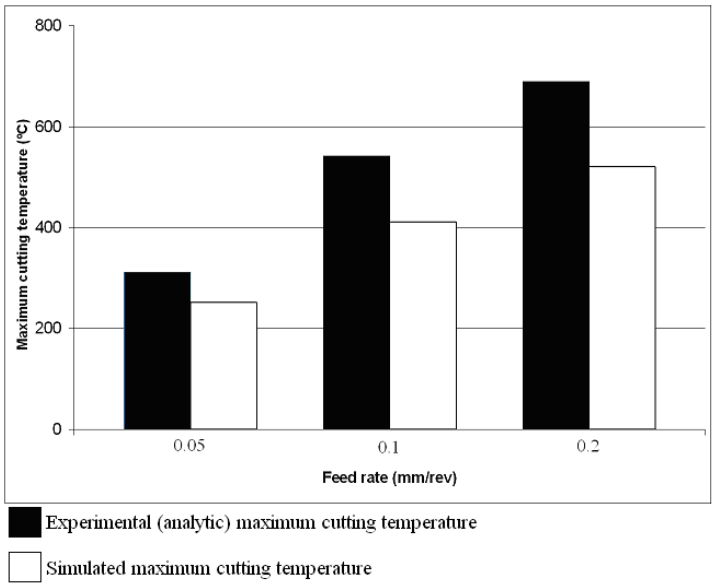

Figure 4.13: Comparison between experimental and simulated maximum cutting temperature when machining the stainless steel with the iterated friction coefficient in function of the feed rate and constant cutting speed of 100 m/min and fixed depth of cut of 1 mm

In figure 4.14, the plastic strain is showed in function of the feed rate. It presents 4.37 deformation in the experimental work and about 3.72 through numerical simulation for 0.05 mm/rev. For 0.1 mm/rev, plastic strain reached 3.18 in the experimental work and about 3.81 through numerical simulation. Lastly, for a feed rate of 0.2 mm/rev, plastic strain reached 3.95 in the experimental work and about 3.91 through numerical simulation.

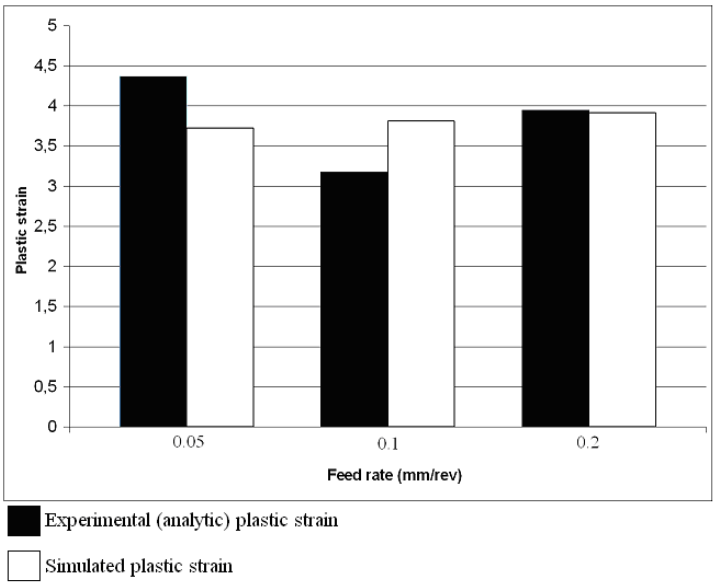

Figure 4.14: Comparison between experimental and simulated plastic strain when machining the stainless steel with the iterated friction coefficient in function of the feed rate and constant cutting speed of 100 m/min and fixed depth of cut of 1 mm

In table 4.9, the differences in percentage between the experimental results and simulated values are shown in function of feed rate in the machining of the stainless steel.

Table 4.9: Differences between experimental and simulated data for the machining of Al 7075 with the PCD cutting tool with a variable feed rate

	Differences (%)				
Feed [mm/rev]	**Cutting force**	**Feed force**	**Cutting Power**	**Maximum Cutting Temperature**	**Plastic strain**
0.05	7.0	15.4	2.5	19.6	15.0
0.1	12.6	13.5	13.2	24.4	19.9
0.2	8.9	13.5	10.1	24.6	1.3

These results are considered acceptable for the machining of the stainless steel although for the cutting temperature, the differences are considerable to be in the limit of being acceptable. When a comparison is made between Coulomb friction coefficient results and the iterated friction coefficient results, it is clear that the iterated friction coefficient should be used. In some cases, the differences are cut in half from the Coulomb friction results to the iterated ones so much more precise results are obtained with an adjustment to the friction coefficient.

4.5 Modelling and prediction

In the following subsections, a more detailed analysis will be addressed for the machining of both materials. Cutting and feed forces, cutting power, maximum cutting temperature, plastic strain and plastic strain rate, maximum shear stress and residual stresses (the latter as an AISI 316 exclusive) will be presented in more in depth detail.

4.5.1 Al 7075 and PCD cutting tool

4.5.1.1 Cutting and feed forces, cutting power and maximum cutting temperature

Regarding the evolution of cutting and feed forces with the variation of feed rate, the obtained results agree with the expected pattern like can be seen in figure 4.15. As the feed keeps increasing, an increase in the feed force is felt, although the increase in the cutting force is much more obvious. This can be explained by the fact that, as the feed keeps increasing, the amount of material being removed also keeps increasing. In fact, as the feed rate doubles, the

amount of removed material also doubles and this reflects itself in the cutting force that, like expected, almost doubles (by default). This leads to a pattern, with the increase in feed rate from 0.05 mm/rev to 0.1 mm/rev and then 0.2 mm/rev, the cutting force increases from 97.8 N to 171.8 N to 315.2 N accordingly. This makes sense because when the amount of material to be removed doubles, also the force to extract it should double.

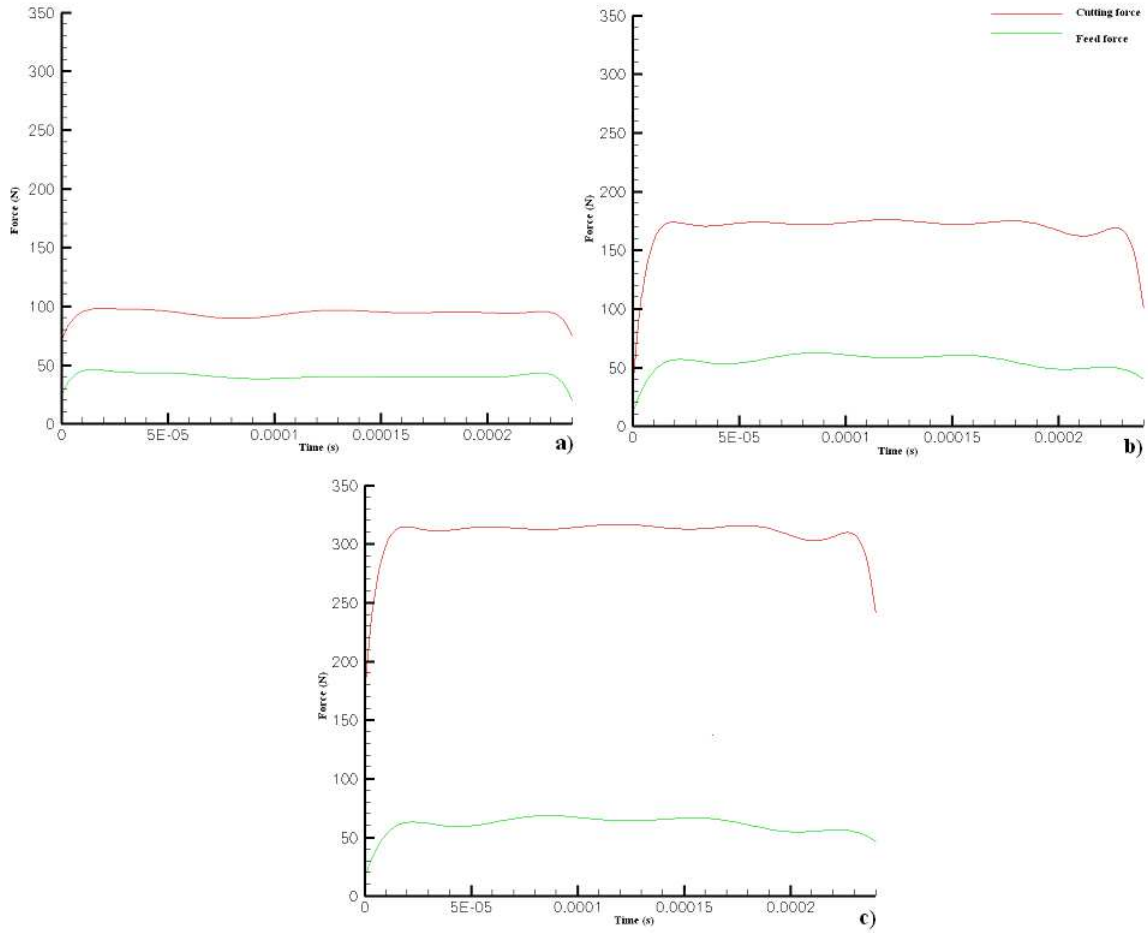

Figure 4.15: Comparison of cutting and feed forces along the time in the machining of the aluminium alloy with a cutting speed of 500 m/min and a depth of cut of 2 mm with the variation of the feed rate. a) 0.05 mm/rev b) 0.1 mm/rev c) 0.2 mm/rev

The cutting power and maximum cutting temperature (which is felt in the tool), can be seen, in function of the cutting time, in figure 4.16. Once again, the results agree with what was initially expected. The cutting power, which is function of the cutting force, keeps growing as the feed rate increases. Like already explained, the cutting force almost doubles with the increase of the feed rate so, the cutting power being directly dependent of the cutting force, has the same pattern.

The maximum cutting temperature increases with the variation of the feed rate but not by a considerable margin. Despite the increase in temperature being faint, this behavior can cause a decrease in tool life like already explained under state of the art. The increase in temperature might be due to the fact of the cutting and feed forces kept increasing with the rise of the feed rate. PCD also have good thermal conductivity so part of the generated heat is being conducted through the cutting tool. Of relevance is that PCD transforms into graphite at about 700ºC. Like can be seen in figure 4.16, this critical temperature isn't achieved for all feed rates.

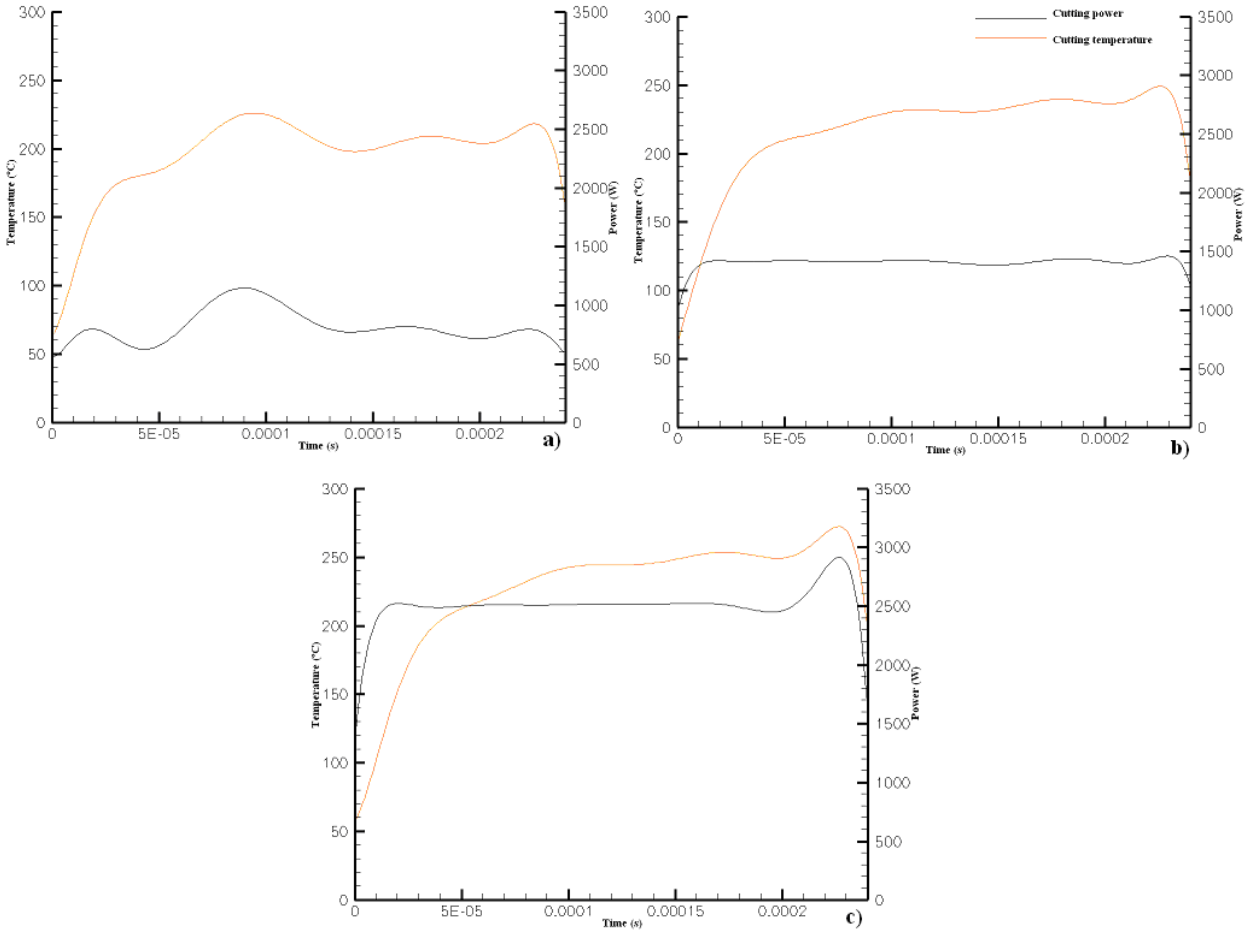

Figure 4.16: Maximum cutting temperature and cutting power along the time in the machining of the aluminium alloy with a cutting speed of 500 m/min and a depth of cut of 2 mm with the variation of the feed rate. a) 0.05 mm/rev b) 0.1 mm/rev c) 0.2 mm/rev

In figure 4.17, a detailed view of the distribution of the cutting temperature in the tool, workpiece and chip can be seen. The figure was taken at the end of the length of cut because it is at this zone that the higher temperatures are felt and steady state conditions are present. The maximum temperature is felt in the primary shear zone for all cases of study (although for a feed rate of 0.2 mm/rev, the chip has a noticeable hotter zone). Like can be seen, the cutting temperature is increasing with the feed rate and the principle mechanism to remove the heat from the cutting zone is the chip (the outside of the chip curling is hotter than the inside zone). Also worth noting is that aluminium and PCD cutting tool both have good heat conductivity so the majority of produced heat is evacuated (being the chip the principal mechanism). This is beneficial and helps to reach a longer tool life. There is also a thermal affected layer in the workpiece that increases with the feed rate (more heat is generated).

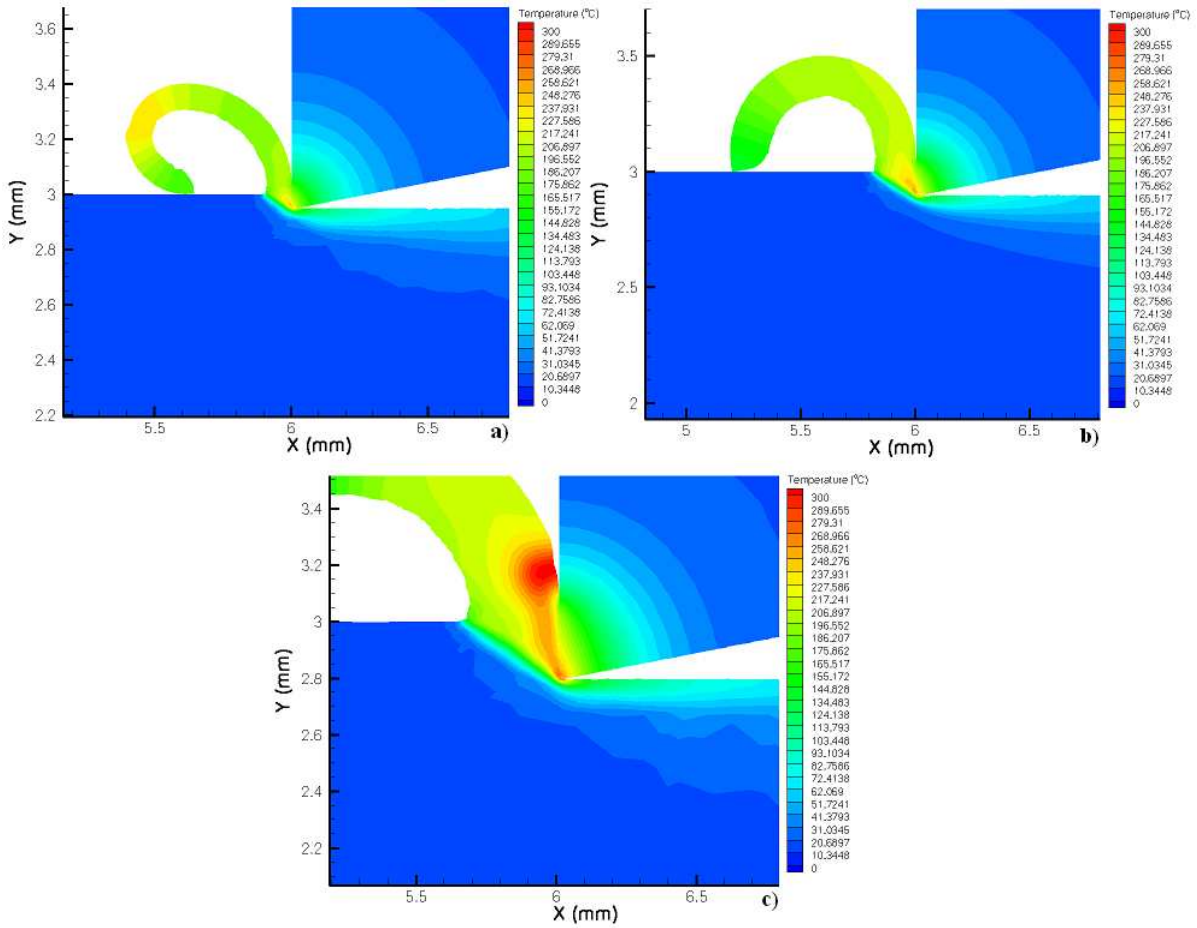

Figure 4.17: Detailed comparison of maximum cutting temperature in the tool, workpiece and chip at the end of length of cut in the machining of the aluminium alloy with a cutting speed of 500 m/min and a depth of cut of 2 mm and a variable feed rate. a) 0.05 mm/rev b) 0.1 mm/rev c) 0.2 mm/rev

4.5.1.2 Plastic strain and plastic strain rate and maximum shear stress

A detailed plastic strain distribution can be seen in figure 4.18 in the workpiece and chip (the figure was taken at the end of length of cut where steady state conditions are present). At first glance, differences in the plastic strain seem to be inexistent with the variation of the feed rate, being a bigger deformed zone in the chip with a feed rate of 0.05 mm/rev the most obvious difference between all cases. However, the plastic strain rate has a trend to slightly increase with the increasing of the feed rate if the primary shear zone is considered. The fact that the plastic strain is increasing with the increase of the feed rate can be explained with the fact that the maximum shear stress is also increasing with the increase of the feed rate. There is also a bigger affected layer by the plastic strain when machining with higher feed rates.

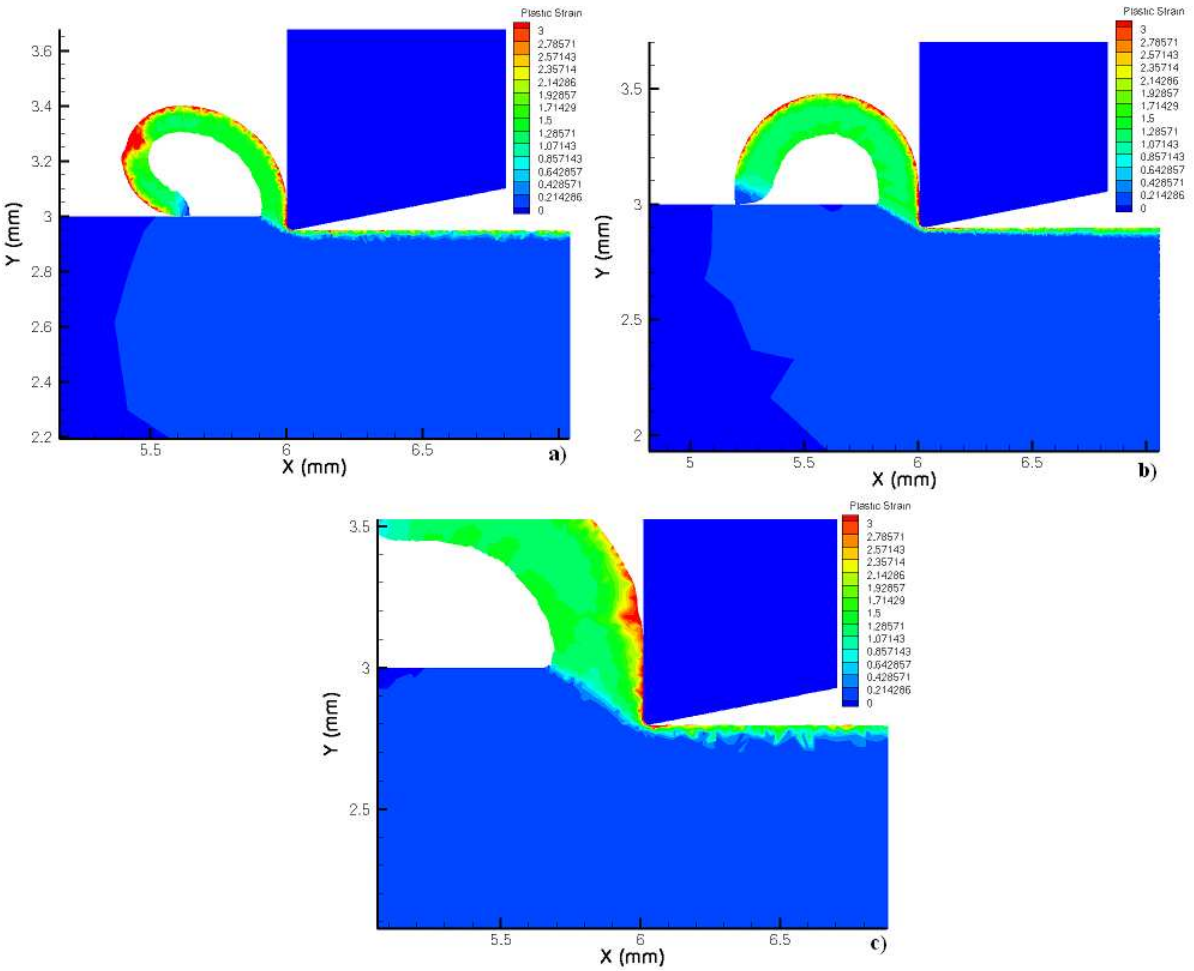

Figure 4.18: Detailed comparison of plastic strain in the tool, workpiece and chip at the end of length of cut in the machining of the aluminium alloy with a cutting speed of 500 m/min and a depth of cut of 2 mm and a variable feed rate. a) 0.05 mm/rev b) 0.1 mm/rev c) 0.2 mm/rev

Regarding plastic strain rate, a detailed distribution can be seen in figure 4.19 in the workpiece and chip (the figure was taken at the end of length of cut where steady state conditions are present). The cutting parameter that affects the most the plastic strain rate is the cutting speed. However, the cutting speed is kept constant between all cases of study, being the feed rate the only variation. In a matter of fact, the higher the feed rate, the bigger affected zone by the plastic strain rate. However, higher peaks in strain rate are achieved when machining at lower feed rates. Also of note is because the cutting temperature kept almost constant between all cases, the plastic strain rate also shows close values between different feed rates.

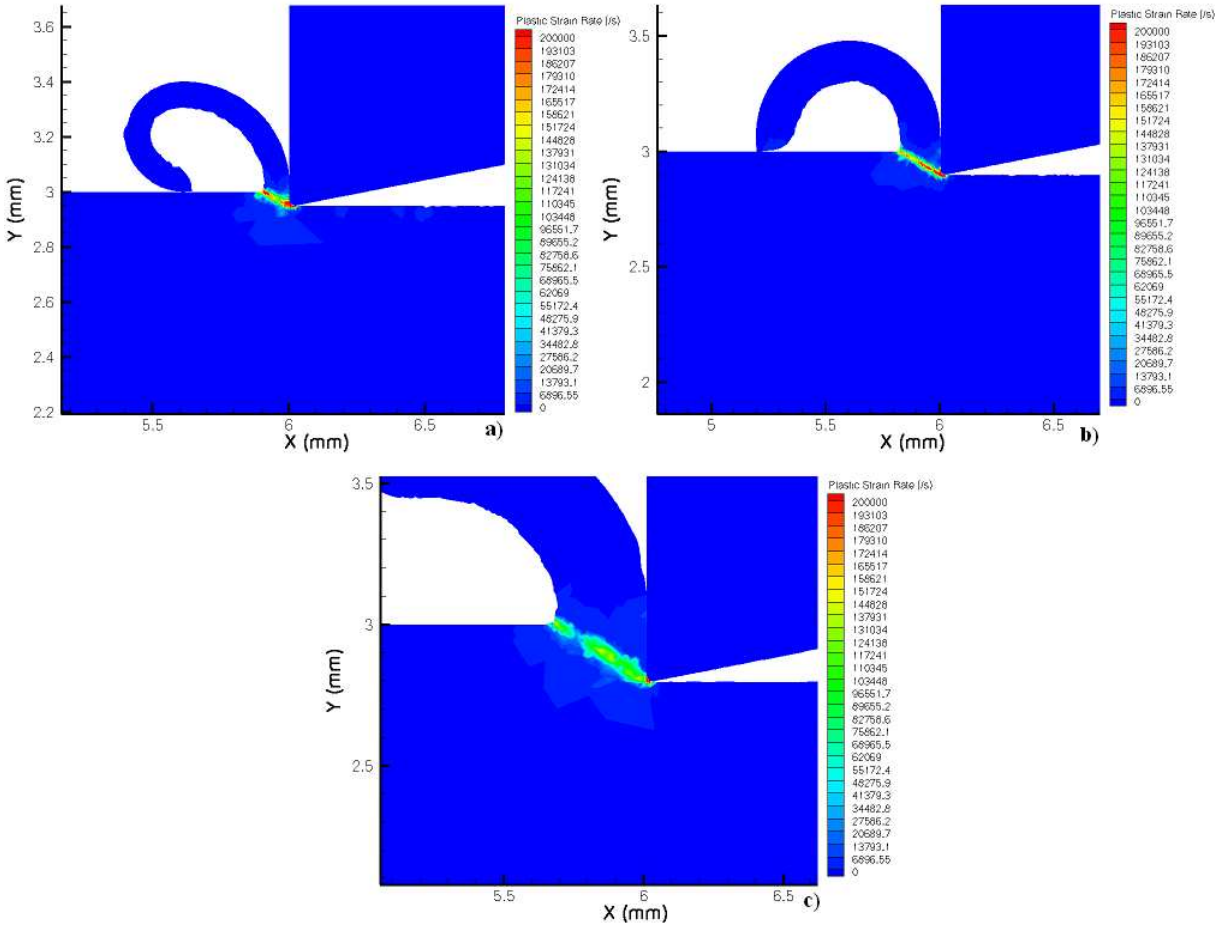

Figure 4.19: Detailed comparison of plastic strain rate in the tool, workpiece and chip at the end of length of cut in the machining of the aluminium alloy with a cutting speed of 500 m/min and a depth of cut of 2 mm and a variable feed rate. a) 0.05 mm/rev b) 0.1 mm/rev c) 0.2 mm/rev

As to what maximum shear stress is concerned, a detailed distribution can be seen in the tool, workpiece and chip in the figure 4.20 (the figure was taken at the end of length of cut where steady state conditions are present). Regarding the cutting tool, it can be seen that as the feed rate increases to double, the amount of removed material also doubles and this is reflected in the affected zone by the maximum shear stress (the tool is being submitted to a more challenging task). Regarding the workpiece, as the feed rate increases, a bigger affected zone is present although by a similar magnitude. The stress is, by definition, the force divided by area. Like already seen, the force almost doubles with the increase of the feed rate and the area doubles therefore, a reduction of the shear stress was expected. Although similar values of maximum shear stress among all cases of study in the primary shear zone are found, the affected zone increases with the increase of the feed rate. Also of note is that the stress decreases with the increasing of the temperature and decreasing of the plastic strain rate like already shown.

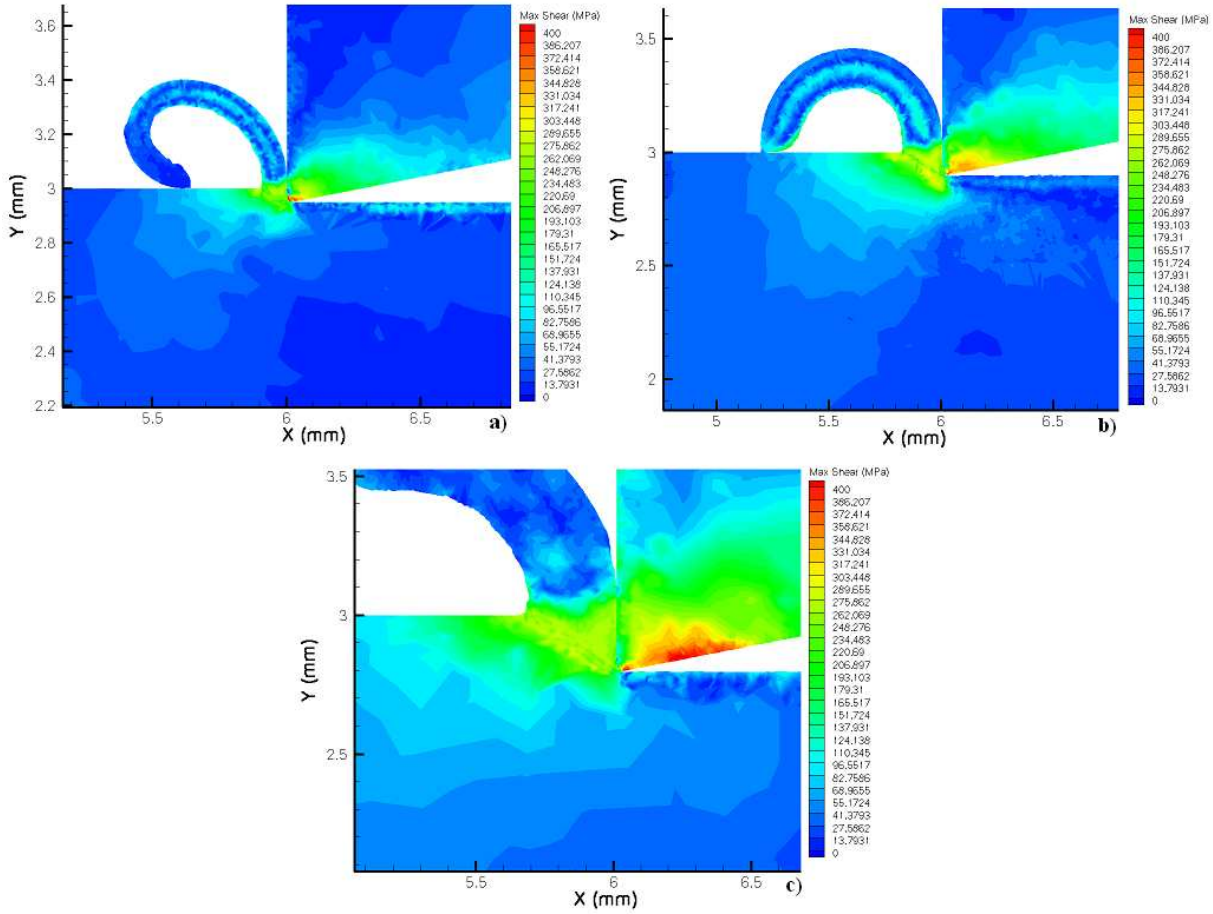

Figure 4.20: Detailed comparison of maximum shear stress in the tool, workpiece and chip at the end of length of cut in the machining of the aluminium alloy with a cutting speed of 500 m/min and a depth of cut of 2 mm and a variable feed rate. a) 0.05 mm/rev b) 0.1 mm/rev c) 0.2 mm/rev

4.5.2 AISI 316 and coated cemented carbide cutting tool

4.5.2.1 Cutting and feed forces, cutting power and maximum cutting temperature

In Figure 4.21, the evolution of the cutting and feed forces along the cutting time is presented. It can be observed that as the feed rate kept increasing, the cutting force kept increasing as well with the feed force showing a faint increase. Like already explained for the machining of the aluminium alloy, this is due to the fact that the amount of removed material doubles as the feed rate also doubles.

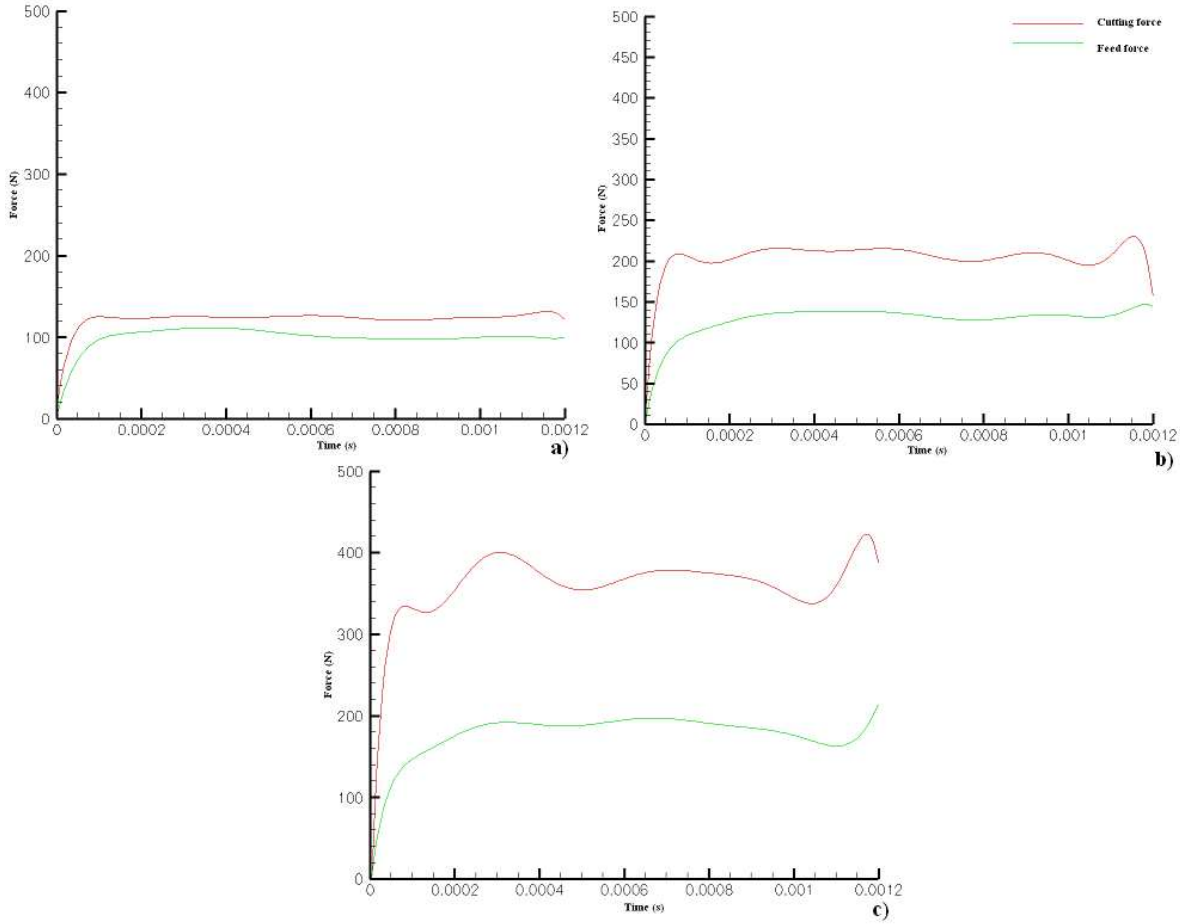

Figure 4.21: Comparison of cutting the feed forces along the time in the machining of the stainless steel with a cutting speed of 100 m/min and a depth of cut of 1 mm with the variation of the feed rate. a) 0.05 mm/rev b) 0.1 mm/rev c) 0.2 mm/rev

In figure 4.22, the evolution of the cutting power and the maximum cutting temperature along the cutting time is showed. What was said before in the machining of the aluminium alloy is also valid in the machining of the stainless steel, although only for the cutting power. The cutting power almost doubles with the increase of the feed rate due to the fact that the cutting force almost doubles from one case to another. The maximum cutting temperature (in the cutting tool) shows a considerable increase with the increase of the feed rate and this wasn't verified in the machining of the aluminium alloy. This can be explained by the fact that the stainless steel has a low thermal conductivity (tends to concentrate heat) and the tool and the chip are the main mechanisms removing the heat from the shear zone.

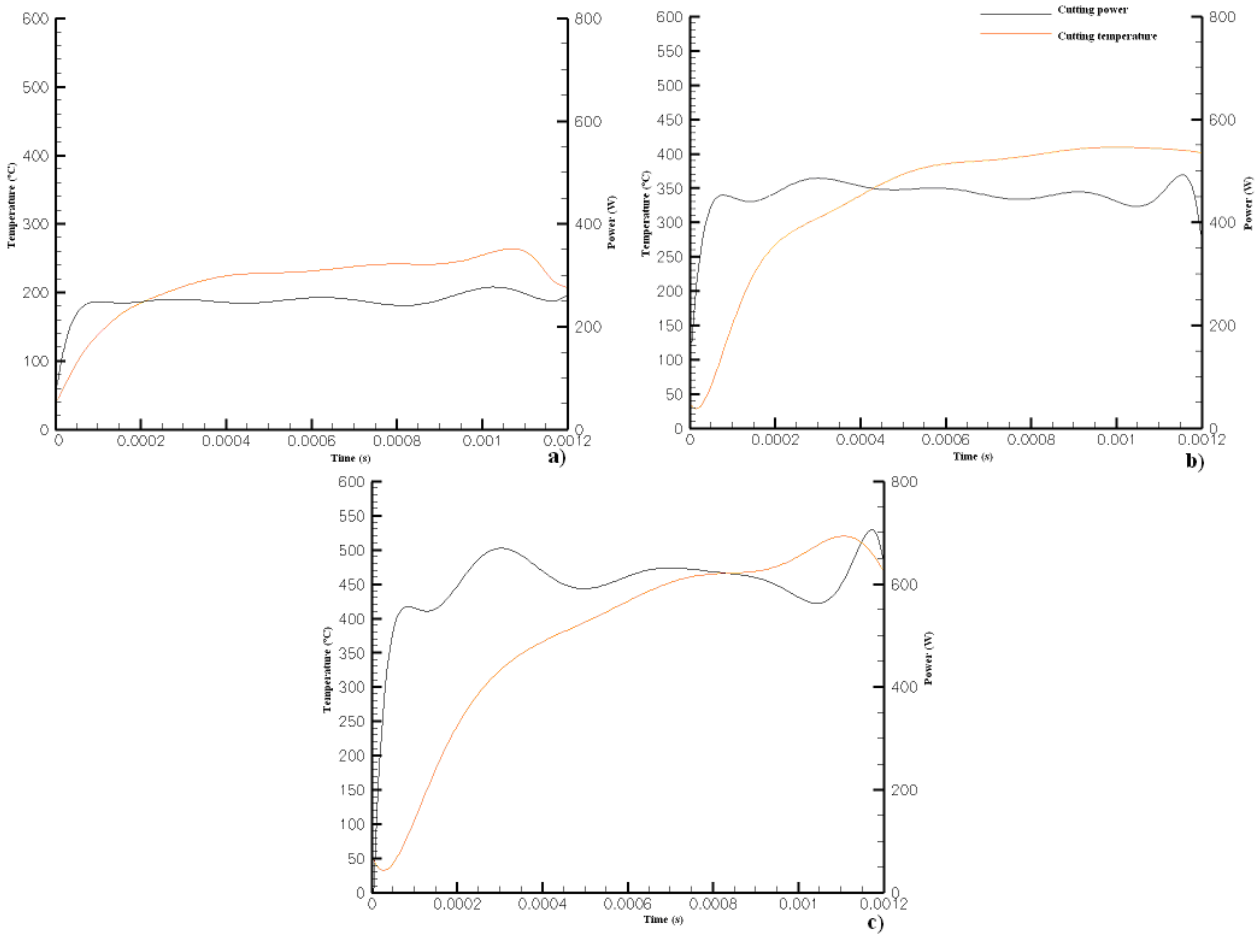

Figure 4.22: Maximum cutting temperature and cutting power along the time in the machining of the stainless steel with a cutting speed of 100 m/min and a depth of cut of 1 mm with the variation of the feed rate. a) 0.05 mm/rev b) 0.1 mm/rev c) 0.2 mm/rev

In figure 4.23, a detailed distribution of the cutting temperature in the tool, workpiece and chip is presented (the figure was taken at the end of the length of cut where the temperature reaches its peak and steady state conditions are present). Like already said, the tool and chip are the principal mechanisms removing the heat from the primary shear zone. This fact is pretty obvious when a feed rate of 0.2 mm/rev is used. The thermal affected layers are bigger when the feed rate increases, leading to more residual stresses with the increase of the feed rate.

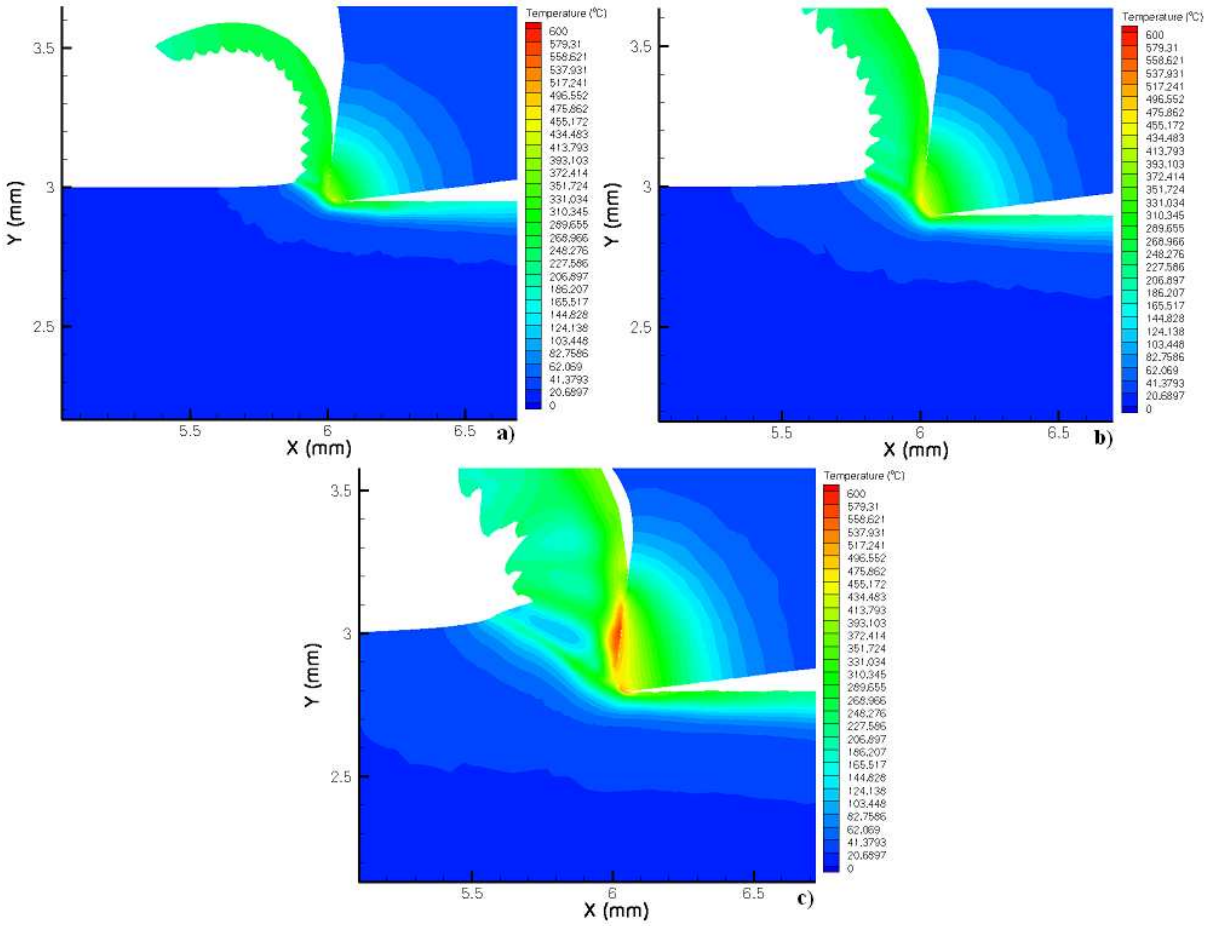

Figure 4.23: Detailed comparison of maximum cutting temperature in the tool, workpiece and chip at the end of length of cut in the machining of the stainless steel with a cutting speed of 100 m/min and a depth of cut of 1 mm with a variable feed rate. a) 0.05 mm/rev b) 0.1 mm/rev c) 0.2 mm/rev

4.5.2.2 Plastic strain and plastic strain rate and maximum shear stress

Regarding plastic strain, a detailed view of its distribution in the tool and chip is shown in figure 4.24 (taken at the end of length of cut for steady state condition purposes). The deformation has a trend to increase, fact which can be explained by the reason of the maximum shear stress also showing an increase with the increase of the feed rate. The outside of the chip curling is obviously more affected by the plastic strain when compared to the inside zone.

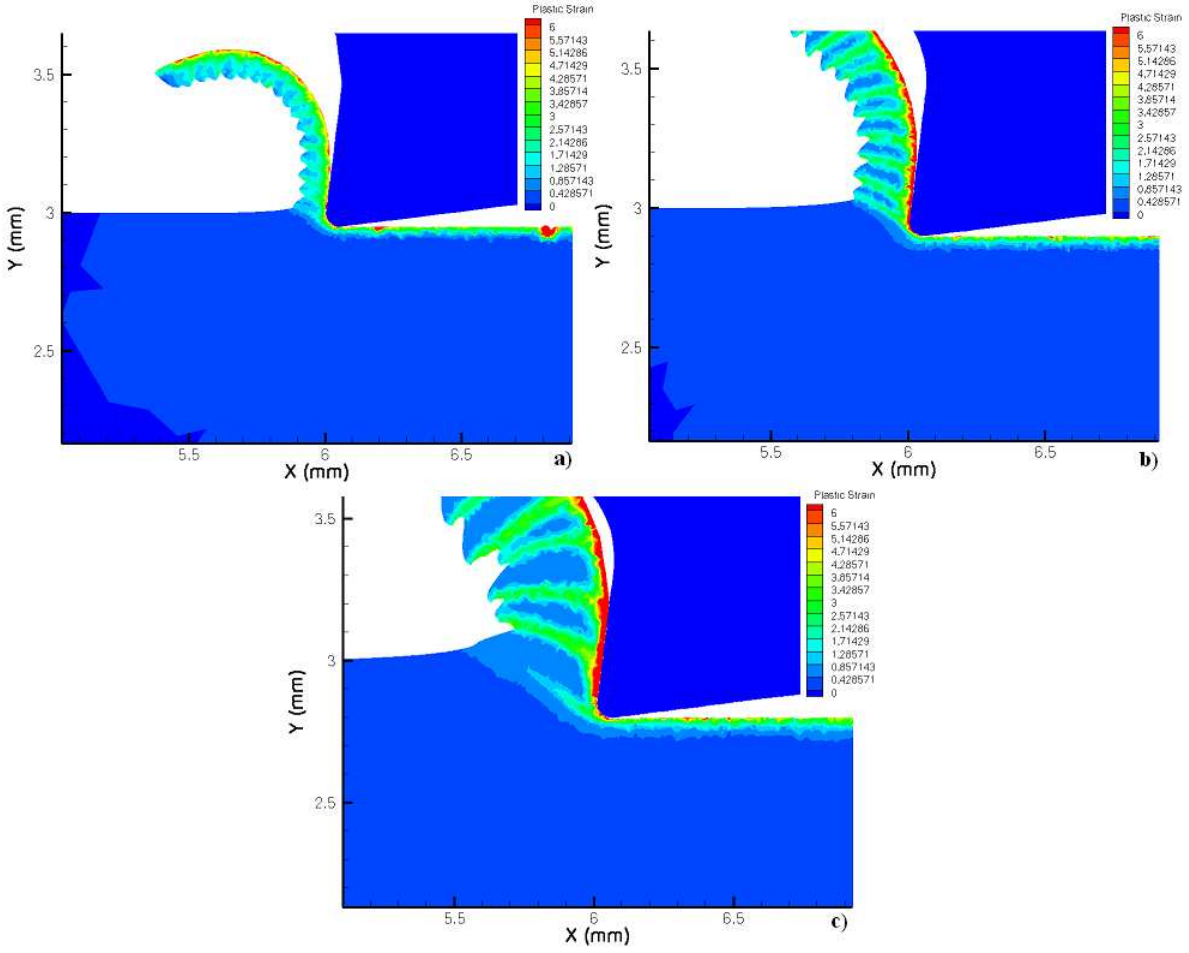

Figure 4.24: Detailed comparison of plastic strain in the tool, workpiece and chip at the end of length of cut in the machining of the stainless steel with a cutting speed of 100 m/min and a depth of cut of 1 mm with a variable feed rate. a) 0.05 mm/rev b) 0.1 mm/rev c) 0.2 mm/rev

What was said regarding plastic strain rate for aluminium is not valid for the machining of the stainless steel. A detailed distribution is presented in figure 4.25 for the workpiece and chip (taken at the end of length of cut due to reach steady state cutting conditions). What was said for aluminium regarding plastic strain rate isn't valid for stainless steel because of the cutting temperature. In aluminium, the cutting temperature was somewhat constant for all cases and the same cannot be said in the machining of the stainless steel. The noticeable increase in temperature with the increase of the feed rate causes a thermal softening of the workpiece material, which leads to an increase in the plastic strain rate.

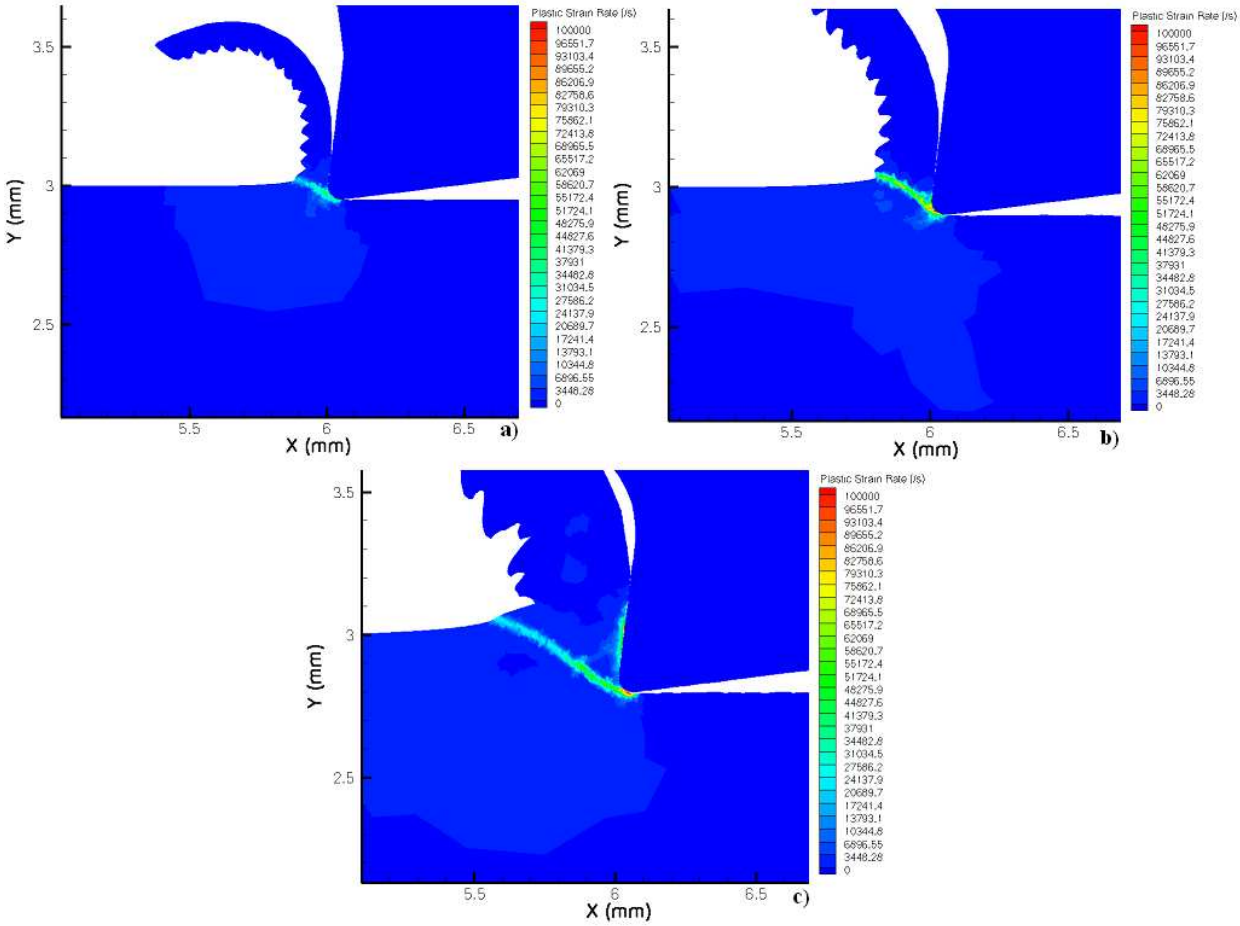

Figure 4.25: Detailed comparison of plastic strain rate in the tool, workpiece and chip at the end of length of cut in the machining of the stainless steel with a cutting speed of 100 m/min and a depth of cut of 1 mm with a variable feed rate. a) 0.05 mm/rev b) 0.1 mm/rev c) 0.2 mm/rev

A distribution of maximum shear stress in the tool, workpiece and chip can be seen in figure 4.26 (taken at the end of length of cut due to steady state conditions). What was initially said for aluminium is not valid for stainless steel. As the feed increases to double, the force almost doubles and the expected shear stress should be decreasing with the increase of the feed rate. This is not verified and, in fact, the maximum shear stress keeps increasing with the feed rate and the affected zone growing as well. The only reasonable explanation for this fact is that the plastic strain showed an increase with the feed rate and this forced the maximum shear stress to increase as well.

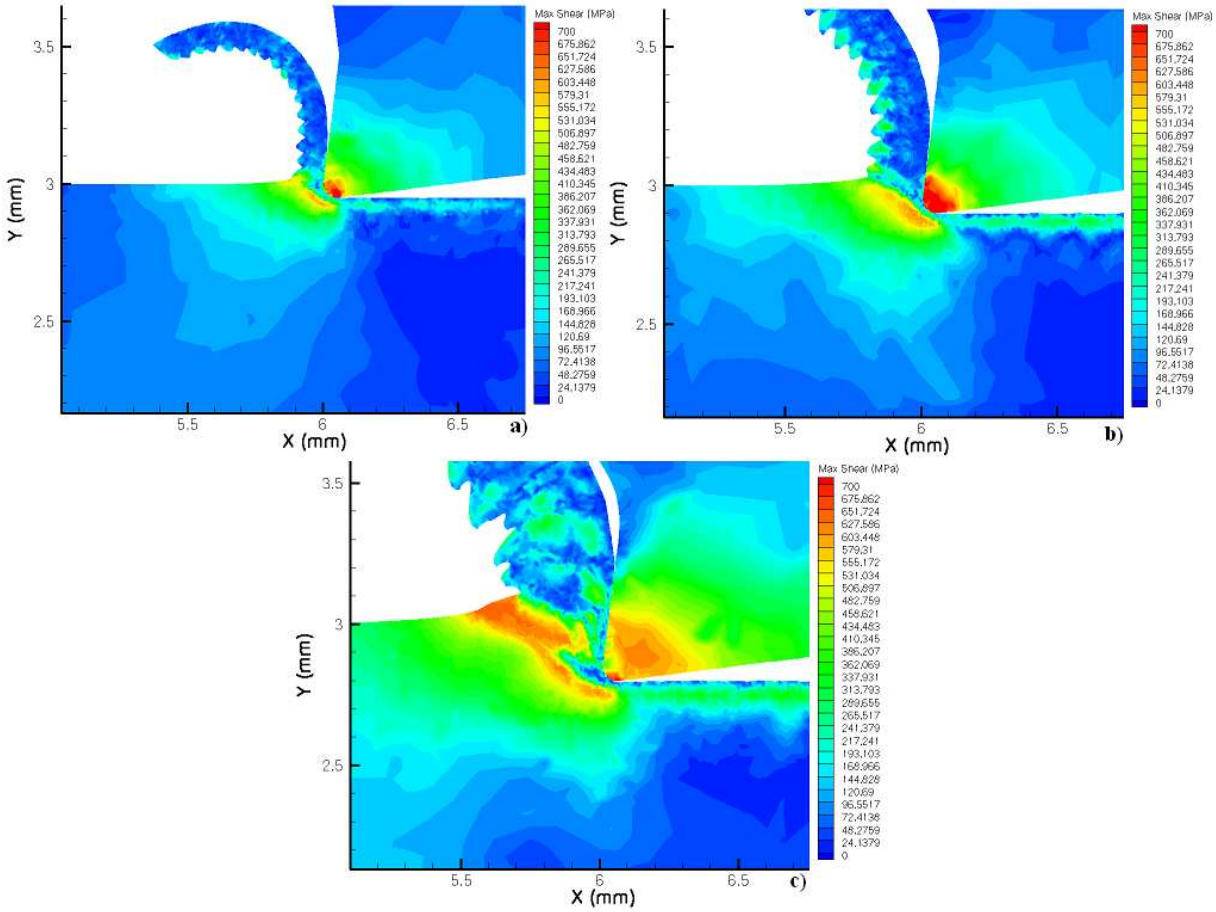

Figure 4.26: Detailed comparison of maximum shear stress in the tool, workpiece and chip at the end of length of cut in the machining of the stainless steel with a cutting speed of 100 m/min and a depth of cut of 1 mm with a variable feed rate. a) 0.05 mm/rev b) 0.1 mm/rev c) 0.2 mm/rev

4.5.2.3 Residual stresses

In figure 4.27, the distribution of the circumferential residual stress can be seen along the depth of the workpiece for the coated cemented carbide cutting tool. Although the maximum tensile residual stress has common values among all feed rates (varying from 250 MPa to 300 MPa), the same cannot be said for the compressive residual stresses. About -100 MPa were reached with a feed rate of 0.05 mm/rev. The compressive residual stress keeps increasing with the increase of the feed rate reaching about -150 MPa for a feed rate of 0.1 mm/rev and about -200 MPa for a feed rate of 0.2 mm/rev. These maximums are reached at 0.26 mm, 0.35 mm and 0.42 mm respectively. The tensile stressed layer also increases with the feed rate being about 0.1 mm for a feed rate of 0.05 mm/rev, about 0.17 mm for a feed rate of 0.1 mm/rev and about 0.2 mm for a feed rate of 0.2 mm/rev.

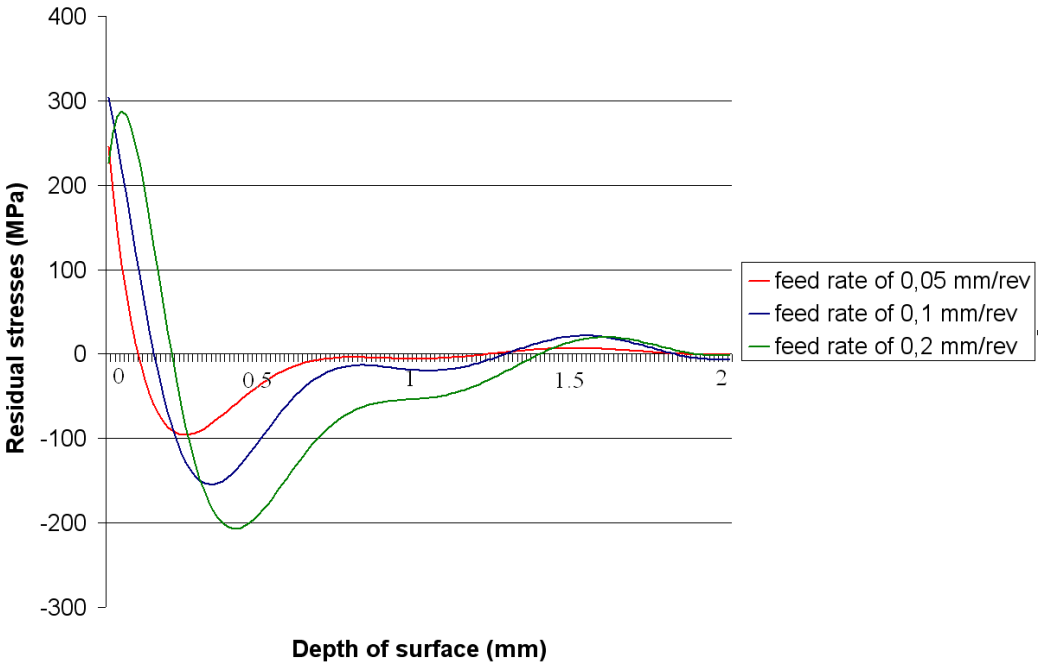

Figure 4.27: Residual stress distribution along the depth of surface in the machining of the stainless steel with a cutting speed of 100 m/min and a depth of cut of 1 mm in function of feed rate

It is also worth noting that the superficial roughness might be related with the residual stress profile. In table 4.10, the obtained roughness profile is shown in function of the feed rate in the machining of the stainless steel. For a feed rate of 0.05 mm/rev, the surface roughness is 1.05 μm. For a feed rate of 0.1 mm/rev and 0.2 mm/rev, the surface roughness is, respectively, 1.16 μm and 3.17 μm. From the simulation work, it is possible to conclude that the lower the feed rate, the lower the residual stresses. This fact can be related with the superficial roughness because the lower the feed, the best roughness is obtained. Having that

said, it is possible to conclude that, for this material and for these machining conditions, the best surface roughness, the less residual stresses are present.

Table 4.10: Experimental roughness values for the machining of the stainless steel with the coated cemented carbide cutting tool in function of the variable feed (an average of 6 measures)

Feed [mm/rev]	Ra (µm)	RzD (µm)	Rt (µm)
0.05	1.05	6.02	8.38
0.1	1.16	6.31	9.78
0.2	3.17	15.05	24.10

Other studies were conducted regarding residual stresses, although with different cutting tools, under different cutting conditions and in AISI 316L instead. In figure 4.28, the distribution of the circumferential residual stress can be observed along the depth of the workpiece (obtained by numerical simulation with uncoated tools with 0 and 15º of rake angle). If both distributions are compared, a big reduction of the maximum tensile residual stress can be verified (in the workpiece surface) for the tool with a superior rake angle (it diminished from 450 MPa to about 200 MPa from the tool with a rake angle of 0º to the tool with a rake angle of 15º respectively). The tensile residual stress thickness layer is the same for both tools (about 0.156 mm) and the compressive residual stress thickness layer is the same as well (about 0.75 mm). The maximum compressive residual stress reached -100 MPa in the tool with a rake angle of 0º and about -50 MPa in the tool with a rake angle of 15º.

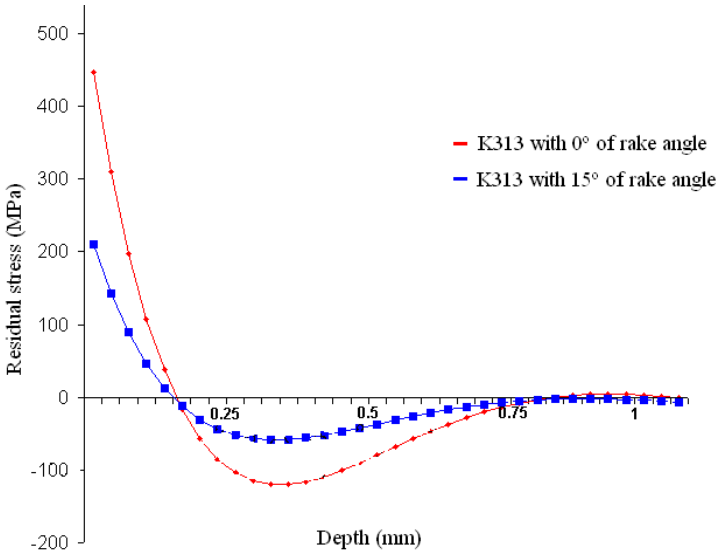

Figure 4.28: Residual stress distribution along the depth of surface in the orthogonal cut of the AISI 316L stainless steel with a friction coefficient of 0.57 with a cutting speed of 150 m/min, a depth of cut of 4 mm and feed rate of 0.1 mm/rev

In figure 4.29, a study of residual stresses in function of the cutting edge radius was conducted. However, like shown in the figure, this parameter seems to not influence the

residual stresses in any way. The tensile residual stresses are almost the same, the affected layers have the same depth and the compressive residual stress also has similar values. It can be concluded that the cutting edge radius does not influence circumferential residual stresses.

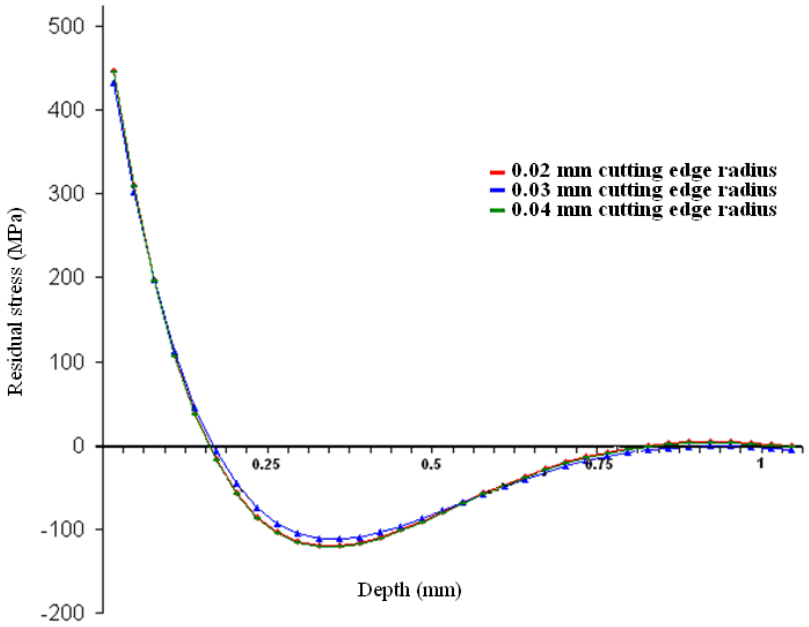

Figure 4.29: Residual stress distribution along the depth of surface in the orthogonal cut of the AISI 316L stainless steel with a friction coefficient of 0.57 with a cutting speed of 150 m/min, a depth of cut of 4 mm and feed rate of 0.1 mm/rev

Chapter 5)

Conclusions

From all the simulations that were made, it is possible to withdraw that the friction coefficient greatly influences the cutting and feed forces, cutting power, maximum cutting temperature and plastic strain. Unfortunately, friction coefficient cannot be measured with precision and it needs to be iterated. Using the experimentation tests, a Coulomb friction coefficient was found for each case of study and this value was the starting point to simulate the machining operations. However, when evaluating the output results of the simulations when the Coulomb friction coefficient is used, it was found that the results didn't met the experimental values (the software predicted all variables by excess in aluminium alloy and with enormous differences in some cases and by defect in the stainless steel, also with

enormous differences in some cases). Regarding this matter, several iterations on the Coulomb friction coefficient were conducted in order to decrease these differences.

Coulomb model predicts friction by excess when turning aluminium alloy because this model is used under static conditions and when metal cutting, dynamic conditions are present along with deformation and thermal gradients, decreasing the friction coefficient. Also of relevance is that the hardness of the experimental workpiece was a bit higher than the simulated workpiece, which suggests near identical flow stress curves between experimental and simulated workpieces. This can be related with the reduction of the Coulomb friction coefficient when machining the aluminium alloy. When turning stainless steel, Coulomb friction model predicts friction by default. This is because the stainless steel flow stress curve that the software uses is below the curve of the workpiece material used in the workshop (the hardness of the experimental workpiece is higher than the hardness of the simulated workpiece). In this case, the friction coefficient had to increase in order to increase the output parameters. Having that said, in aluminium alloy the Coulomb friction coefficient was decreased while for stainless steel it was increased. By default, the software uses the standard friction coefficient (0.5) but Coulomb model is more helpful because it gives a better approximation to the “correct” friction coefficient that should be used. Coulomb model is helpful as a starting point for further iterations, therefore it shouldn’t be used as a final input value. Friction coefficients for all cases of study are within the expected values (lower than 0.5 for the aluminium alloy and higher than 0.5 for the stainless steel). These values are typical like mentioned in state of the art.

Differences between experimentation and simulation when machining the stainless steel are generally bigger than the differences when machining the aluminium alloy. It is believed that the depth of cut might be influencing the results. The validity of the analytic models is called into question if orthogonal conditions are not present. In the machining of the aluminium alloy, the depth of cut is 2 mm, so the tool nose radius has a small impact in the chip formation and the chip is plane. On the other hand, in the machining of the stainless steel, the depth of cut is only 1 mm and the tool nose radius might be influencing the chip formation because its shape is almost plane and not perfectly plane like when machining aluminium. That being put, when applying the analytic models, the measured values are supposed to be taken from a perfect orthogonal cut and that didn’t happen when machining the stainless steel, being the cut almost orthogonal. Also of note is that the used cutting tool in

the machining of the stainless steel has a chip breaker and this also induces deformation in the chip.

It is believed that using numerical simulation is a valid approach to determine parameters like cutting forces, feed forces, cutting power, maximum cutting temperature, plastic strain and plastic strain rate, maximum shear stresses and residual stresses in the orthogonal (almost) cut of the Al 7075 and AISI 316 if the correct friction coefficient is used. Otherwise, the output results have unacceptable differences.

In this investigation 80 simulations were realized along 9 months in order to obtain the presented results.

In the future it would be interesting to change the constitutive law parameters and see if better results are achieved and if Coulomb friction coefficient is capable of better results with the constitutive law parameters adjustment. Because of computational time, all simulations were done under 2D conditions. It would be interesting to simulate in 3D instead of 2D and see what major differences are present.

With the realization of this work, it is possible to conclude that:

- Friction coefficient greatly influences the simulated results
- Friction coefficient cannot be measured with precision
- Coulomb model is helpful as a starting point for further iterations and it shouldn’t be used as a final input value
- Coulomb model predicts the friction by excess when turning aluminium and by default when turning stainless steel
- Numerical simulation is a valid approach to determine parameters like cutting forces, feed forces, cutting power, maximum cutting temperature, plastic strain and plastic strain rate, maximum shear stresses and residual stresses

REFERENCES

Abukhshim N., Mativenga P., Sheikh M. (2006) *Heat generation and temperature prediction in metal cutting: A review and implications for high speed machining*, International Journal of Machine Tools & Manufacture 46 782–800

Aslan E., Camusçu N., Birgoren B. (2007) *Design optimization of cutting parameters when turning hardened AISI 4140 steel (63 HRC) with Al2O3 + TiCN mixed ceramic tool*, Materials and Design 28 1618–1622

Astakhov V. (2007) *Effects of the cutting feed, depth of cut, and workpiece (bore) diameter on the tool wear rate*, The International Journal of Advanced Manufacturing Technology 34 631-640

Astakhov V., Outeiro J. (2005) *Modeling of the contact stress distribution at the tool-chip interface*, Machine Science and Technology, 9:85–99

Barge M., Hamdi H., Rech J., Bergheau J. (2005) *Numerical modelling of orthogonal cutting: influence of numerical parameters*, Journal of Materials Processing Technology 164–165: 1148–1153

Bil H., Kiliç S., Tekkaya A. (2004) *A comparison of orthogonal cutting data from experiments with three different finite element models*, International Journal of Machine Tools & Manufacture 44 933-944

Boothroyd G., Knight W. (1989) *Fundamentals of Machining and Machine Tools*, Marcel Dekker, New York

Bouzid W. (2005a) *An investigation of tool wear in high-speed turning of AISI 4340 steel*, Int J Adv Manuf Technol 26: 330–334

Bouzid W. (2005b) *Cutting parameter optimization to minimize production time in high speed turning*, Journal of Materials Processing Technology 161 388–395

Capello E. (2005) *Residual stresses in turning Part I: Influence of process parameters*, Journal of Materials Processing Technology 160 221–228

Ceretti E., Fallbohmer P., Wu W., Altan T. (1996) *Application of 2D FEM to chip formation in orthogonal cutting*, Journal of Materials Processing Technology 59 169-180

Dahlman P., Gunnberg F., Jacobson M. (2004) *The influence of rake angle, cutting feed and cutting depth on residual stresses in hard turning*, Journal of Materials Processing Technology 147 181–184

Das N., Dundur S. (2006) *A Slipline field analysis of free-chip orthogonal machining with adhesion friction at rake face*, Machining Science and Technology 10:371–387

Davim J., Maranhão C., Jackson M., Cabral G., Grácio J. (2007) *FEM analysis in high speed machining of aluminum alloy (Al7075-0) using polycrystalline diamond (PCD) and cemented carbide (K10) cutting tools*, International Journal Advanced Manufacturing Technology (Springer), in press

Duan C., Wang M., Pang J., Li G. (2006) *A calculational model of shear strain and strain rate within shear band in a serrated chip formed during high speed machining*, Journal of Materials Processing Technology 178 274–277

El-Axir M. (2002) *A method of modeling residual stress distribution in turning for different materials*, International Journal of Machine Tools & Manufacture 42 1055–1063

Ezugwu E., Bonney J., Yamane Y. (2003) *An overview of the machinability of aeroengine alloys*, Journal of Materials Processing Technology, 134, 233-253

Fang N. (2005) *Tool-chip friction in machining with a large negative rake angle tool*, Wear 258 890–897

Filice L., Micari F., Rizzuti S., Umbrello D. (2007) *A critical analysis on the friction modelling in orthogonal machining*, International Journal of Machine Tools & Manufacture 47 709–714

Fratini L., Casto S., Valvo E. (2006) *A technical note on an experimental device to measure friction coefficient in sheet metal forming*, Journal of Materials Processing Technology 172 16–21

Fukui H., Okida J., Omori N., Moriguchi H., Tsuda K. (2004) *Cutting performance of DLC coated tools in dry machining aluminium alloys*, Surface and Coatings Technology, 187 (1), 70-76

Geiger M., Kleiner M., Eckstein R., Tiesler N., Engel U. (2001) *Microforming Annals* CIRP 50(2):445–462

Gilat A., Wu X. (1997) *Plastic deformation of 1020 steel over a wide range of strain rates and temperatures*, International Journal of Plasticity, Vol. 13, Nos. 6-7, pp. 611~32

Gnevko A., Kazakov N., Lazarev D., Velichkovskii V. (2002) *Effect of the loading rate on the microhardness of metallic materials and the micromechanism of plastic strain*, Metal Science and Heat Treatment Vol. 44, Nos. 9 – 10

Gokkaya H., Nalbant M. (2007) *The effects of cutting tool geometry and processing parameters on the surface roughness of AISI 1030 steel*, Materials and Design 28 717–721

Grzesik W. (2008) *Advanced Machining Processes of Metallic Materials Theory Modelling and Applications*, Elsevier

Grzesik W., Nieslony A., Bartoszuk P. (2005) *Finite element modelling of temperature distribution in the cutting zone in turning processes with differently coated tools*, Journal of Materials Processing Technology 164: 1204-1211

Gunnberg F., Escursell M., Jacobson M. (2006) *The influence of cutting parameters on residual stresses and surface topography during hard turning of 18MnCr5 case carburised steel*, Journal of Materials Processing Technology 174 82–90

Ikawa N., Donaldson N., Komanduri R., Koenig W., Aachen T., Mckeown P., Moriwaki T., Stowers I. (1991) *Ultra-precision metal cutting—the past, the present and the future*, Ann. CIRP 40/2 587–594

Kelly J., Cottrell M. (2002) *Minimal lubrication machining of aluminium alloys*, Journal of Materials Processing Technology 120, 327-334

Kim J., Kang Y. (1997) *High speed machining of aluminium using diamond endmills*, International Journal Machining Tools Manufacturing. Vol. 37, No. 8, 1155-1165

Korkut I., Boy M., Karacan I., Seker U. (2007) *Investigation of chip-back temperature during machining depending on cutting parameters*, Materials and Design 28 2329–2335

Lee W., Yeh G. (1997) *The plastic deformation behaviour of AISI 4340 alloy steel subjected to high temperature and high strain rate loading conditions*, Journal of Materials Processing Technology 71 224-234

Li L., He N., Wang M., Wang Z. (2002) *High speed cutting of Inconel 718 with coated carbide and ceramic inserts*, Journal of Materials Processing Technology 129 127-130

Li Q., Lovell M. (2005) *On the critical interfacial friction of a two-roll CWR process*, Journal of Materials Processing Technology 160 245–256

List G., Nouari M., Gehin D., Gomez S., Manaud P., Petitcorps Y., Girot F. (2005) *Wear behaviour of cemented carbide tools in dry machining of aluminium alloy*, Wear 259 1177–1189

Liu R., Guo B. (2005) *Finite element analysis of the effect of sequential cuts and tool–chip friction on residual stresses in a machined layer*, International Journal of Mechanical Sciences;42:1069–86.

MacGinley T., Monaghan J. (2001) *Modelling the orthogonal machining process using coated cemented carbidel cutting tools*, Journal of Materials Processing Technology 118: 293-300

Mackerle J. (2003) *Finite-element analysis and simulation of machining: an addendum bibliography* (1996–2002), Journal of Materials Processing Technology 43 103–114

Mahrenholtz O., Bontcheva N., Iankov R. (2005) *Influence of surface roughness on friction during metal forming processes*, Journal of Materials Processing Technology 159 9–16

Maity K., Das N. (2001) *A class of slipline field solutions for metal machining with Coulomb friction at the chip-tool interface*, Journal of Materials Processing Technology 116 278 – 288

Marusich T., Ortiz M. (1995) *Modelling and Simulation of High Speed Machining* Int. J. Num. Meth. Eng., 38:3675-3694

Merchant E. (1945) *Mechanics of the Metal Cutting Process. I. Plasticity Conditions in Orthogonal Cutting*, J. Appl. Phys. 16, 318

M'Saoubi R., Outeiro J., Changeux B., Lebrun J., Dias A. (1999) *Residual stress analysis in orthogonal machining of standard and resulfurized AISI 316L steels*, Journal of Materials Processing Technology 96 225±233

Odeshi A., Al-ameeri S., Bassim M. (2005) *Effect of high strain rate on plastic deformation of a low alloy steel subjected to ballistic impact*, Journal of Materials Processing Technology 162–163 385–391

Outeiro J. (2007) *Influence of tool sharpness on the thermal and mechanical phenomena generated during machining operations, International.* Journal of Machining and Machinability of Materials, Vol. 2, Nos. 3/4

Outeiro J., Dias A., Jawahir I. (2006a) *On the Effects of Residual Stresses Induced by Coated and Uncoated Cutting Tools with Finite Edge Radii in Turning Operations*

Outeiro J., Umbrello D., M'Saoubi R. (2006b) *Experimental and numerical modelling of the residual stresses induced in orthogonal cutting of AISI 316L steel*, International Journal of Machine Tools & Manufacture 46 1786–1794

Ozel T. (2006) *The influence of friction models of finite element simulations of machining*, International Journal of Machine Tools & Manufacture 46, 518-530

Ozel T., Zeren E. (2007) *Numerical modelling of meso-scale finish machining with finite edge radius tools*, International Journal of Machining and Machinability of Materials, Vol. 2, Nos. 3/4

Ozel T., Altan T. (2000) *Determination of workpiece flow stress and friction at the chip–tool contact for high-speed cutting*, International Journal of Machine Tools & Manufacture 40 133–152

Raman S., Longstreet A., Guha D. (2002) *A fractal view of tool–chip interfacial friction in machining*, Wear 253 1111–1120

Sahin Y., Motorcu A. (2005) *Surface roughness model for machining mild steel with coated carbide tool*, Materials and Design 26 321–326

Shen C. (1996) *The importance of diamond coated tools for agile manufacturing and dry machining*, Surface and Coatings Technology, 86-87 (part 2) 672-677

Sartkulvanich P., Altan T., Gocmen A. (2005) *Effects of flow stress and friction models in finite element simulation of orthogonal cutting – a sensitivity analysis*, Machine Science and Technology 9, 1-26

Trent M., Wright P. (2000) *Metal Cutting*, Butterworth-Heinemann

Umbrello D., M'Saoubi R., Outeiro J. (2007) *The influence of Johnson–Cook material constants on finite element simulation of machining of AISI 316L steel*, International Journal of Machine Tools & Manufacture 47 462–470

Velasquez J., Bolle B., Chevrier P., Geandier G., Tidu A. (2007) *Metallurgical study on chips obtained by high speed machining of a Ti–6 wt.%Al–4 wt.%V alloy*, Materials Science and Engineering A 452–453 469–474

Xue Q., Liao X., Zhu Y., Gray G. (2005) *Formation mechanisms of nanostructures in stainless steel during high-strain-rate severe plastic deformation*, Materials Science and Engineering A 410–411 252–256

Yang X., Liu C. (2002) *A new stress-based model of friction behaviour in machining and its significant impact on residual stresses computed by finite element method*, International Journal of Mechanical Sciences 44 703–723

Yen Y., Söhner J., Lilly B., Altan T. (2004) *Estimation of tool wear in orthogonal cutting using the finite element analysis*, Journal of Materials Processing Technology 146: 82–91

Zorev N., Wallace P., Boothroyd G. (1964) *Tool forces and tool-chip friction in orthogonal machining*, Journal of Mechanical Engineering Science 6: 422-&